Fatigue Life of Hybrid FRP Composite Beams

by

Jolyn Louise Senne

Thesis submitted to the Faculty of the
Virginia Polytechnic Institute and State University
in partial fulfillment of the requirements for the degree of

Master of Science
in
Engineering Mechanics

John J. Lesko, Chair
Scott W. Case
Thomas E. Cousins

July 10, 2000
Blacksburg, Virginia

Keywords: fiber-reinforced polymer (FRP) composites, fatigue, hybrid composites, pultruded composites, life prediction, infrastructure

Fatigue Life of Hybrid FRP Composite Beams

Jolyn Louise Senne

(ABSTRACT)

As fiber reinforced polymer (FRP) structures find application in highway bridge structures, methodologies for describing their long-term performance under service loading will be a necessity for designers. The designer of FRP bridge structures is faced with out-of-plane damage and delamination at ply interfaces. The damage most often occurs between hybrid plys and dominates the life time response of a thick section FRP structure. The focus of this work is on the performance of the 20.3 cm (8 in) pultruded, hybrid double web I-beam structural shape. Experimental four-point bend fatigue results indicate that overall stiffness reduction of the structure is controlled by the degradation of the tensile flange. The loss of stiffness in the tensile flange results in the redistribution of the stresses and strains, until the initiation of failure by delamination in the compression flange. These observations become the basis of the assumptions used to develop an analytical life prediction model. In the model, the tensile flange stiffness is reduced based on coupon test data, and is used to determine the overall strength reduction of the beam in accordance the residual strength life prediction methodology. Delamination initiation is based on the out-of-plane stress σ_z at the free edge. The stresses are calculated using two different approximations, the Primitive Delamination Model and the Minimization of Complementary Energy. The model successfully describes the onset of delamination prior to fiber failure and suggests that out-of-plane failure controls the life of the structure.

ACKNOWLEDGEMENTS

This work could have never been completed without the patience, assistance and friendship of so many people. The past two years have been better than I could have ever anticipated. If I thanked everyone for everything, the people who bind this thing wouldn't be very happy. Hopefully I'll hit most of the important points…..

First and foremost, **Dr. John "Jack" Lesko** - I remember meeting you, walking out of your office and being 100% sure that you were the right advisor for me. Now, two years later, I'm still certain I made the right choice. Your patience, encouragement and advice were essential to my success here. I appreciate all the confidence and respect you had for my work. Beyond the research, I think we had some pretty good laughs. More than once I've had people comment on how well I got along with my advisor. Maybe we weren't always super professional, but I think we still got the job done. In fact, it was done so well, I don't think I need to stick around for a Ph.D!

Dr. Scott Case the number of things you've helped me with, from how to use the quick keys to put in the ° sign in Word, to some crazy complicated math, can't be counted. I think I will forever be amazed with the fact that I can ponder something for a week, be stumped, ask you and 15 minutes later the solution is crystal clear. I really do appreciate all of your assistance, especially in the development stages of this code. Finally, I hope you can find someone to blame all the computer problems on after I'm gone.

Dr. Tommy Cousins, thanks for the insight from the Civil Engineering side of things. Your assistance with everything in the structures lab, including with the MEGA-DUH, was essential in getting the fatigue test going, and going, and going.

I'm pretty sure the MRG has two of the best secretaries around, **Bev Williams** and **Shelia Collins**. Thanks for keeping enough zip disks and transparency covers around; I don't know how I went through so many of those things. Also, it was great to have you ladies around when I had questions about getting fitted for dresses and things of that sort. Bev, a special thanks for dealing with all my POs and reimbursements – I think I finally have the system down.

Much of my experimental work would have not have been completed without the assistance of **Brett Farmer, Dennis Huffman, Mac McCord, Bob Simmonds** and **Dave Simmons.** All of you are excellent at what you do, and are extremely patient and helpful to those of us who don't necessarily know what we are doing. Brett and Dennis and anyone else subjected to the non-stop fatigue test, sorry about the noise, and hope I haven't caused any permanent damage to your eardrums.

The insight and experience of my fellow grad students was also essential to getting things done. **David Haeberle** I've truly enjoyed working with you, it's been far from "typical". I really appreciate all the help you've given me getting things done in the structures lab and checking on my tests when I'm gone, etc. I will always strive to strain gage to your

standards, and will try to remember to not put my pencil written notes in the same stack with my transparencies. **Doug Neely**, thanks for making the lab and field tests a highly amusing time. I don't think there was more than five minutes of silence when we were working, but we always got everything done. I'm really glad you got to help me figure out how fashionable waders and safety glasses really could be. **Joe South** working on the Strength and Life project was quite an experience, I appreciate you being able to deal with the Jolyn-way-of-doing-things. Thanks for all your help in naming variables and making sure I was caffeinated by the many trips to the "King". **Blair Russell,** thanks for all the free advice and keeping me rational through my thesis writing days. My thesis brought together lots of people's research that had been completed prior to my arrival. **Steve Pfifer, Michael Hayes, Kyle Garcia** and **Greg Ariff** thanks for doing such superb work.

I think working in the MRG has been one of the greatest work environments I'll ever encounter. The people in the group are extremely dynamic, and make just about every day an experience. Each and everyone of you have contributed to my success here. It truly has been an honor to follow **Celine Mahieux** as *Queen Bee* of the group. **Rob Carter** and **Blair Russell** thanks for being "right on" time for the most important part of the day – lunch. May you always think of me when you see a turkey sandwich, and "wing-pie" will always remind me of you guys. **Jason Burdette,** you had a very respectable attendance record at lunch too, and it was great to have a fellow hockey fan around, it really should have been the Red Wings and Flyers in the finals! **Tozer Bandorowalla**, I don't think the office would be the same without you, thanks for helping me expand my vocabulary to include things like spectacles and buggies.

The other friendships I've made outside of the office, during my short stint away from the mid-west, have been fundamental to me succeeding here. **Amy Dalrymple**, your friendship and ability to totally know what I'm always thinking was incredible; I truly think we lead parallel lives before arriving at VT. **Linda Harris,** we really should have lived together, we would have had a blast – I can't wait for Europe! **Rich Meyerson** thanks for being here for the duration, we had some good laughs and delicious dinners. Football games, hiking, and weekend life in general would not have been the same without **Mark Boorse, Trevor Kirkpatrick, Marybeth Miceli, Mike Neubert, John Ryan, Tony Temeles** and **Donna Senn.**

A special thanks to my parents, **Steve and Judi Senne** who have made most all of this possible. Sorry you had to put up with me choosing schools that were at least 8 hours from home. I know you guys thought I was crazy when I decided to go to get my M.S. without ever visiting where I would spend the next two years of my life, but amazingly it all worked out fine. You have been more than generous to me – and certainly deserved to still claim me as dependant on the income tax returns. Finally, my sister **Ann,** thanks for being the best kid sis I could ask for.

TABLE OF CONTENTS

LIST OF FIGURES

LIST OF TABLES

CHAPTER 1: INTRODUCTION AND LITERATURE REVIEW

1.1 Introduction

Fiber reinforced polymeric (FRP) composites have great potential for use in infrastructure and other civil engineering applications. Composites may offer a number of advantages over traditional materials, including environmental durability and ease of construction due to high specific strength and stiffness. However, a number of technical issues remain that must be addressed before the civil engineering community can develop confidence in structural design with composite members. These issues include, but are not limited to, low stiffness, connection details, cost, confirmation of improved durability, and availability of design codes.

Enviro-mechanical durability is often cited as a key advantage of FRP composite materials over steel designs. Yet, composite performance under the non-deterministic service environment of a bridge structure is neither well understood nor can it currently be modeled with any level of confidence. From the perspective of the highway bridge designer, the inability to quantify service life either through experience or proven predictive schemes presents a formidable barrier to the use of composites in even an experimental structure.

The problem is complicated by the need to develop a life prediction tool for a path dependent damage material system, in the face of combined and synergistic enviro-mechanical loading. Although polymer composites do not exhibit corrosion (material state change) as does steel, polymers and their composites do experience loss in stiffness and strength under the influence of time, temperature, moisture and stress. For example, polymer stiffness, toughness and strength can be reduced when exposed to moisture, UV, and temperature. These issues inhibit our ability to accelerate these processes and extend the credibility of predictions to the design lives of bridges, which may be as long as 100 years.

One other factor plays a role in how life prediction is approached for the civil infrastructure composites; most structural elements are composed of thick sections, hybrid composites and in some cases adhesively bonded components. These characteristics present the opportunity for out-of-plane failures to dominate the life time performance of the structure. Typically, highway structural design is stiffness critical to ensure rider comfort (reducing deflection so that it is neither not perceptible or awkward to the driver) and reduce tensile strains in concrete structures. This leads to low operating stress levels that make it unlikely that in-plane fiber damage will dominate the response. Thus, delaminations and failures in adhesively bonded regions will most likely lead to global reduction in structural stiffness. This has been observed by Lopez *et al*. during strength and fatigue testing of an FRP deck system composed of a thick multi-layer pultruded section adhesively bonded together [1]. Similar observations on failure of FRP shapes were reported in [2], where beams tested to failure in bending exhibited onset of delamination on top flanges.

The focus of the thesis work presented here considers the fatigue response of a hybrid pultruded structural section presently employed in the Tom's Creek Bridge, Blacksburg, Virginia [3]. The loading considered is only mechanical and forms the basis for future efforts that consider other degradation mechanisms. Experimental four-point bend fatigue results will be compared to an analytical life-prediction model considering the same loading. The model is developed based on coupon fatigue characterization and considers the delamination failure mode that occurs under bending.

1.2 Tom's Creek Bridge Overview

1.2.1 Bridge Construction and Testing

The original Tom's Creek Bridge, constructed in 1932 and reconstructed in 1964 in Blacksburg, Virginia was rehabilitated in 1997 using hybrid FRP composite beams. [3,4,5] The bridge is a small structure with a HS20-44 load rating and is shown in Figure 1- 1. The twelve steel stringers have been replaced with 24 composite beams in a project involving Virginia Tech, Strongwell Corp., the Virginia Transportation Research Council (VTRC), the Virginia Department of Transportation (VDOT) and the Town of Blacksburg, Virginia. The project provides an opportunity to investigate the material behavior under vehicular loading and environmental effects over a 10-15 year period.

Figure 1- 1: Rehabilitated Tom's Creek Bridge

The bridge has a span of 5.33 m (17.5 ft) and is 7.32 m (24 ft) wide with a skew angle of 12.5°[4] Prior to installation of the bridge, a full-scale laboratory test of the bridge was completed to validate the design. A loading frame was built to simulate axle load and the foundation of the bridge. Different scenarios were simulated to evaluate the connections and overall response of the structure. [5]

Several field tests have been conducted since the installation of the bridge. The tests were conducted using a controlled vehicle of known weight at various speeds to assess static and dynamic response of the structure. The tests indicate no chanige in stiffness. Beams were also removed from the bridge after fifteen months of service; and the composite girders had not lost a significant amount of either stiffness or ultimate strength.

[6] Additionally, temperature, moisture and UV effects are being investigated, and this research is ongoing. The environmental conditions are being monitored in an effort to understand their impact on the system on an individual basis and as combined effects. The effects of saturation and freeze-thaw fatigue on pultruded vinyl ester E-glass composites is under investigation [7,8]. In the pultruded materials, the voids and interfacial cracking provide locations for water to reside. Experimental results indicated that the volume increase during freezing results in damage accumulation in the composite. Fatigued samples showed a decrease in stiffness and strength, although no relationship was found between diffusivity and crack density [9]. Combined moisture and thermal effects on the laminates appear to influence the residual strength [10,11] and durability [12]. All of the damage mechanisms need to be understood including sequencing and combined effects to properly predict the fatigue performance of the beams in the unpredictable infrastructure environments.

1.2.2 The Hybrid Double Web I Beam

1.2.2.1 Beam Design

The structural shape employed in the bridge is a double web I beam, coined Extren DWB^{TM} [13]. The cross section was designed as part of an Advanced Technology Program through the national Institute of Standards and Technology (NIST) lead by the Strongwell Corporation of Bristol, Virginia, with input from Dr. Abdul Zureick of Georgia Tech. A 20.3 cm (8 in) deep section (see Figure 1- 2) is serving as a sub-scale prototype for a 91.4 cm (36 in) beam being developed for 10 to 18 meter span bridges [14,15]. Optimization of the design was focused on structural efficiency and ease of manufacture. Since the flanges provide the majority of the stiffness in such a beam, increasing flange thickness can add significant stiffness to the structure. In a standard I-beam, without lateral support, increasing the thickness of the flanges can results in twisting or buckling of the web. In the double web design, the webs are connected using supplemental internal flanges improving the stiffness and torsional rotation response. [16]

The beam is a pultruded section composed of both E-glass and carbon fiber in a vinyl ester resin. The approximate fiber volume fraction (both glass and carbon) for the structure is 55%. The carbon is located in the flanges to increase the section's bending stiffness and is oriented at 0°. Glass fiber is present in the pultruded structure primarily in the form of stitched angle ply mats, roving and continuous strand mat. In the flanges, mats are primarily oriented at angles of 0° and 90°, with respect to the direction of the length of the beam with a few mats oriented at +/-45°. The webs are predominantly +/-45° layups.

The geometrical properties of the section are:

$$\text{Area} = 88.4\ \text{cm}^2\ (13.7\ \text{in}^2)$$

$$I_{zz} = 5328\ \text{cm}^4\ (128\ \text{in}^4)$$

$$I_{yy} = 1320\ \text{cm}^4\ (31.7\ \text{in}^4)$$

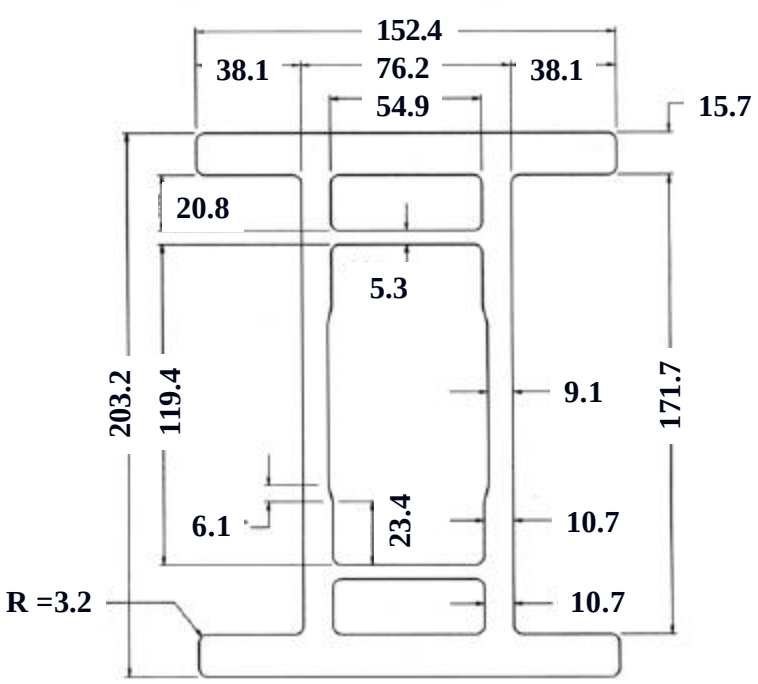

Figure 1- 2: Cross Section of the 20.3 cm (8 in) Double Web I – Beam

1.2.2.2 Beam Manufacture

The Tom's Creek Bridge beams are manufactured using the pultrusion process and consist of unidirectional carbon and stitched mat E-glass in a vinyl-ester resin. The pultrusion process is the lowest cost and most efficient way to manufacture the structural members used in infrastructure. Similar to extrusion used in metals and plastics, pultrusion is continuous process for which a constant cross section can be created. Carbon or glass fibers in various forms, including continuous axial fibers, continuous strand mat, stitched mat or woven fabrics, can be used within a section. The material is cured as the fibers are pulled though a resin bath and heated die [17].

Unlike high performance composite materials used in military and aerospace applications, composites created by pultrusion are often inconsistent. Fiber undulation, voids and variable ply thickness influence the performance of these materials under fatigue loading. The influence of these flaws can best be understood by looking at their experimental response [18].

1.2.2.3 Stiffness and Strength Characterization

Static strength and stiffness testing has been conducted on the beams as part of a design manual development. Two series of beams were tested, the 400-series and the 500-series, at various lengths. The two series contain carbon fiber from two different manufacturers. The loading was four-point bend at the triple points, up to failure at 2.44 m, 4.27m and 6.10 m (8 ft, 14 ft and 20 ft) spans. The set-up is shown schematically in Figure 1- 3 for a 6.10 m beam. All of the beams failed in a catastrophic manner, characterized by delamination of the top flange exhibited in Figure 1- 4. Note that the two photographs shown are not from the same beam. The average resulting stiffness, deflections, strains, failure moment and KGA (shear stiffness) values are summarized in Table 1- 1. [19]

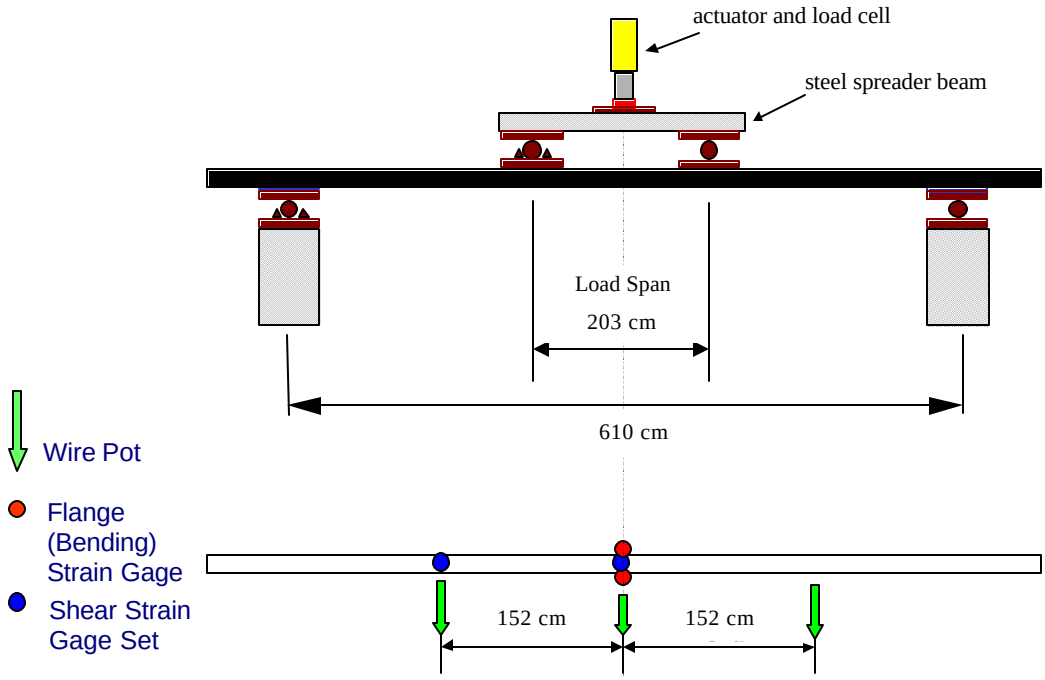

Figure 1-3: Schematic of quasi-static testing to failure

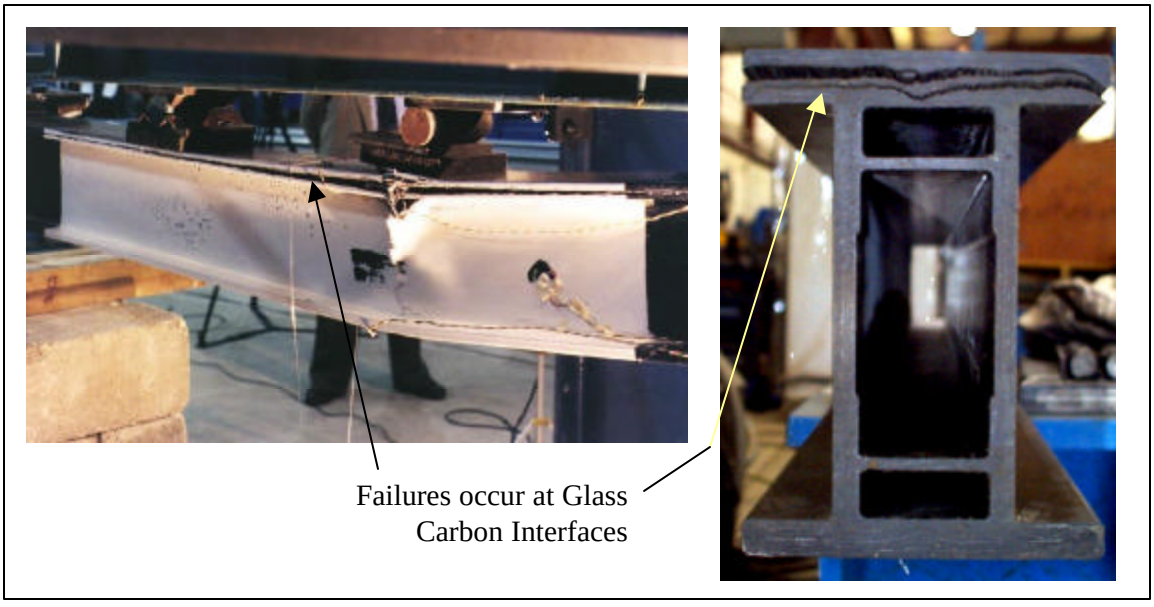

Figure 1-4: Delamination Failure of the beam under quasi-static testing

Table 1- 1: Results of Static Tests to Failure on Hybrid Beams

		Stiffness		Failure Moment		Center Deflection		Top Flange Strain	KGA	
		GPa	Msi	kN-m	kip-ft	cm	in	με	N	lbs
400 Series	Mean	43.3	6.28	129.2	95.3	4.57	1.8	5874	1.17E+07	2.64E+06
2.4 m (8 ft)	*Std. Dev*	*0.12*	*0.18*	*21.8*	*16.1*	*0.48*	*0.19*	*620*	*7.56E+05*	*1.70E+05*
400 Series	Mean	42.8	6.21	139.0	102.5	12.7	5.0	6232	1.40E+07	3.14E+06
4.3 m (14 ft)	*Std. Dev*	*0.62*	*0.09*	*15.6*	*11.5*	*1.47*	*0.58*	*829*	*3.60E+06*	*8.10E+05*
500 Series	Mean	45.8	6.64	100.6	74.2	17.5	6.9	4333	1.03E+07	2.31E+06
6.1 m (20 ft)	*Std. Dev*	*1.45*	*0.21*	*17.9*	*13.2*	*3.00*	*1.18*	*753*	*3.25E+06*	*7.30E+05*

The failure due to delamination consistently occurs between the glass and carbon layers in the top flange. The results indicate that the stiffer beams had a lower ultimate failure load. This is most likely due to the idea that the carbon stiffness dictates the overall stiffness of the beam. But, it is has also been shown that a greater mismatch in material stiffness results in higher interfacial stresses between layers [20]. Therefore, although a stiffer carbon fiber increases the overall stiffness, it also inherently decreases the overall strength of the hybrid member. In addition to the material mismatch, the sizings used on the carbon fiber were developed for use in aero-space applications and are generally incompatible with the vinyl ester resins used in the pultruded products. [21,22]

In addition to the hybrid beams, glass beams of the same shape were also tested in the same manor. The failure mode was the same as the hybrid beams, although failure occurred at a higher ultimate moment and strain, despite the structure being less stiff. This confirms the idea that the material mismatch and interfacial concerns induce the failure by delamination. The results of the glass tests are shown in Table 1- 2.

Table 1- 2 : Results of Static Tests to Failure on Glass Beams

		Stiffness		Failure Moment		Center Deflection		Top Flange Strain	KGA	
		MPa	Msi	kN-m	kip-ft	cm	in	με	N	lbs
400 Series	*Mean*	31.4	4.56	179.5	132.4	8.89	3.5	11980	1.37E+07	3.08E+06
2.4 m (8 ft)	*Std. Dev*	*0.4*	*0.06*	*11.5*	*8.5*	*0.81*	*0.32*	*1226*	*3.39E+06*	*7.62E+05*
400 Series	*Mean*	30.3	4.39	199.0	146.8	27.18	10.7	13740	1.91E+07	4.30E+06
4.3 m (14 ft)	*Std. Dev*	*0.4*	*0.06*	*9.9*	*7.3*	*1.65*	*0.65*	*888*	*4.42E+06*	*9.93E+05*
500 Series	*Mean*	32.2	4.67	163.8	120.8	43.18	17.0	9942	9.56E+06	2.15E+06
6.1 m (20 ft)	*Std. Dev*	*1.0*	*0.15*	*8.1*	*6.0*	*2.62*	*1.03*	*679*	*4.76E+06*	*1.07E+06*

1.2.2.4 Out of Plane Strength Characterization

Testing was completed in an attempt to characterize the out-of-plane strength of the top flange of the beam [23]. The specimens were machined and mounted with aluminum tabs on the top of the flange. A hole was machined in the web to complete the centric load path through the sample. The specimens were then loaded in tension. The failure appeared to be failure between the carbon fiber and the vinyl ester resin at the first carbon-resin interface from the bottom of the flange, as was seen in the failure of the overall structure, Figure 1- 5. The Weibull characteristic strength of the specimens was found to be 276 psi. The crack initiated at the center of the specimen (1) and continued to grew toward the edge (2) and was through the entire thickness of the specimen.

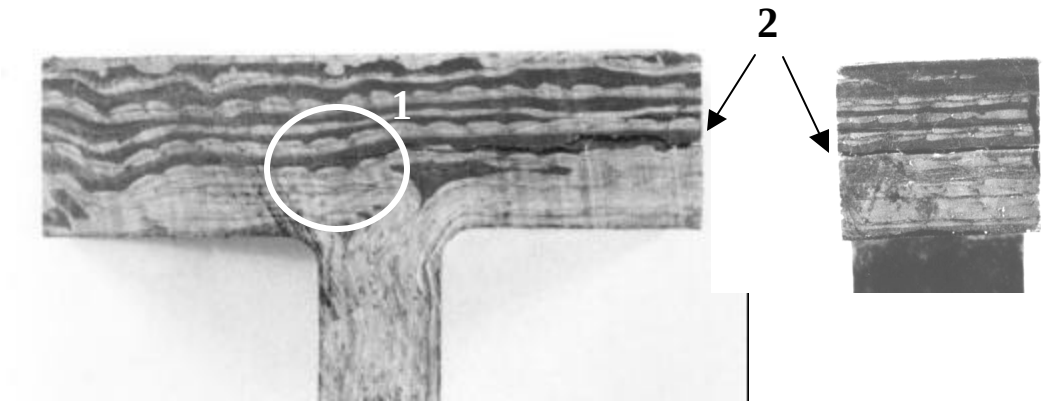

Figure 1- 5: Resulting failure from out-of-plane strength test

1.3 Literature Review

The ability to predict the out-of-plane failure mode of delamination, the main focus of this thesis, requires an understanding of the three dimensional stress state, especially at

the free edge. Understanding the interlaminar stresses requires analysis beyond standard Classical Lamination Theory for in-plane effects. Additionally, since the beam is loaded in both tension and compression multiple strength values need to be quantified and understood in order to effectively evaluate a failure criterion. A review of the literature considering the flexural response, the free edge problem and delamination prediction is summarized below.

1.3.1 Flexural Response

Buckling and compressive failures in pultruded FRP I-beams has been reported on by Bank for pultruded E-glass / polyester and E-glass / vinyl ester I-beams under four-point bend loading. [24] All of the beams failed through local buckling of the compressive flange, as seen for the Tom's Creek Bridge beams. There was a difference noted in the actual buckling failure for the two material types. The vinyl ester beams failed at the junction between the web and flange due to a longitudinal crack at this interface, but the flange remained intact. Therefore, the failure was actually a local geometry dependent failure. The polyester beams failed due to compression of the material within the top flange. A comparison of the vinyl ester beams in Bank's tests to the in-house tests shows very different ultimate moment values but similar modulus values. This results from the continuous mats used in the double-web I-beam, which shifts the failure from the web-flange interface to within the flange itself, encouraging the design used in the Tom's Creek Bridge beams.

Thick section hybrid composite response to three-point bend loading has been considered by Khatri, for unidirectional and cross ply laminates. [25] 16 and 40-ply symmetric E-Glass and AS4 samples were tested. The samples had an AS4 (graphite) core sandwiched between E-glass. 100%, 75%, 50%, and 25% AS4, and 100% E-glass combinations were considered. The flexural rigidity is seen to be very dependent on the content of AS4. Since flexural rigidity is a function of EI, the maximum rigidity is attained by placing the graphite on the outermost surface. In reality, an increase in the failure strain is accomplished by placing the E-glass on the surface, since it buckles at a higher strain. The glass layers therefore restrict the graphite from buckling prior to matrix failure in the

off-axis plies or delamination at the interface. This "hybrid effect" was verified experimentally, the maximum failure strain is reached for a sample containing 75% AS4 fibers. The ultimate bending moment was also increased for the hybrid layups.

The failure in the tests by Khatri, in most cases was catastrophic with no obvious damage prior to the drop in the load. In all of the tests, the compressive mode controlled the failure and resulted in the propagation of delamination. For the 100% graphite and hybrid composite, the outermost graphite layer is where the failure initiated and propagated as kink bands. For the $[0/90]_s$ hybrid samples, the failure normally initiates in the 90° layer, resulting in kink band formation and propagation in the 0° layer. The kinking in the graphite layer is the result of matrix cracking and yielding of the matrix in the glass region. For the 100% glass samples, failure is compressive, but the extensive delamination is seen at the 90° ply interfaces with the 0° plies.

1.3.2 Interfacial Stresses and Delamination

1.3.2.1 The Free Edge Problem

When considering laminated material systems, the solution for the stresses is complex near the free edge. Classical Lamination Theory (CLT) [26] assumes plane stress, and therefore is only appropriate away from the free surface. At a given free surface $\sigma_x = \tau_{xy} = 0$ or $\sigma_y = \tau_{xy} = 0$. Equilibrium arguments then require the presence of interlaminar stresses (σ_z,τ_{xz} and τ_{yz}) in a boundary layer region at the free edge. These stresses are critical since they often lead to delamination-type failures at loads below what is required for in-plane failures. A general plot of the stresses is shown in Figure 1-6 where the y face is the free surface. The values of τ_{xy} and σ_y are at their CLT value outside of the boundary layer region and become zero at the free edge. σ_z and τ_{xz} are zero until the bondary layer, and attain their maximum value at the free edge. Many exact solutions indicate a singularity at the free edge for these values, although a finite value in reality must be reached there. The value of τ_{yz} reaches a maximum within the boundary layer, but returns to zero at the free edge. The magnitude of the interlaminar stresses are of significant magnitude and can not be neglected.

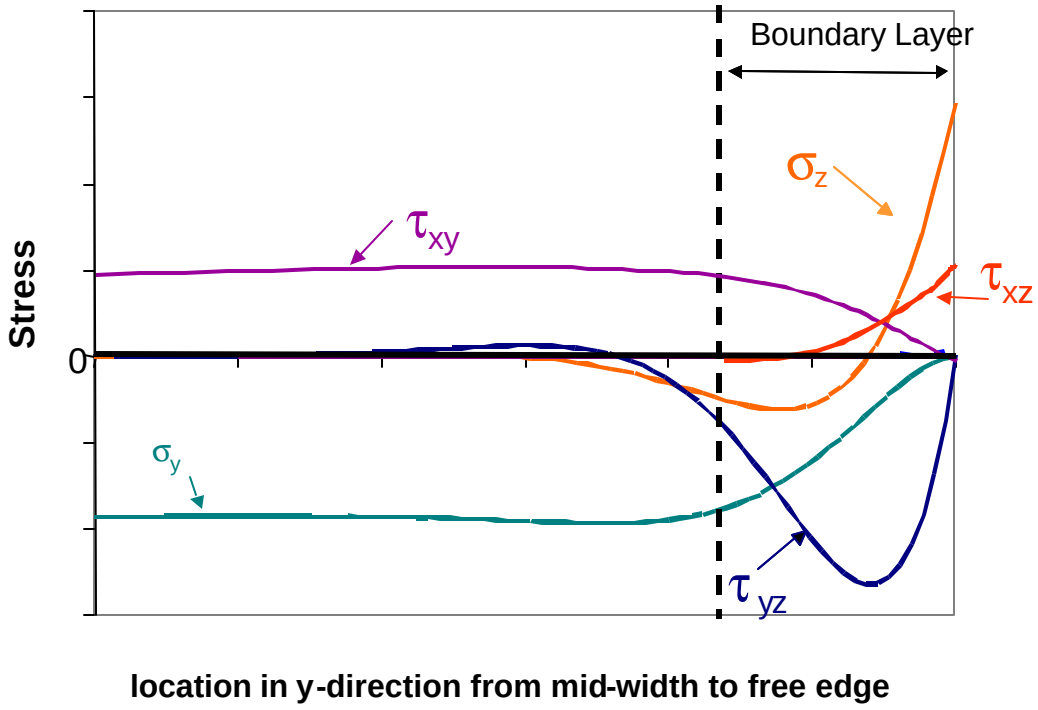

Figure 1- 6: Distribution of stresses at the free edge

The interlaminar stresses are caused by material property mismatch in adjacent layers and non-continuous stress components between plies. Interlaminar shear (τ_{yz}) and normal (σ_z) results from a Poisson ratio mismatch. The coefficients of mutual influence quantify the axial shear coupling in off-axis laminae ($h_{xy,x} = g_{xy} / e_x$). A mismatch between layers of these values can result in large values of the interlaminar shear stress τ_{xz}. The stacking sequence is also influential to the magnitude and type of stresses developed. [27] Herakovich [28] examined the influence of the material property mismatch for adjacent ($\pm q$) layer combinations. From this analytical and experimental study, interlaminar shear stresses are primarily a function of the coefficient of mutual influence mismatch that can be ten times larger than the poisson ratio mismatch. The largest mismatch and therefore largest stresses are reached for laminates with orientations between ±10° and ±15°. The normal stresses are primarily dependent on the stacking sequence selected rather than the material properties. The special case of the cross ply laminate (0/90) results in the interfacial shear stress being zero and delamination resulting only from σ_z.

1.3.2.2 Interlaminar Boundary Layer Stresses

Quantification of the stresses developed in the "free edge problem" was first done by Pipes and Pagano. Following their initial work, several Finite Element solutions and experimental studies were conducted to understand the influence of the free surface. The delamination failure resulting from the interlaminar stresses and methods to predict this failure mode have also been investigated. A *chronological* look at the development of work in this area will be presented below.

The first solution by Pipes and Pagano (1970) [29] considers the response of a finite-width symmetric four layer laminate under tractions applied in the x-directions at the ends. The theory of elasticity is used to establish the relations for the solution and finite-difference techniques are used to solve the system. The results of this solution are most useful for giving an indication of how the shear transfer mechanism occurs in the laminate. The in-plane shear stress creates a moment that must be balanced over the boundary layer with the free edge interlaminar shear stress. Since the distance the interlaminar stress acts over is small, the stress developed is significant and it appears that a singularity exists at the intersection of the interface and the free edge. The idea of a singularity existing at this intersection is also shown in work by Bogy [30] and Hess [31]. The numerical solution was completed for several geometries, and indicated that the interlaminar stress components quickly decay from the free edge. The boundary layer that the interlaminar stressed are confined to are approximately equal to the thickness of the laminate. Beyond this region, in-plane stress calculations using CLT are appropriate.

A second paper by Pagano and Pipes (1971) [32] focuses on the how delamination, namely the normal (σ_z) stress is influenced by the stacking sequence of a laminate. This work was encouraged by experimental results from Foye and Baker [33] on angle-ply ($\pm 15°$, ± 45) boron-epoxy laminates in different configurations resulted in a difference in strength of as much as 25,000 psi. Lamination theory yields the same in-plane stress levels for a symmetric laminate regardless of the sequence, indicating something else was influencing the onset of delamination. In conjunction with the assumptions for the shear transfer mechanism and ideas of equilibrium, the distribution of σ_z on a surface will be a

couple which that a gradient at the free edge which could be infinite, and depending on the width of the laminate, approach zero in the middle. Analysis of free body diagrams of the stress state show that by varying the stacking sequence, σ_z can change from tensile to compressive at the free edge. The interlaminar shear stresses are independent of the stacking arrangement, and were therefore considered minor contributors to delamination. The conclusions from this work were that the normal σ_z stresses are influential on differences in strength of the laminates.

The concepts presented in the finite difference solution and the influence of stacking sequence were confirmed in subsequent work by Rybicki [34]. The theorem of minimum complementary energy was used for the analysis. A finite element representation was used for the Maxwell stress functions. The obtained solution closely matched the interlaminar shear results from the Finite Difference solution by Pipes and Pagano. It also verified that a change in sign for σ_z can be accomplished by changing the stacking sequence. Several other finite element models have been used in solving this problem and look at mesh refinement and different types of elements at the free edge. [27, 35]

The 1972 paper by Pagano and Pipes [36] develops an approximate distribution and solution for the interlaminar stresses and report on experimental results to support their hypothesis. This method later became known as the Primitive Delamination Model [37]. Previous numerical solutions yielded a mathematical singularity at the free edge, encouraging an approximate stress analysis to be considered. A piece-wise linear distribution is then assumed for σ_z across the width of the laminate, shown in Figure 1-7. Since the resultant of the distribution is a couple, the areas under the curves can then be balanced, and a solution for the stress can be obtained. (It should be noted that there is an error in Ref. [36] and the correct form of the moment equation is shown in Ref [37]. There is also an error in the stress distribution figure in Ref [36], but it is properly shown in Ref [37] and in Figure 1-7 below)

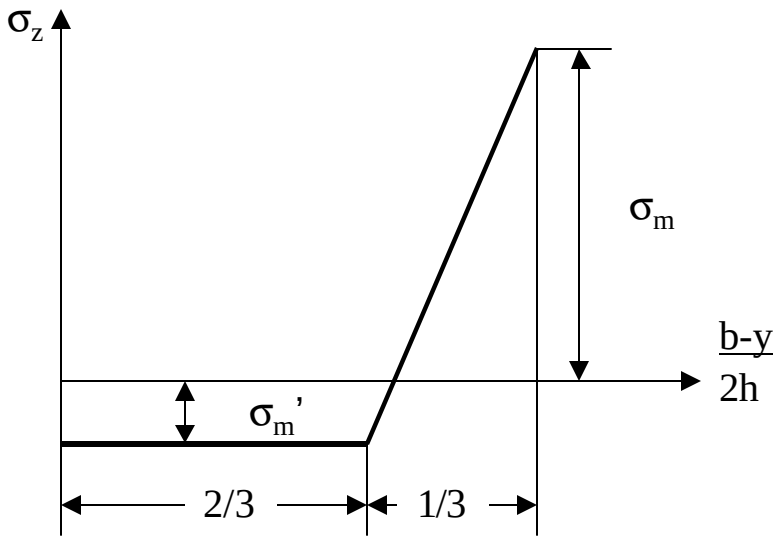

Figure 1- 7: Assumed linear stress distribution in the Primitive Delamination Model

Specimens were then designed which were considered susceptible to delamination. The stacking sequences were arranged so one laminate would have tensile values for the interlaminar normal stresses and one would be compressive. The predicted tensile σ_z specimen did in fact delaminate, whereas the compressive did not. Additional testing indicated that the crack did initiate at the point of predicted maximum σ_z, and the crack opened in a manner that made the cross section appear like a deformed double cantilever beam. Further confirmation of the approximations for σ_z and its influence on delamination was done by Whitney and Browning [38] who investigated (±45, 90) graphite-epoxy laminates. Delamination occurred for the predicted tensile interlaminar normal samples under both static and fatigue loading. Kim and Aoki [39] also used this method to predict the failure loads in quasi-static tests for laminates with stacking sequences of $(0/90_n/\pm45)$ and $(0/\pm45/90_n)$. The results matched well for n = 1 and 3, but a discrepancy existed when n = 6.

An approximate analytical elasticity solution (Pipes and Pagano, 1974) was then evaluated and agreed very well with the numerical finite difference solution. [40] The approximation was used to investigate the response of multi-layer layer laminates that

were computationally intense for the numerical solution. Evaluation of this solution for laminates of varying thickness confirmed that the boundary layer region is equal to the laminate thickness.

A global-local variational model was introduced in 1983 by Pagano and Soni [41] to further streamline the computation process. In this methodology, the laminate is divided into global and local regions. The region of interest is the "local" region wherein stresses are considered on a ply-level basis. The remaining plies are grouped together as a "global" region, over which the laminate properties are smeared. Matching conditions are then in place at the interface and stresses in critical plies can be computed for much larger structures. The model predicts well for stresses outside of the transition region.

Wang and Choi [42,43] used an eigenvalue approach to the problem and confirmed that the singularity at the free edge of the laminate controls the response in the boundary layer region. They also concluded that the boundary-layer width is dependent on the lamination and geometric variables, loading and environmental conditions. Their solution allows for asymmetric lamiates to be considered under various loading conditions, beyond the axial tension considered in the previous models.

The accuracy of finite element models and the idea of a singularity at the interface and the free edge was looked at experimentally by Herakovich *et. al* [44] in 1985. Moiré interferometry was used to characterize the out-of-plane shear strain γ_{xz} at the free edge. The results showed that the shear strains on the free edge are in fact finite; and the ratio of the strain did not exceed a ratio of 7.5 when compared to the applied strain. Comparison of the moiré results to finite element results suggest that a four-node isoperimetric rectangular element mesh yields the best results.

In order to analyze thick laminates, Kassapoglou and Lagace [45, 46,47] presented an efficient method to evaluate the stresses for symmetric laminates under uniaxial and thermal loading. The method is based on assumed stress shapes and is optimized by minimizing the complementary energy of the entire laminate. The solutions compared

well with previous solutions completed using finite element analysis and convergence to the solution was attained for up to 100 plies in under 70 iterations. This model was then expanded to a more general loading case by Lin and Hsu [48].

Based on the minimization of complementary approach, Kassapoglou [49] presented a closed form solution, that employs variational calculus approach to determine the functional form of the stress shapes. Yin [50] used a similar but simplified variational approach to approximate the interlaminar stresses at the free edge. (The Lekhnitskii stress functions are used along the interfaces.) The method is simple and demonstrated satisfactory agreement for cross-ply and angle-ply laminates.

1.3.2.3 Delamination and Crack Growth

Knowledge of analysis techniques for the free edge stresses allows for delamination initiation and the crack growth that follows to be investigated. An understanding of these phenomenon is important in predicting when failure occurs in the beams. An overview of the literature in this area will be presented in the following section.

O'Brien has done extensive work in determining the effects on the fatigue life of a laminate once delamination initiates. [51-54]. A delamination at the free edge or within the matrix, results in isolation of a ply and inhibits its ability to carry load, thus changing modulus and load distribution of the entire laminate. This effect was seen both under quasi-static loading to failure and under tension-tension fatigue. A rule of mixtures approach was suggested to understand the influence of delamination and crack length on the change in modulus of the laminate. Such an approach resulted in the laminate modulus decreases linearly with delamination size.

O'Brien characterized the onset of delamination and then the crack growth which follows using fracture mechanics. The strain energy release rate, G, was found to be dependent on the in-plane strain, laminate thickness and the modulus before and after delamination. Using a finite element model, a critical value for G can be attained and used as a prediction for delamination. Crack growth can then be found using a different value for

G which accounts for the region that has delaminated. The value of *G* is dependent on the stacking sequence of the laminate and there is also an indication that delamination is the result of both opening and shear modes. The disadvantage of such a model is that it is extremely sensitive to uncertainties in the applied load and due to the multiple load paths available in a composite, and failure may not be as catastrophic as would be predicted.

In order to justify the use of strain energy release rate, O'Brien and Hooper conducted studies to better understand how matrix cracks can influence delamination (Ref 52 and 53). Tension tests were conducted on $(0_2/q_2/-q_2)$ graphite/epoxy laminates and a quasi-3D finite element analysis was conducted to calculate the stresses. Experimentally it was shown that matrix cracking in the central $-q$ resulted in local delamination onset in the $q/-q$ interface at the intersection of the matrix crack and the free edge. The finite element model indicated that in-plane stresses may not be capable of properly predicting these matrix cracks, since they represent the minimum values in the interior of the laminate. Fatigue testing indicated that for constant amplitude tension tests, matrix cracking in the central plies always preceded the onset of delamination. Additionally, calculations show that the strain energy release rate for local delamination exceeded that of edge delamination. This suggests that delaminations from matrix cracks would initiate prior to edge delamination.

Strain energy release rates were also considered by Rybicki *et. al* [55]. Ultrasonic pulse-echo methods were used to measure crack propagation during the test. Energy release rates were calculated using a finite element model for specific amount of delamination. The study did indicate that the method predicted stable crack growth and was an accurate methodology.

Prediction of delamination based on stress type criterions has also been investigated. Initial work in this area was done by Kim and Soni [20] in 1983. The criterion used was essentially a maximum stress criterion, assuming that σ_z is solely responsible for the failure. The transverse strength of the laminate was used as the interlaminar strength of the material, and the stresses were calculated using the global-local model. Several

laminates were loaded and acoustic emission techniques were used to quantify when delamination occurred. When a maximum point stress at the free edge was used to predict failure, the results were very conservative. Averaging the stress value over a distance from the free edge equal to the ply thickness gave a good prediction to the onset of delamination.

A maximum stress criterion approach was also used by Kim and Aoki [39] for $(0/90_n/\pm45)$ and $(0/\pm45/90_n)$ quasi-isotropic laminates. As previously mentioned in the discussion on interlaminar stresses, the Primitive Delamination Model was used to predict the failure well for $n = 1$ and 3, but a discrepancy existed when $n = 6$. Their experimental study also looked at crack density and growth in the laminates. They found that with increasing layer thickness, crack density decreases, but cracks extends at lower stresses and fatigue cycles and will continually grow versus arresting for a period of time as seen in the thinner laminates. They also concluded that delamination is controlled by a combination of tensile interlaminar normal stresses and the size of a transverse crack.

A quadratic delamination criterion was proposed by Brewer and Lagace [56]. Similar to Kim and Soni, an average stress at the free edge is used to avoid the effects of a stress singularity. The length to average over is experimentally determined, and found to differ slightly from the ply thickness but appears to be a property of the material. The criterion only considers out-of-plane stresses and assumes failure is independent of the sign on the shear stress. No interaction terms are present, but the difference in compressive and tensile normal strengths is accounted for. As with other criterions of this nature, attaining the appropriate out-of-plane strengths is a complication to the method. Experimental testing resulted in delamination between plies of different angular orientation prior to any transverse cracking. The criterion could be correlated to the tests and data in the literature. This prediction appeared to be more consistent than the strain energy release rate methodology proposed by O'Brien which also requires a finite element analysis to determine G_c.

A modified Tsai-Wu criterion has been proposed by Naik *et. al* [57] to try to characterize failure under combined loading. The assumption in the criteria is that only interlaminar stresses interact to influence interlaminar failure; and are therefore decoupled from in-plane stresses. This proposed criteria was then compared with other interactive criteria by Greszczuk, Sun and Hashin. The samples under combined compression and shear indicated an increase in shear strength for small values of transverse compression. The modified Tsai-Wu and Sun criteria predicted this well, whereas the Greszczuk and Hashin criteria under predicted the strengths.

CHAPTER 2: EXPERIMENTAL PROCEDURE AND RESULTS

2.1 Experimental Overview

In order to understand the fatigue characteristics of the entire bridge, the beam level characteristics must too be understood. In order to do this, full-scale static and fatigue tests were run at a 4.27 m (14 ft) span, similar to the bridge. The stiffness response of the beam under four-point bend mechanical loading was monitored for the two different beam batches. Four beams were tested in fatigue in an effort to create an S-N curve for the beam.

2.1.1 Hybrid Beam Static Test to Failure

The maximum moment capacity of the beam was determined based on static load to failure tests completed on beams as discussed in Chapter 1. The average results of the 3 sets of test run have been included again in Table 2- 1 for convenience with the A and B allowable values as described in the Strongwell Extren DWB^{TM} Design Guide [13].

Table 2- 1: Results of Static Tests to Failure on Hybrid Beams

	Stiffness			**Failure Moment**		
	Mean GPa (Msi)	A-Allow GPa (Msi)	B-Allow GPa (Msi)	Mean kN-m (kip-ft)	A-Allow kN-m (kip-ft)	B-Allow kN-m (kip-ft)
400 Series 8'	43.3 (6.28)	39.0 (5.66)	41.2 (5.97)	129.2 (95.3)	65.3 (48.2)	91.6 (67.6)
400 Series 14'	42.8 (6.21)	40.7 (5.90)	41.7 (6.05)	139.0 (102.5)	89.7 (66.2)	112 (82.4)
500 Series 20'	45.8 (6.21)	40.8 (5.92)	43.2 (6.27)	100.6 (74.2)	48.9 (36.1)	70.0 (51.6)

2.2 Hybrid Beam Bending Fatigue Test

2.2.1 Test Setup

The fatigue test selected was a four-point bend test loaded at 1/3 points. This test configuration was similar to the quasi-static tests and simplifies the analysis due to the constant moment region [13]. The test configuration can be seen in Figure 2- 1.

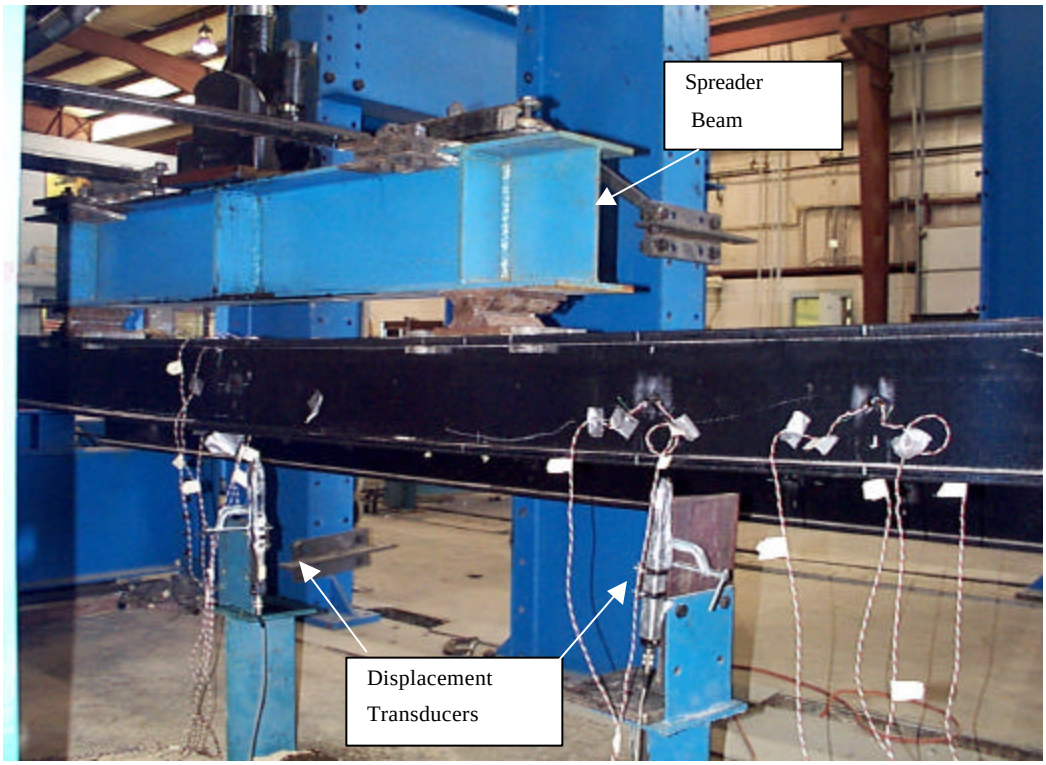

Figure 2- 1: Four Point Bend Fatigue Test

The data collected from the test was predominately to monitor stiffness reduction throughout the test, and ensure there was no torsional loading on the beam. The data was collected using the MEGADAC 3108 data acquisition system, which allows for 200 scans/second/channel. The data collected was:

1. Actuator Load
2. Actuator Deflection
3. Mid-span Deflection
4. Quarter Point Deflection
5. Top Center Bending Strain
6. Top Right Bending Strain

7. Top Left Bending Strain
8. Top Right Flange Bending Strain
9. Top Left Flange Bending Strain
10. Bottom Center Bending Strain
11. Shear Strain 1" outside of the constant moment region
12. Torsional Strain at the ¼ point.

The loading and gage locations are shown in Figure 2- 2

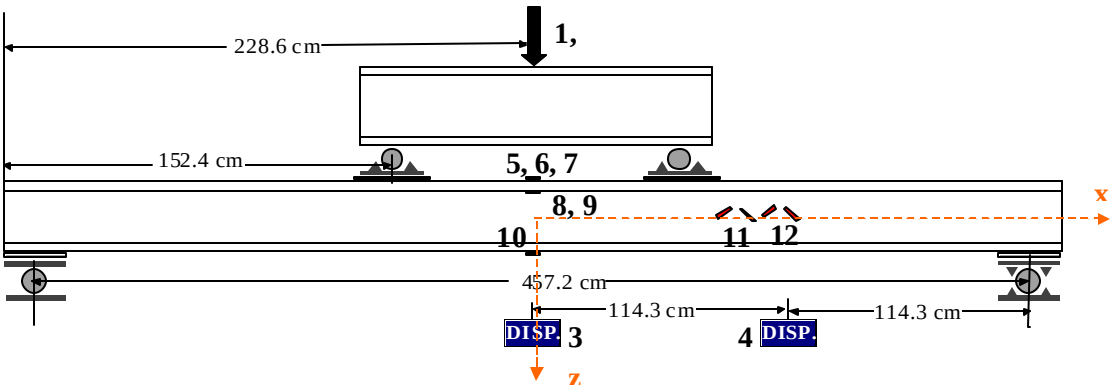

Figure 2- 2: Schematic of fatigue test set up

The loads applied were based on the moment capacity found in the static tests discussed above. Two batches of beams were tested, the 400 series and the 500 series. The 400 series beams had a higher average ultimate moment and lower average stiffness values than the 500 series beams. Four beams were subjected to the fatigue loading, two from each batch. These loads are at approximately 9 times the actual loading the bridge beams will see in service at the Tom's Creek Bridge [6]. The testing matrix comparing the loading to the ultimate moment and strains at failure is show in Table 2- 2 . The loading is compared to the batch properties and also to an overall average of both batches.

Table 2- 2: Test matrix of beams subjected to fatigue loading

	Actuator Load kN (kips)	Applied Moment kN-m (kip-ft)	% M_{ult} Batch A-Allow B-Allow	% M_{ult} Average	Top Strain ($\mu\varepsilon$)	% $\varepsilon_{failure}$ Batch	% $\varepsilon_{failure}$ Average
Beam 425	71 (16)	50.6 (37.3)	36% 56% 45%	42%	2824	37%	43%
Beam 421	89 (20)	63.3 (46.7)	45% 71% 57%	53%	2277	46%	54%
Beam 514	89 (20)	63.3 (46.7)	63% 129% 91%	53%	2664	62%	51%
Beam 517	120 (27)	85.4 (63.0)	85% 175% 122%	71%	3689	86%	70%

The tests were run in load control, using an MTS controller. The R-ratio (min load/ max load) was desired to be 0.1. In actuality, due to the large deflections, the pump controlled the load ratios and speed of the test; the maximum and minimum actuator loads and the frequencies are summarized in Table 2- 3. These values were consistently held throughout the test.

Table 2- 3: Fatigue test conditions for each beam

	Max Actuator Load (lbs)	Min Actuator Load (lbs)	R-Ratio (Min/Max)	Frequency (Hz)
Beam 425	16,000	1720	0.11	0.85
Beam 421	20,100	1300	0.06	0.60
Beam 514	20,010	2700	0.13	0.82
Beam 517	27,085	7500	0.28	0.70

Periodic quasi-static tests were completed on the beams and the strains and deflections listed above were collected. The load was applied in displacement control up to the maximum load of the respective test. From the data, stiffness values could be calculated and the influence of cyclic loading on the system analyzed. The data analysis procedures are outlined below.

2.2.2 Data Analysis

As the beam undergoes fatigue, there is a reduction in stiffness, and a related shift in the neutral axis. Modulus values were calculated using top and bottom strain values and also deflection data. Comparison of these values allows for the shear influence and neutral axis shift to be quantified.

Mid-span top and bottom strain values were used to determine the modulus based on beam theory, Equation 2-1.

$$E_{strain} = \frac{Mc}{Ie} \tag{2-1}$$

In this expression, M is the moment in the constant moment region, the moment of inertia is $I = I_{zz} = 5328$ cm^4 (128.5 in^4) and e is the gage reading at the top or bottom of the beam. The value of c is taken as either the distance from the section mid-plane to the gage or the distance from the neutral axis to the beam. Using the mid-plane as the reference point will result in different values of E in the top and bottom flange, showing how each are independently influenced by the loading. To determine an overall effective modulus of the beam, the value of c is used as the distance from the neutral axis of the beam to the gage. The location of the neutral axis was simply found as the intercept of the line connecting top and bottom strain values.

The modulus was also calculated using the mid-span deflection value. This calculation includes the influence of shear deformation and results in a lower modulus value than when calculated based on strain alone:

$$E_{deflection} = \frac{M}{2Iy}\left(\frac{L^2}{4} - \frac{L^2}{2} + \frac{a^2}{3}\right) \quad (2\text{-}2)$$

In Equation 2-2, M is the moment, $I=I_{zz}=$ 5328 cm^4 (128.5 in^4) and y is the measured deflection value under the maximum load. L represents the length of the beam, and a is the distance from the load point to the support.

From the modulus values, calculated using strain and deflection, KGA is calculated. The KGA term is from shear deformable beam theory (Timoshenko). The predicted deflection without shear can be found as:

$$y_{strain} = \frac{M}{2E_{strain}I}\left(\frac{L^2}{4} - \frac{L^2}{2} + \frac{a^2}{3}\right) \quad (2\text{-}3)$$

The measured deflection is a combination of this value and the shear contribution:

$$y_{measured} = y_{shear} + y_{strain} \quad (2\text{-}4)$$

Equation 2-4 can be solved for the y_{shear}, based on the known deflection ($y_{measured}$). KGA is then found from Equation 2-5, where P is the actuator load, and L is the length of the beam.

$$y_{shear} = \frac{PL}{8\,KGA} \quad (2\text{-}5)$$

2.3 Results

The initial stiffness properties and neutral axis location for the beams tested are summarized in Table 2-4 The data collected for each beams is shown and discussed in detail below. In the plots of data for each beam, the lines connecting the data are used to demonstrate a trend between data points, and are in no way a prediction of the actual response of the beam under loading. The error bars shown on the modulus plots are

conservative and account for error all of the inputs into the respective stiffness calculation.

Table 2- 4 : Intial Properties of tested beams and batch data

	Initial Properties			Batch Properties	
	Modulus Deflection GPa (Msi)	Modulus Strain GPa (Msi)	NA Location From Bottom cm (in)	Beam Modulus GPa (Msi)	NA Location cm (in)
Beam 421	39.5 (5.74)	42.9 (6.23)	10.0 (3.94)	42.8 (6.21)	10.2 (4.03)
Beam 425	39.9 (5.79)	43.5 (6.31)	9.78 (3.85)		
Beam 514	42.0 (6.09)	47.1 (6.83)	9.73 (3.83)	45.8 (6.64)	10.1 (3.98)
Beam 517	39.6 (5.74)	44.1 (6.39)	10.0 (3.95)		

2.3.1 Test Results at 45% of M_{ult}

The first beam tested was beam 421 at 45% of the average ultimate load of its batch. The beam failed after 130,000 cycles. The failure mode was delamination of the top flange in the constant moment region (Figure 2- 3) and was located at the carbon-glass interface. This served as an initial verification that the fatigue failure mode is the same as that of quasi-static failure.

Very little stiffness reduction is evident prior to beam failure, shown in Figure 2- 4. After delamination, the beam remained capable of carrying load, and about 60% of the stiffness was retained. The bottom (tensile) flange calculation indicates a higher modulus value than the compression side, possibly because the carbon acts stiffer in tension than in compression. The modulus found from deflection is about 7% lower than the strain values, indicating there are shear contributions at this load and span. Because of the top

and bottom modulus mismatch, the neutral axis was initially offset below the midplane (Figure 2- 5). The plot also indicates that after delamination there is a significant shift in the neutral axis away from the failed flange. Similar to the other data trends for this beam, the mid-span deflection is constant until delamination, and then increases significantly thereafter (Figure 2- 6). The deflection values shown are normalized by dividing the deflection value by the load, and multiplying by the maximum desired load of 89 kN (20 kips)

Figure 2- 3: Delamination failure of Beam #421 after 130,000 cycles, at 47% of the ultimate moment.

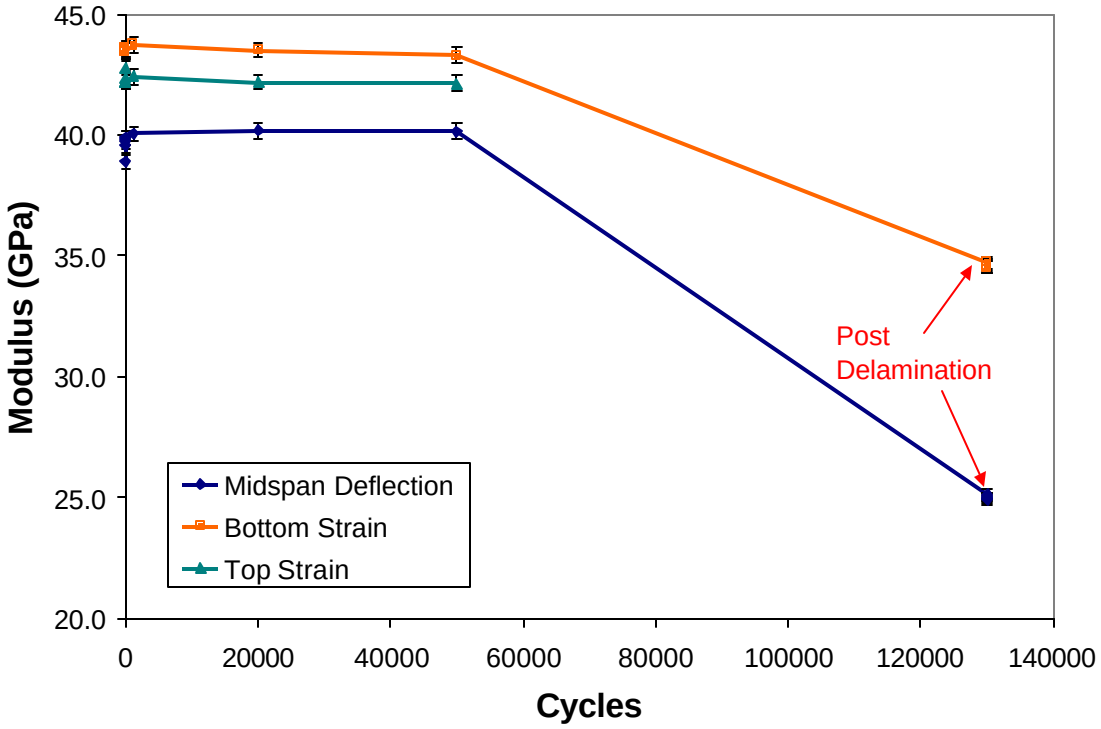

Figure 2- 4: Modulus Reduction of Beam #421, loaded to 45% of the Ultimate Moment

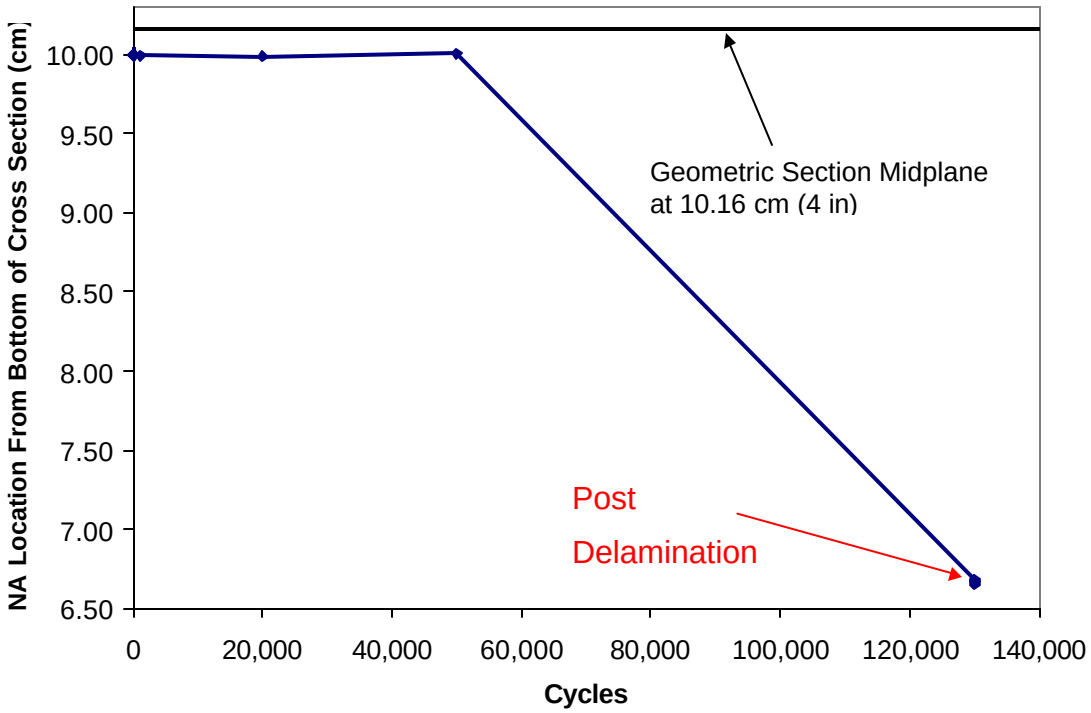

Figure 2- 5: Neutral Axis location of Beam #421, loaded to 45% of the Ultimate Moment

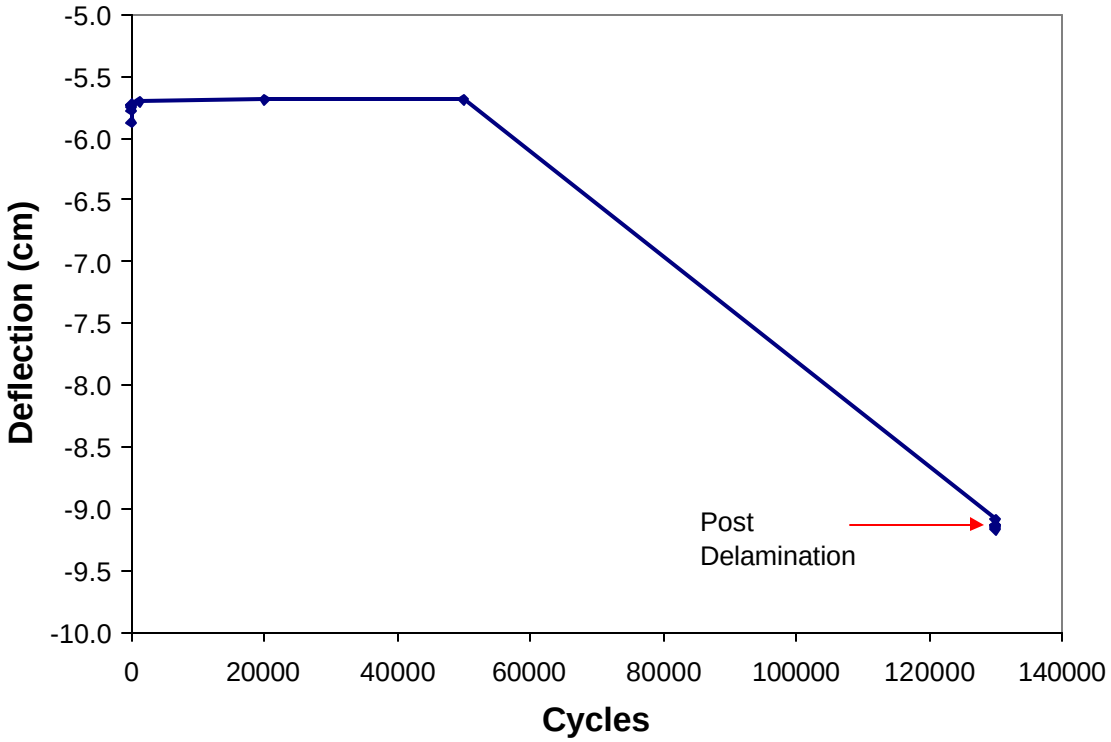

Figure 2- 6: Mid-span deflection of Beam #421, loaded to 45% of the Ultimate Moment

2.3.2 Test Results at 36% of M_{ult}

The low number of cycles to failure of the first beam suggested a lower load be used for second test. Beam #425 was then tested at 36 % of the average ultimate moment of the batch. In this case, the beam did not fail and was removed after 10 million cycles. As in the previous test, the tensile flange had a higher stiffness value than the compression flange. This difference was higher than before, resulting in a larger neutral axis shift (Figure 2- 7 and Figure 2- 8). Some initial degradation in stiffness was noted at the very beginning of the test, following this, it appears that the data flattens out. There is a stiffness increase in the data around 2 million cycles, at this point the load cell was replaced, and this shift coincides with the load cell replacement. Additionally at 3.5 million cycles the load frame was moved which resulted in another shift in the data. Based on the data from the beams after this test, it is assumed that the stiffness remained constant after the initial degradation. The deflection data followed the same trend, but is not included here.

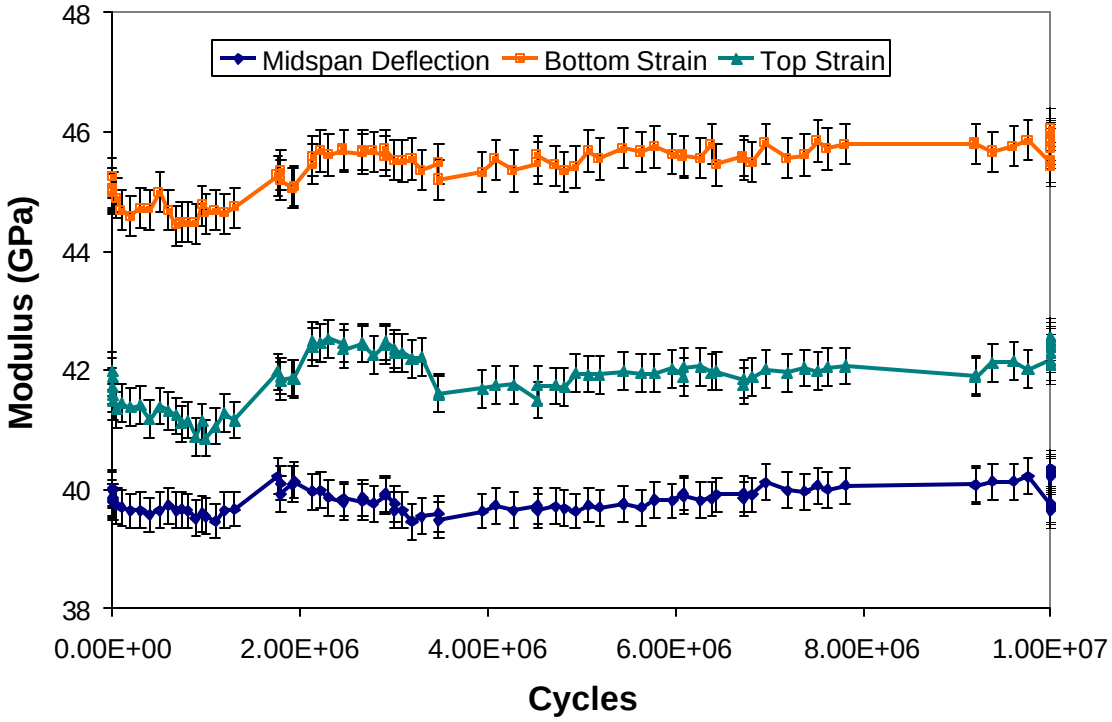

Figure 2- 7: Modulus Reduction of Beam #425, loaded to 36% of the Ultimate Moment

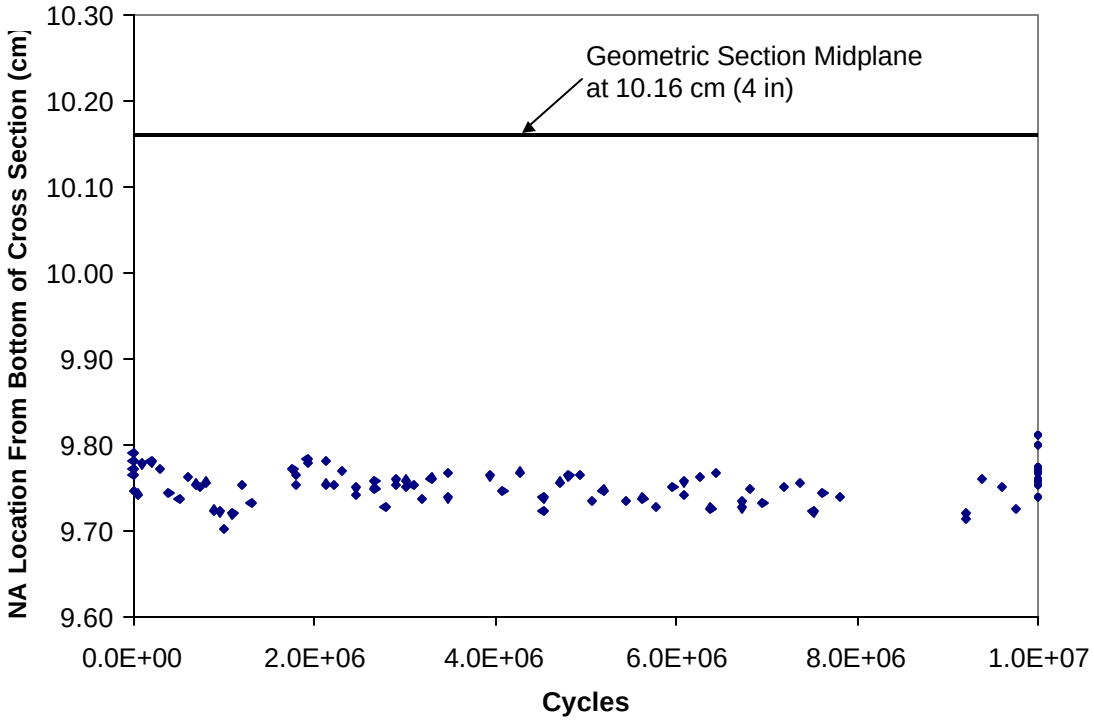

Figure 2- 8: Neutral Axis location of Beam #425, loaded to 36% of the Ultimate Moment

2.3.3 Test Results at 63% of M_{ult}

To understand if stiffness or moment capacity dominated the response of the beams, the next test was at the same applied actuator load as the first test, for a beam from the second batch. Beam #514 was loaded at 63% of the average ultimate moment of the batch. The initial 2% stiffness degradation and was captured well in this data as shown in Figure 2- 9, and is notably higher than in the 400 series beams. The loss in stiffness appears to be constrained to the first 90,000 cycles. It appears that the overall stiffness reduction is controlled by the tensile flange, as it correlates best with the stiffness trend shown by the deflection calculations. Initially, the neutral axis is located closer to the tensile flange. As the stiffness is reduced, there is a neutral axis shift away from the tensile flange, toward the compression side, which maintains its initial properties (Figure 2- 10). After this initial stage, the modulus values and neutral axis locations appear to remain constant. The deflection of the beam was normalized, as discussed above, and underwent a 0.35 cm (0.14 in) increase in deflection over the duration of the test (Figure 2- 11).

The beam was stopped after 7,600,000 cycles, to allow another beam to be tested. Additionally, it appeared to be exhibiting similar trends with the beam from the 400 series. After the beam was removed, there was residual camber deformation in the beam. At midspan the deflection was measured by stretching a string tight from the two endpoints and measuring the distance from the string to the beam. The beam was turned on its side to ensure the weight effects were not included in the measurement. The deflection was roughly 0.5 cm (0.2 in).

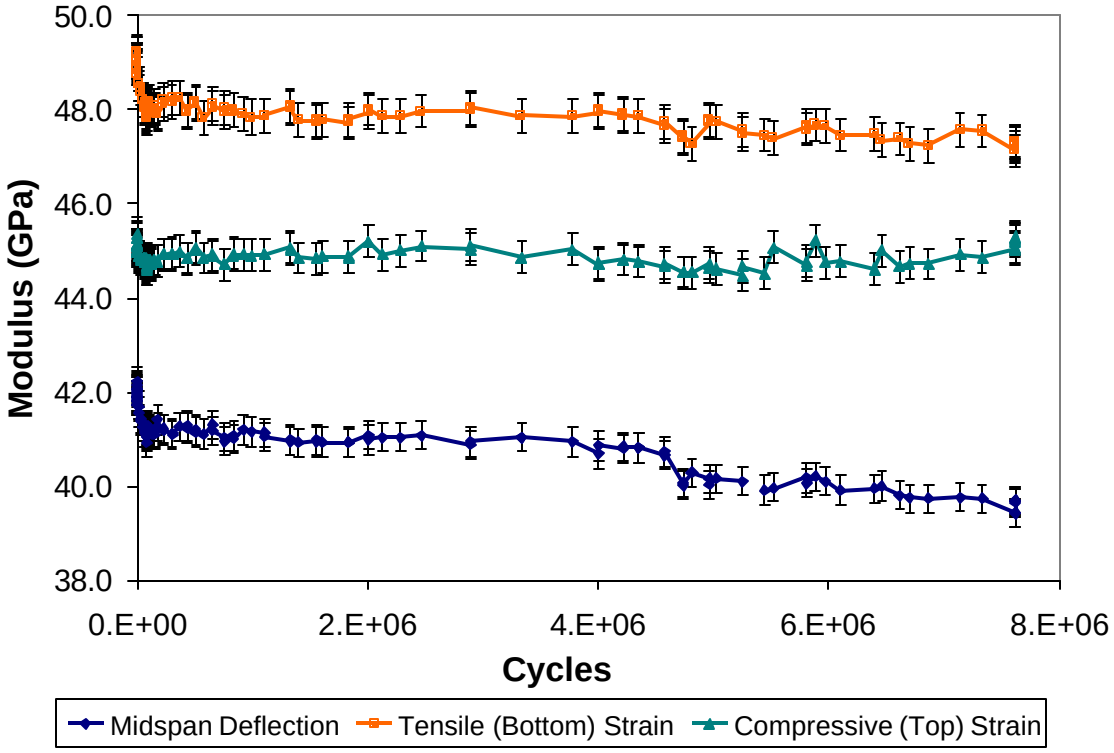

Figure 2- 9: Modulus Reduction of Beam #514, loaded to 63% of the Ultimate Moment

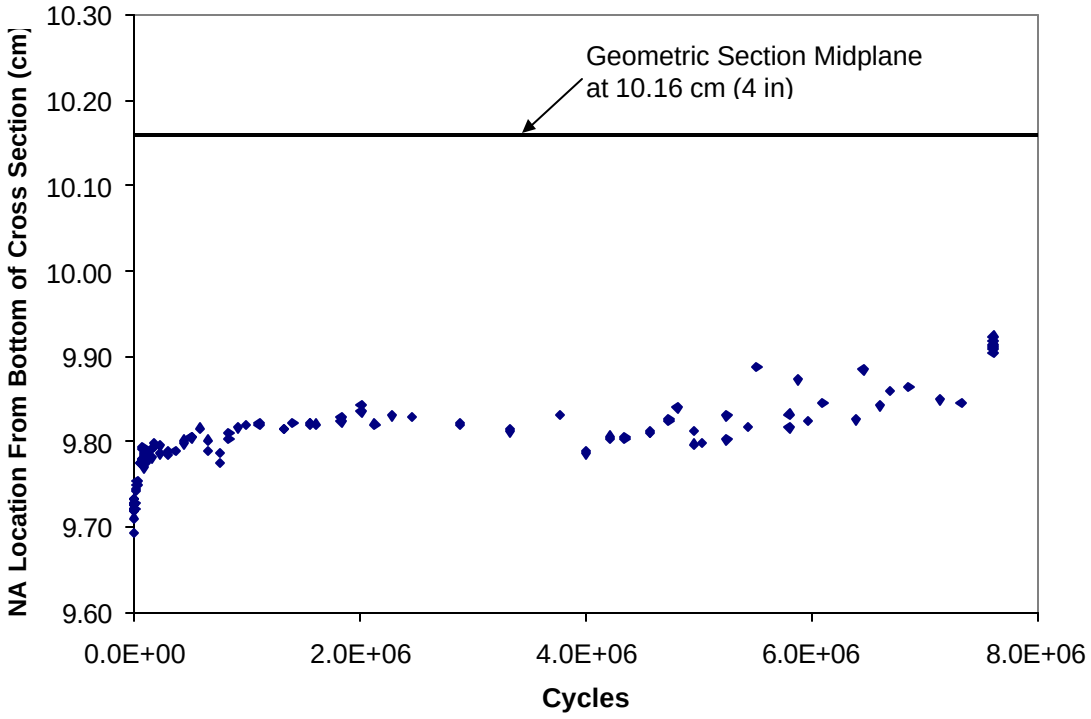

Figure 2- 10: Neutral Axis location of Beam #514, loaded to 63% of the Ultimate Moment

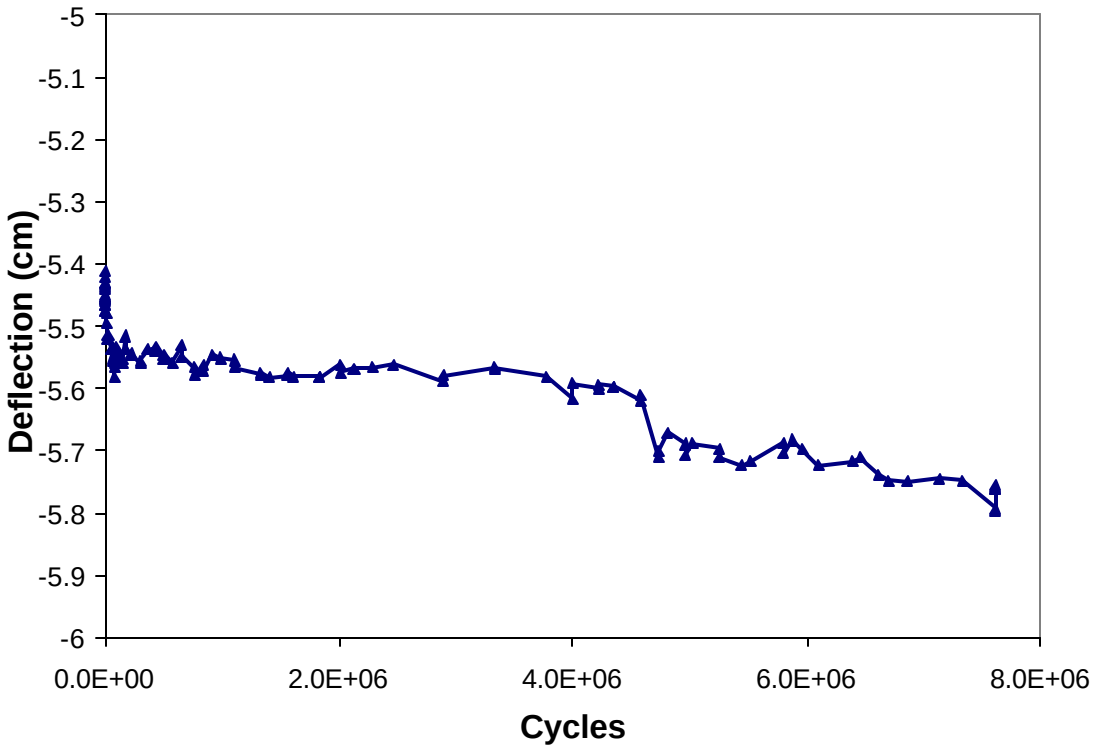

Figure 2- 11: Normalized mid-span deflection of Beam #514, loaded to 63% of the Ultimate Moment

2.3.4 Test Results at 82% of M_{ult}

A second beam from the 500 series was tested at 82% of M_{ult}. The beam failed by top flange delamination after 370,000 cycles. The delamination occurred during fatigue loading, and the initiation of the crack could be heard. The failure appears to have originated under the loading point, seen in Figure 2- 12. The crack then propagated along a single interface in the constant moment region. The location of the crack, shown in Figure 2- 13, seems to coincide with the location of the carbon-glass interface. The crack was on both sides of the beam, but it was not apparent if it was through the entire thickness of the beam. The beam was loaded up to the same maximum test load after the crack initiated. Further cracking could be heard, although no further crack growth was witnessed.

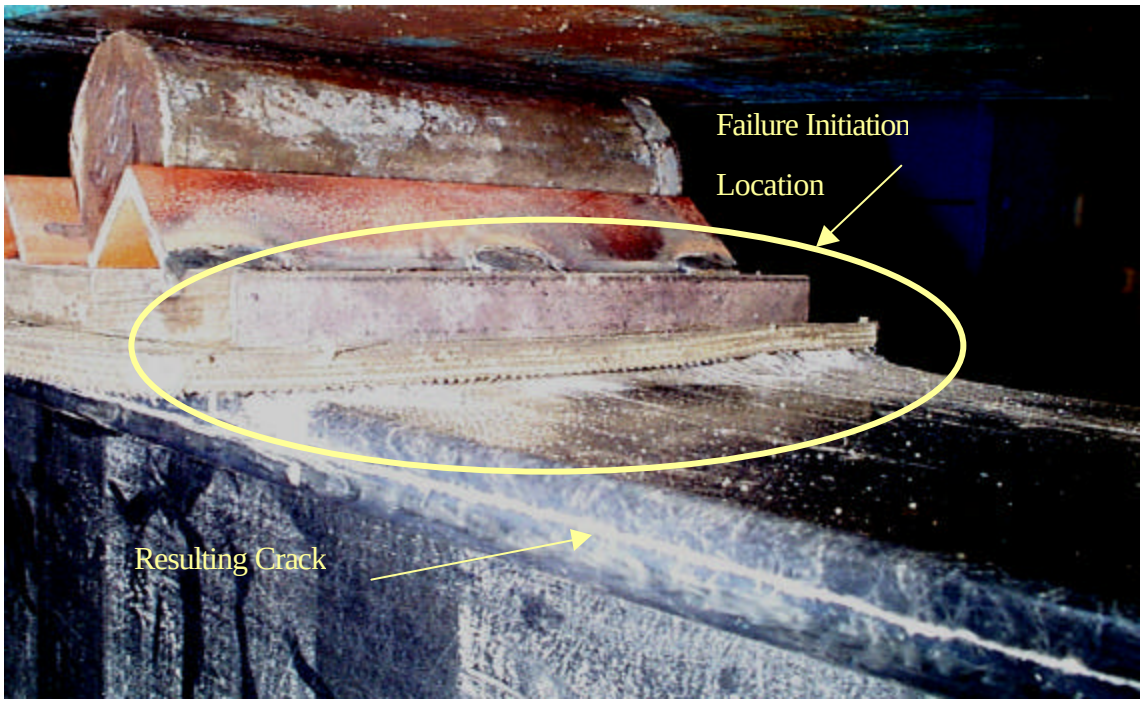

Figure 2- 12: Failure under load point for Beam #517 after 370,000 cycles at 82% of the ultimate load

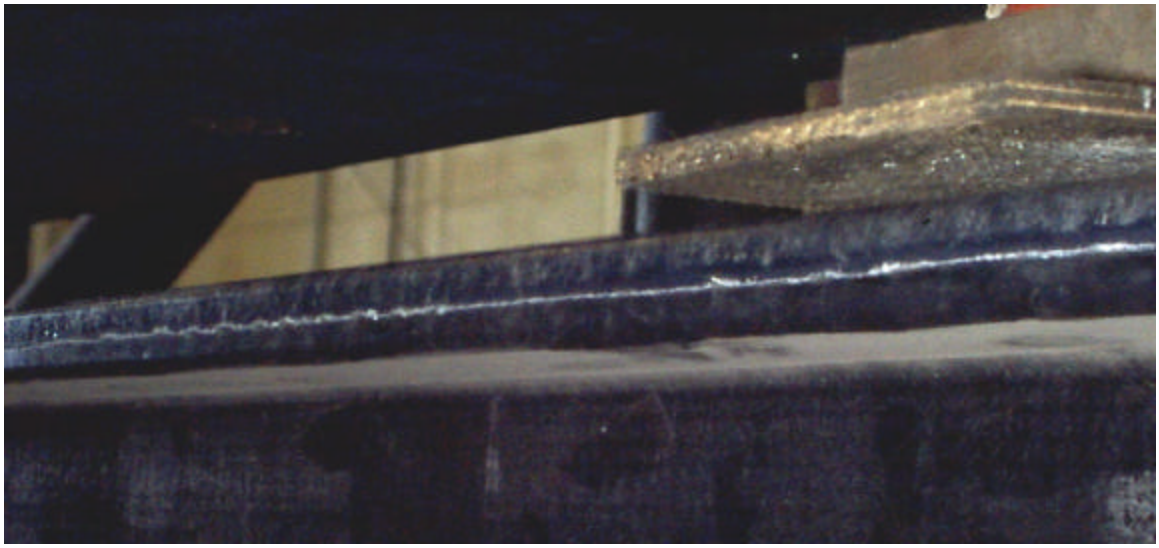

Figure 2- 13: Crack resulting from delamination of the top flange

Similar to Beam #514, the initial stiffness loss was just under 2%, but occurred within the first 10,000 cycles, rather than 90,000 cycles at 63% of the ultimate load. Figure 2- 14 shows this and the second drop in stiffness prior to delamination, after which 80% of the stiffness was maintained. The beam was still capable of carrying the same test load level after delamination. The neutral axis location and deflection plots are Figure 2- 15 and Figure 2- 16 respectively. The anticipated trend is followed for each plot. Once again the tension flange controls the stiffness, and the neutral axis is shifted toward the compression flange until the crack occurs.

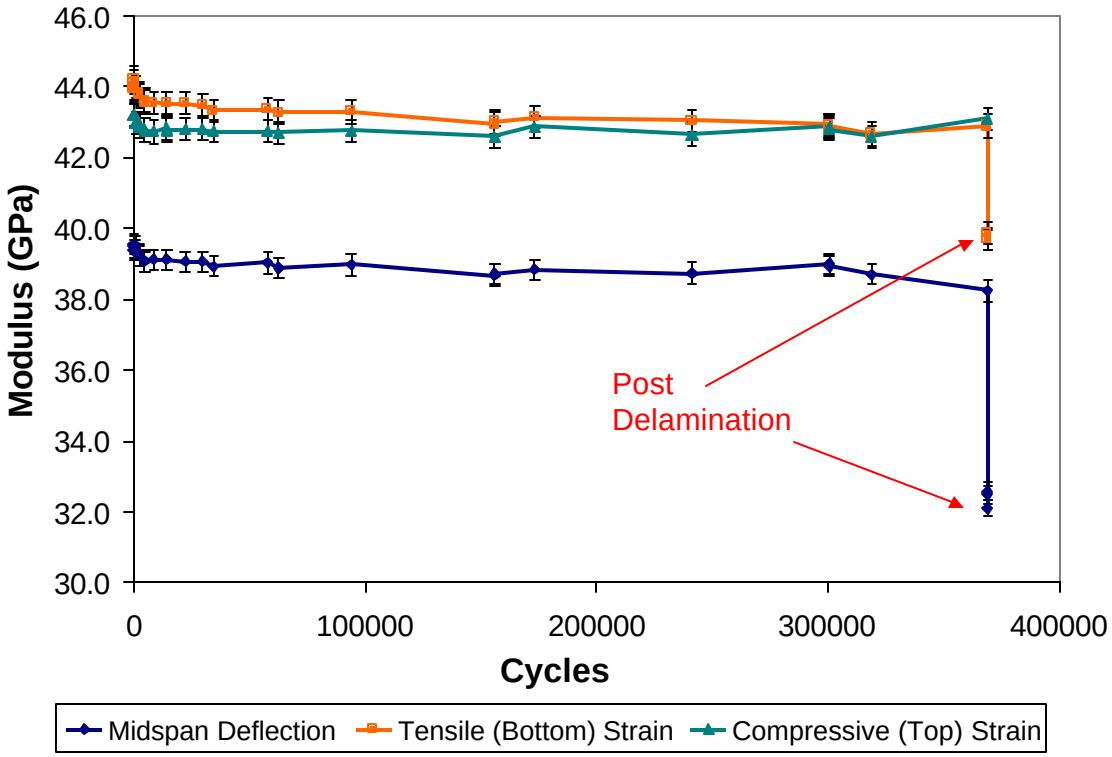

Figure 2- 14: Modulus Reduction of Beam #517, loaded to 82% of the Ultimate Moment

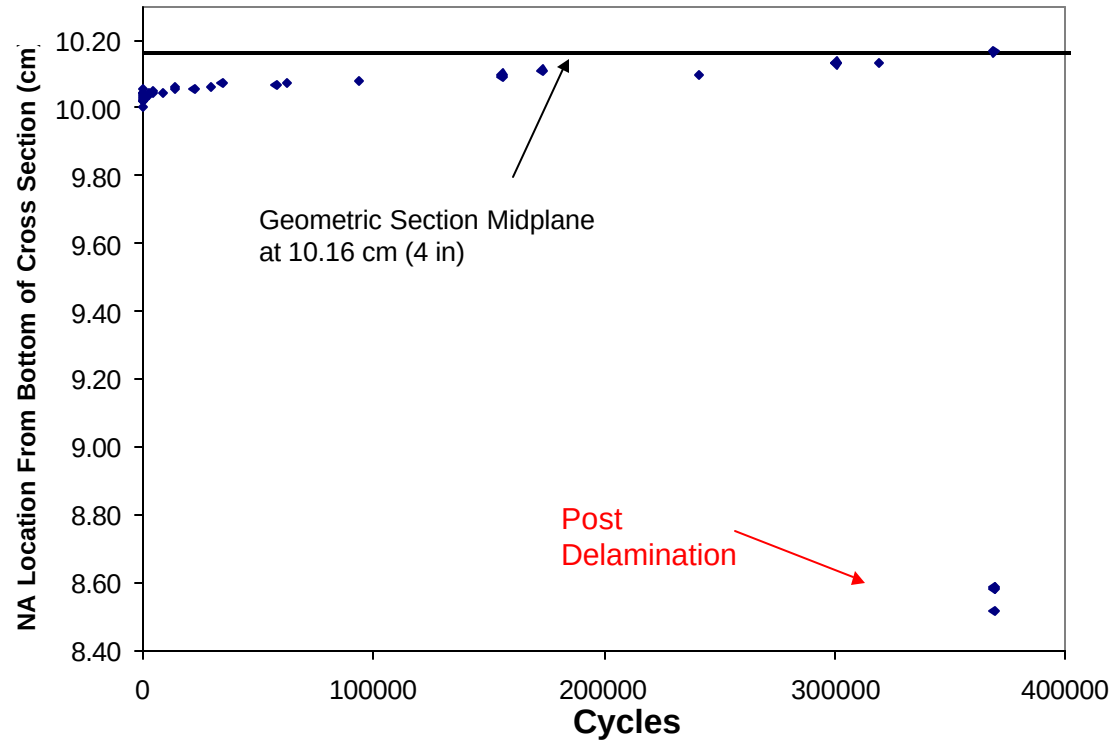

Figure 2- 15: Neutral Axis location of Beam #517, loaded to 82% of the Ultimate Moment

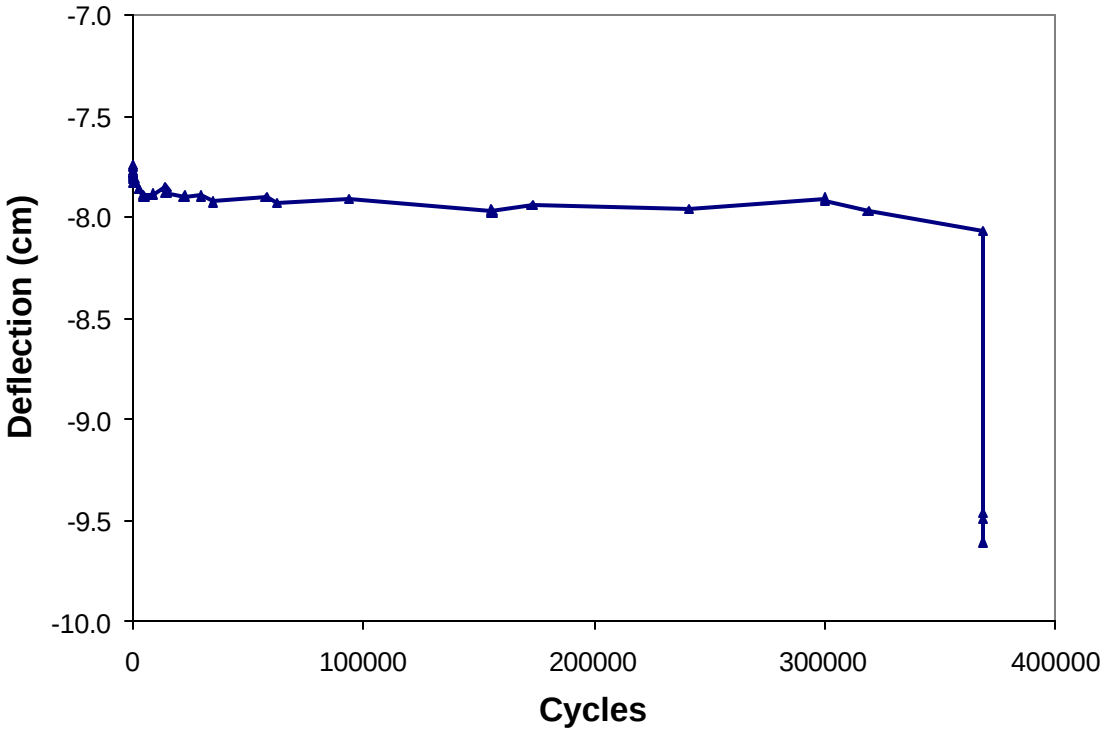

Figure 2- 16: Normalized mid-span deflection of Beam #517, loaded to 82% of the Ultimate Moment

2.3.5 Summary of Test Results

The test results confirm that the fatigue failure mode is the same as had been seen in quasi-static four point bend tests, delamination of the top flange. Following this failure, the structure remains capable of carrying load, and retains between 60% and 80% of the initial stiffness. There is an initial 2% stiffness reduction in the beams, after the reduction, the modulus remains constant up to failure. The amount of stiffness reduction was independent of load, although the speed of the degradation was load dependent. The number of cycles for each beam is summarized in Table 2-5.

Table 2- 5 : Summary of fatigue test results

	% M_{ult} Batch	% M_{ult} Average	% $\varepsilon_{failure}$ Batch	% $\varepsilon_{failure}$ Average	Total Cycles
Beam 425	36%	42%	37%	43%	10,000,000 Runout
Beam 421	45%	53%	46%	51%	130,000 Failed
Beam 514	63%	53%	62%	51%	7,600,000 Runout
Beam 517	85%	71%	86%	70%	370,000 Failed

The two tests run at the same actuator load of 89 kN (20 kips) from the two different batches indicated a significant difference in fatigue life. The 1.5 order of magnitude fatigue life difference cannot be fully explained, but is consistent with the idea that the life is stiffness, rather than strength dominated. The higher the stiffness, the lower the in-plane strain values and the less degradation in the tensile flange. Another explanation for this large difference are inconsistencies in the manufacturing processes.

Trends in the data indicate there is a shear contribution to the deflection, ranging from 9% to 11% of the total deflection. The values for KGA had an average value of 10.9 MN (2.46 (10^6) lbs) for the 400 series and 7.65 MN (1.72 (10^6) lbs) for the 500 series. These values do not appear to be a function of cyclic loading, demonstrated in Figure 2- 17 for Beam #517. The plot shows the total measured deflection, and the calculated value for the deflection based on the strain modulus alone. The difference between the two curves

represents the shear contribution to the deflection and remains constant over the course of the test. The lack of influence of fatigue on KGA enforces the idea that the webs contribute very little stiffness to the overall structure and are of negligible consideration in the fatigue life of the structure.

The mid-span deflections are proportional to the applied load, although permanent deformation does occur after cyclic loading. The stiffness reduction in the compression flange appears to be less than the tension and deflection value reductions. Inherent in this mismatch of stiffness is a shift in the neutral axis, which does not originate at the midplane. Finally, there is an insignificant amount of torsional strain seen on the structure under this loading which is neglected.

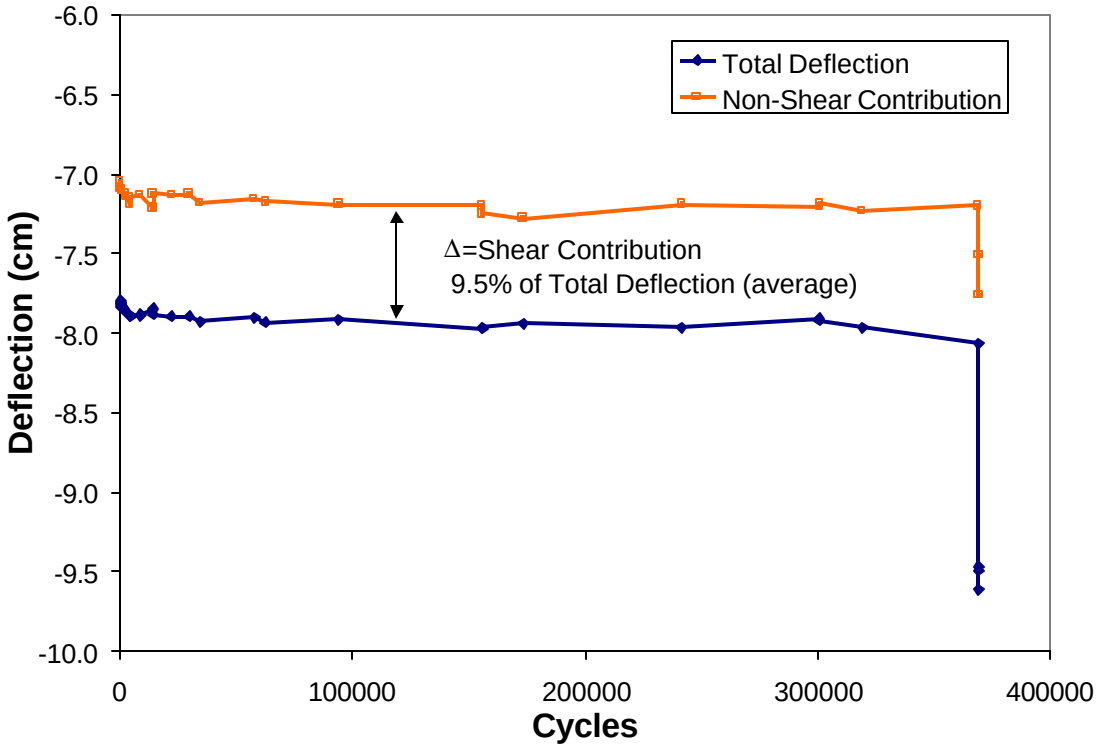

Figure 2-17: Shear contribution to deflection for Beam #517, loaded to 82% of M_{ult}

CHAPTER 3: ANALYTICAL DEVELOPMENT

Due to the limited amount of fatigue data available for structural FRP beams, and the large scale testing required to attain this data, a means must be developed to predict the life of the structural member. Ideally, small-scale coupon test data can be used to characterize the structure in its entirety. A life prediction methodology is developed in this chapter using tension fatigue coupon data in conjunction with assumptions and observations made in the full four-point bend fatigue test of the beam. The model accounts for the out-of-plane failure mode of delamination, and attempts to mimic the stiffness reduction up to failure.

3.1 Laminated Beam Theory

3.1.1 Stiffness Characteristics

Prediction of the stiffness properties is necessary to evaluate the response of the beam. The overall stiffness is calculated based on the known ply-level orientation and properties. The loading considered is the four-point bend configuration discussed in Chapter 2. Laminated beam theory [58], within the constant moment region, is then used to evaluate the ply-level stresses and strains. This approach has been verified in work done by Davalos *et. al* [59]

The cross-section is divided into 4 web and 6 flange subsections for the analysis as shown in Figure 3- 1. The photograph of the beam shows the ply waviness and nonuniform thickness, although for the analysis, the plies are assumed uniform and parallel.

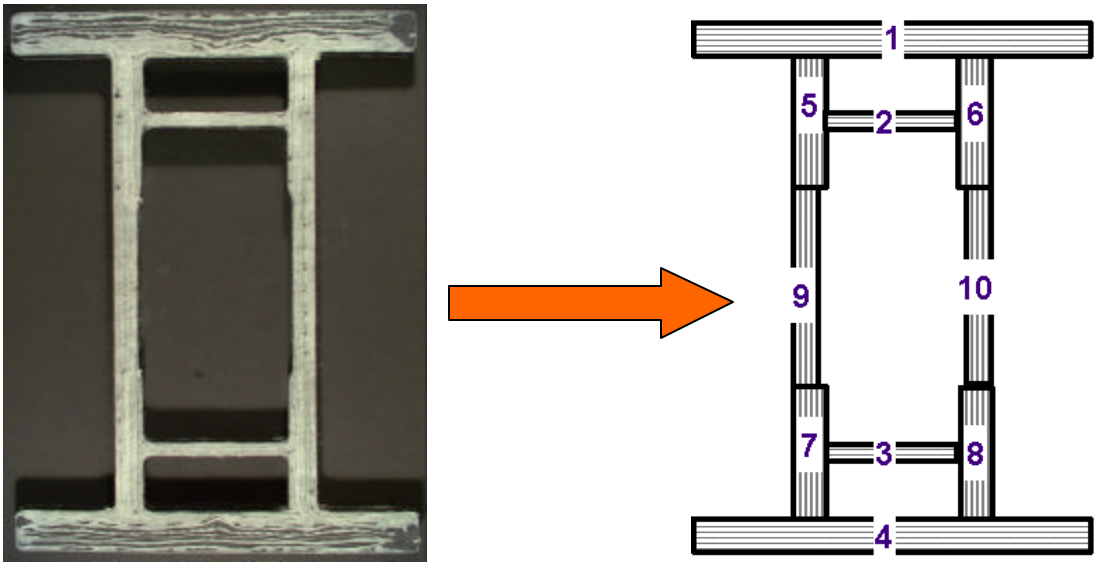

Figure 3- 1: Division of the cross section into 4 flange and 6 web subsections

For the case of bending, the stiffness value is calculated based on the assumptions that the curvature through the cross-section is constant. The total moment in the beam is equal to the sum of the sections.

$$M_{beam} = \sum M_{flange} + \sum M_{web} \tag{3-1}$$

The moment in a given section is:

$$M_i = \frac{(EI)_i}{k_i} \tag{3-2}$$

Since k_i is constant, the effective stiffness of the beam becomes:

$$EI_{eff} = \sum EI_{flange} + \sum EI_{web} \tag{3-3}$$

The EI values for each web and flange are calculated using the ABD matrix used in Classic Lamination Theory (CLT). The EI values for the flanges and webs are then calculated using Equations 3-4 and 3-5. In the expressions, x represents the distance from the NA of the beam to the NA of the section in the z direction. The b and h values are the base and height dimensions with respect to the ply direction of the section. The properties for each section and resulting stiffness is shown in Table 3- 1.

$$EI_{web} = \frac{h_{web}^3}{12 a_{11,web}} + b_{web} h_{web} x^2 \quad (3\text{-}4)$$

$$EI_{flange} = 2 b_{flange} [a_{11} x^2 + (a_{12} + a_{21}) x + a_{22}] \quad (3\text{-}5a)$$

$$a_{11} = A_{11} - \frac{A_{12} A_{21}}{A_{22}} \qquad a_{12} = B_{11} - \frac{A_{12} B_{21}}{A_{22}}$$
$$a_{21} = B_{11} - \frac{B_{12} A_{21}}{A_{22}} \qquad a_{22} = D_{11} - \frac{B_{12} B_{21}}{A_{22}} \quad (3\text{-}5b)$$

Table 3- 1: Sub-Section geometric properties and EI values

Section	Dist to NA (x) cm (in)	b cm (in)	h cm (in)	EI_{eff} MPa-m^4 (psi-in^4)
Top Flange	-9.60 (-3.78)	15.24 (6.00)	1.57 (0.62)	1.14 (4.00 x 10^8)
Bottom Flange	9.60 (3.78)	15.24 (6.00)	1.57 (0.62)	1.17 (4.09 x 10^8)
Top Subflange	-6.22 (-2.45)	5.49 (2.16)	0.70 (0.28)	.037 (1.29 x 10^7)
Bottom Subflange	6.22 (2.45)	5.49 (2.16)	0.70 (0.28)	.038 (1.32 x 10^7)
Left Top Web	-5.96 (-2.35)	5.26 (2.07)	0.42 (1.07)	.002 (8.43 x 10^5)
Right Top Web	-5.96 (-2.35)	5.26 (2.07)	0.42 (1.07)	.002 (8.43 x 10^5)
Left Bottom Web	5.96 (2.35)	5.26 (2.07)	0.42 (1.07)	.002 (8.43 x 10^5)
Right Bottom Web	5.96 (2.35)	5.26 (2.07)	0.42 (1.07)	.002 (8.43 x 10^5)
Left Center Web	0.00 (0.00)	6.65 (2.62)	0.36 (0.91)	.004 (1.54 x 10^6)
Right Center Web	0.00 (0.00)	6.65 (2.62)	0.36 (0.91)	.004 (1.54 x 10^6)

The total EI_{eff} value for the hybrid beam was found to be 2.41 MPa-m^4 (8.41x10^8 psi-in^4). The contribution of the webs and interior flanges is only 3.9% of this value. Because of this fact, and the location of the failure, ply-level stresses are only calculated for the top and bottom flanges.

3.1.2 In-Plane Stress and Strain Analysis

The curvature in the constant moment region is the loading used to determine in-plane ply-level strains and stresses. The curvature of the beam, κ^{o}_{x}, for a given bending moment can be simply calculated using the effective stiffness as shown in Equation 3-6.

$$k^{\circ}_{x} = \frac{EI_{eff}}{M_{beam}} \tag{3-6}$$

The coordinate systems for the analysis are shown in Figure 3- 2.

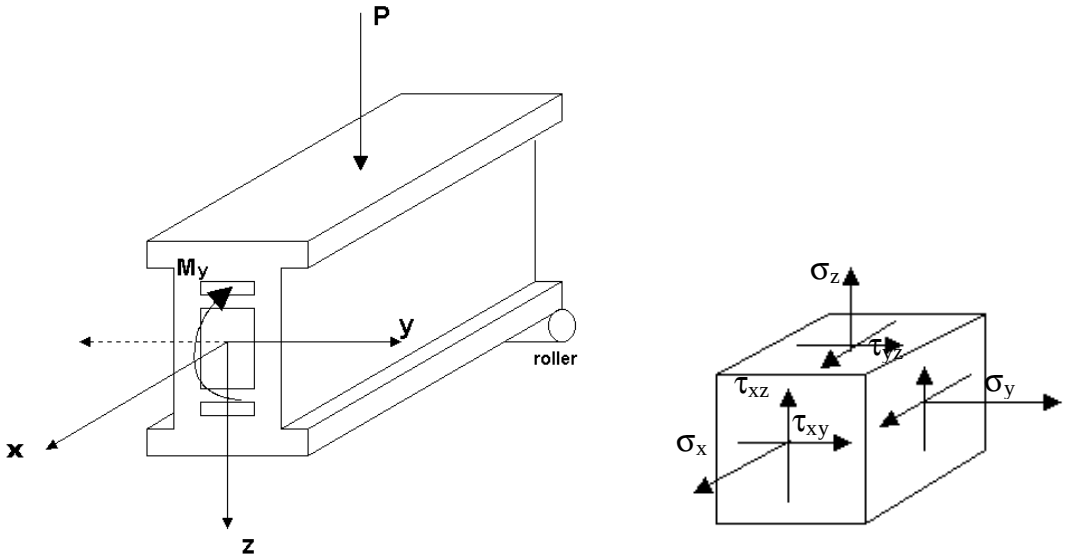

Figure 3- 2: Coordinate systems used in analysis.

The known curvature value can be used to determine the value of M_y required for CLT using the inverse ABD matrix:

$$\begin{Bmatrix} e_x^o \\ e_y^o \\ e_{xy}^o \\ k_x^o \\ k_y^o \\ k_{xy}^o \end{Bmatrix} = \left[\begin{array}{c|c} A & B \\ \hline B & D \end{array}\right]^{-1} \begin{Bmatrix} N_x \\ N_y \\ N_{xy} \\ M_x \\ M_y \\ M_{xy} \end{Bmatrix} \tag{3-7}$$

Knowing that $N_x=N_y= N_{xy}=M_x=M_{xy}=0$, M_y is defined as:

$$M_y = \frac{k_x^o}{d_{12}} \tag{3-8}$$

The value for M_y can be substituted back into (3-7) to attain values for the other mid-plane strain values. The relations for the strain response of the laminates then become:

$$e_x(x,y,z) = e_x^o + zk_x^o \tag{3-9}$$

$$e_y(x,y,z) = e_y^o + zk_y^o \tag{3-10}$$

$$e_{xy}(x,y,z) = g_{xy}^o + zk_{xy}^o \tag{3-11}$$

In these expressions the value of z is measured with respect to the neutral axis of the beam cross section. The strain values shown are the engineering strain values. The stresses can then be calculated in each ply using the Q-bar matrix:

$$\begin{pmatrix} s_x \\ s_y \\ t_{xy} \end{pmatrix} = \begin{bmatrix} \bar{\bar{Q}}_{11} & \bar{\bar{Q}}_{12} & \bar{\bar{Q}}_{13} \\ \bar{\bar{Q}}_{12} & \bar{\bar{Q}}_{22} & \bar{\bar{Q}}_{26} \\ \bar{\bar{Q}}_{13} & \bar{\bar{Q}}_{26} & \bar{\bar{Q}}_{66} \end{bmatrix} \begin{pmatrix} e_x \\ e_y \\ g_{xy} \end{pmatrix} \tag{3-12}$$

3.1.3 Out of Plane Stresses

The delamination failure mode of the beam, is the result of the out-of-plane free-edge τ_{xz} and σ_z stresses. The standard CLT stress calculations do not predict these stresses, and as discussed in Chapter 1, there are several analysis techniques to calculate them. The distance away from the free edge that the stresses act over, the boundary layer, is a constant of the laminate, independent of the loading or the location of the analysis. The boundary layer is directly proportional to the effective ply thickness of the laminate. This has been demonstrated both analytically and experimentally [20, 60]. The free body diagram below (Figure 3-3) demonstrates the stresses influenced by the free edge effect are distributed in a cut away of several plies. Two methods will be considered for the stress analysis, the Primitive Delamination Model [37] and the Minimization of Complementary Energy [49] as discussed in Chapter 1.

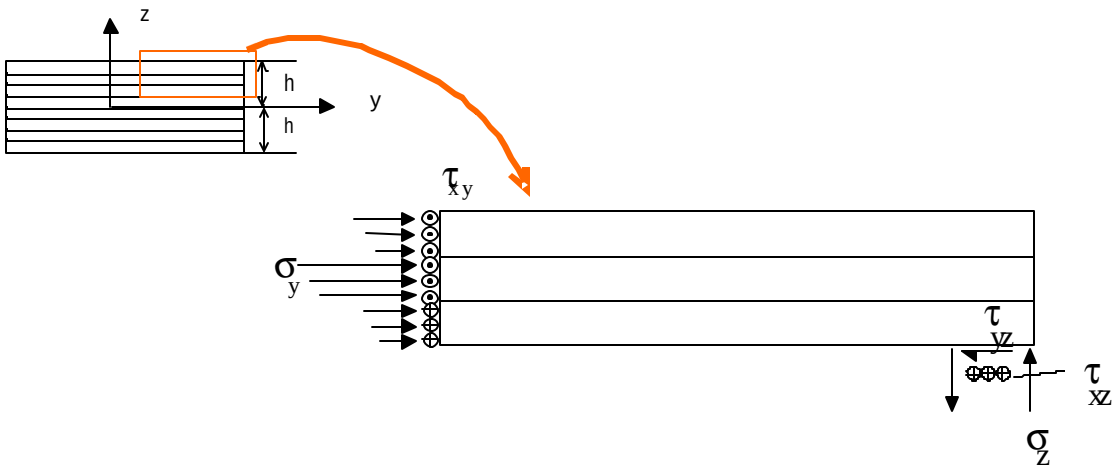

Figure 3- 3: Free body diagram including out-of-plane stresses.

In both methods, the beam is simplified to the symmetric case by representing the webs and internal flange to one equivalent ply (Figure 3- 4), and also as four equivalent plies (Figure 3-5). The overall EI_{eff} of the beam is maintained in this "smearing" process, but this simplification violates the stress free boundary condition on the bottom face of the flange. The boundary layer is often taken as the half-thickness of the laminate, but to

best represent the stress state, the boundary layer is assumed to be the thickness of the top flange.

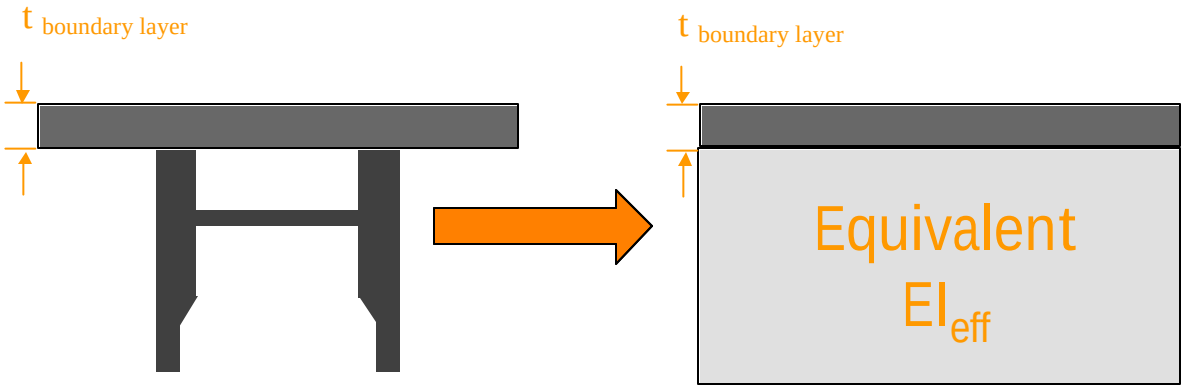

Figure 3- 4: Smearing properties of the web and flanges into one equivalent ply

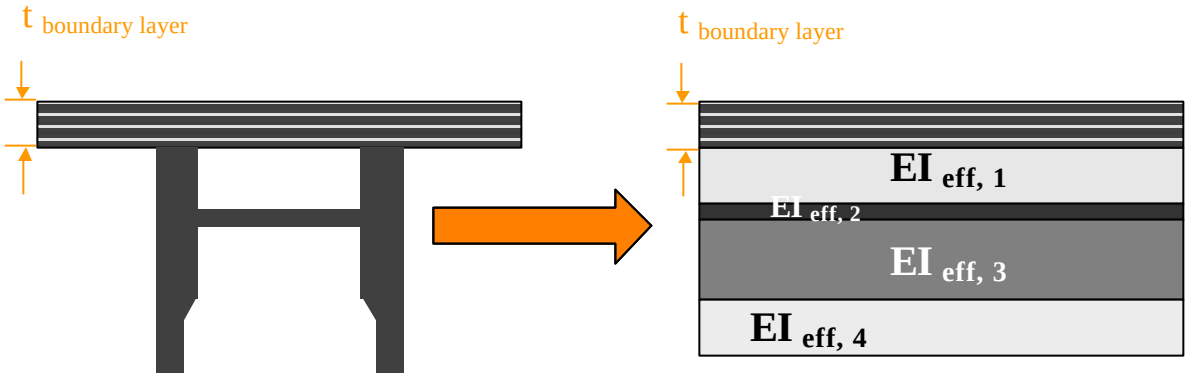

Figure 3- 5: Smearing properties of the web and flanges into 4 equivalent plies

There is some discrepancy between the in-plane stress values calculated using Laminated Beam Theory and the smeared properties. The results are shown comparatively in Figure 3- 6 through Figure 3- 8 below, all normalized to the magnitude of the σ_x value at the top of the flange calculated from Laminated Beam Theory. This maintains the convention that negative stresses are compressive. The plots shown represent the stresses through the thickness of the top flange. The distances are measured from the mid-plane of the beam

in accordance with the coordinate system shown in Figure 3- 2. Normalizing to the same value demonstrates that most of the stress is carried in the x-direction by the carbon plies.

Smearing the subflange and webs separately, is a closer match to the LBT distribution for the x-direction and shear stresses. For the y-direction stresses, it is a mixed response, where the one equivalent ply is better for the positive stress values and the four equivalent plies are more accurate for the negative values. Both models under predict the tensile stresses and over predict the compressive stresses. This is due to the fact the smeared plies are assumed isotropic, increasing the stiffness in the y-direction (i.e. stiffer 90° plies) and reducing the tensile stresses but increasing the compressive stresses. The overall increase in stiffness for the four smeared plies results in lower magnitudes of stresses, thus matching the compressive stresses better. The inverse becomes true for the one smeared ply. Overall, the stiffness of the smeared properties are low, and therefore these plies do not carry any significant amount of load, justifying the approximation.

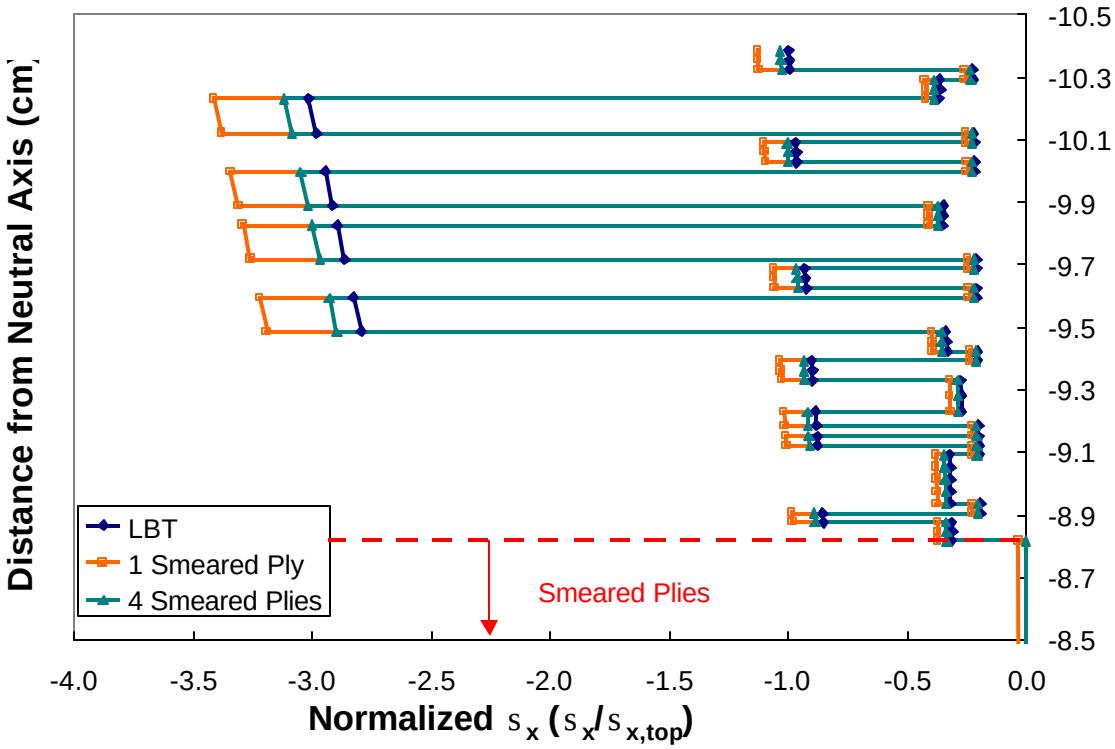

Figure 3- 6: Comparison of axial stresses using Laminated Beam Theory to the smeared cross section results

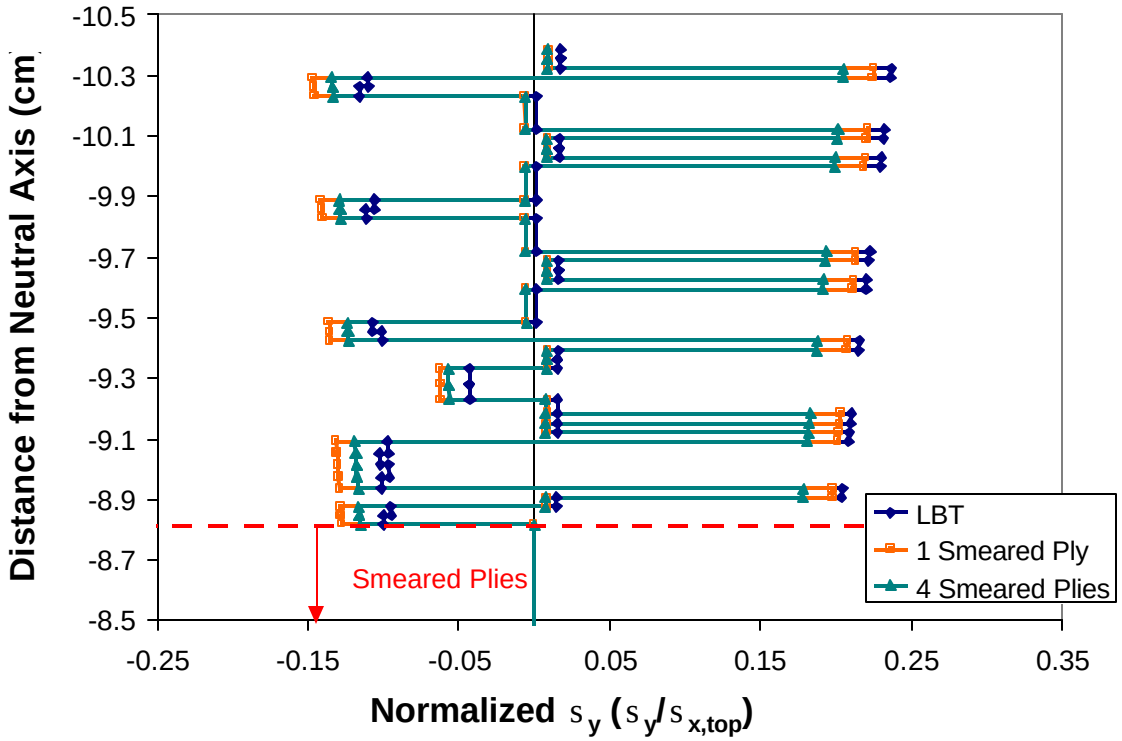

Figure 3- 7: Comparison of transverse stresses using Laminated Beam Theory to the smeared cross section results

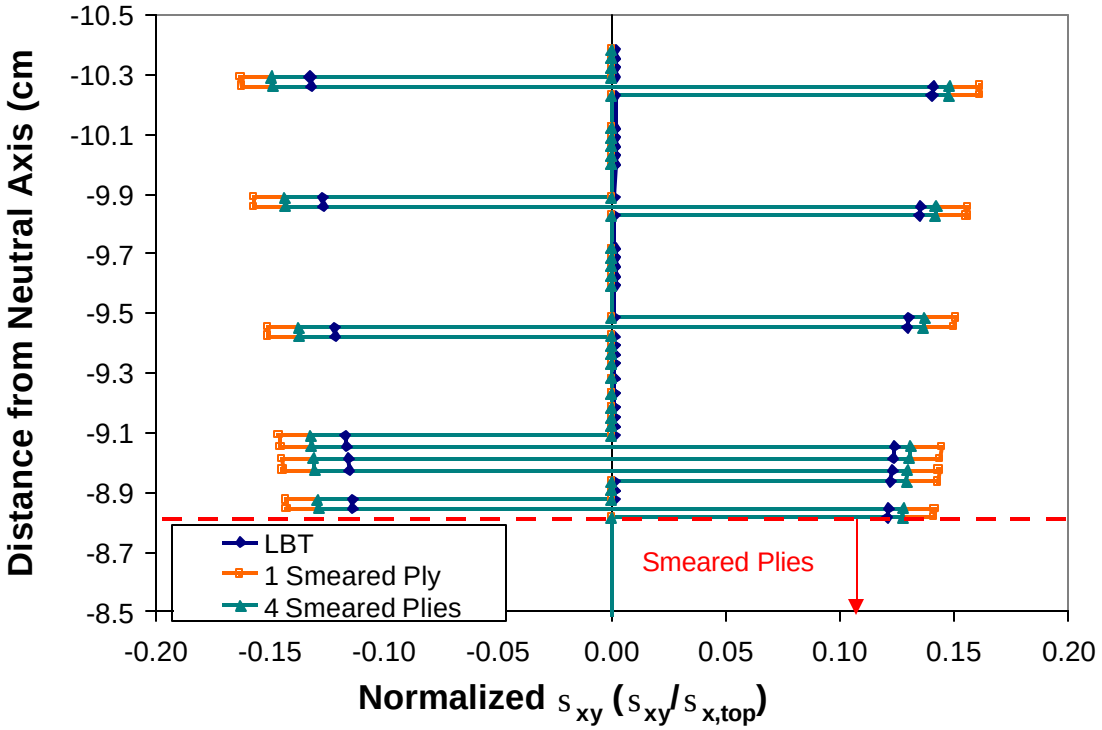

Figure 3- 8: Comparison of the shear stresses using Laminated Beam Theory to the smeared cross section results

3.1.3.1 Primitive Delamination Model

The first model considered for determining the three-dimensional stress state is the "Primitive Delamination Model", developed by Pagano and Pipes, [36,37]. This mathematically simple model is essentially a moment balance of the σ_y stresses with the σ_z stresses, which are a couple at the free edge. Using this method, the value of σ_z reaches a maximum at the free edge, which agrees with the more complicated analysis techniques and also changes sign in the boundary layer. The model assumes that the free edge effects are only contributors over a distance from the edge equal to the laminate thickness. An approximation was made on the stress distribution to linearize it as shown in Figure 3- 9. In the figure σ_m represents the maximum stress at the free edge.

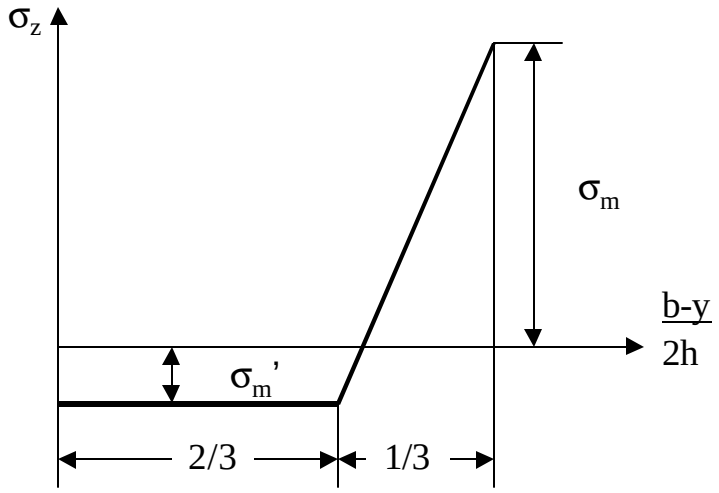

Figure 3- 9: Assumed s_z stress distribution across laminate half-width

Equating the areas under the curve, the stresses are related by Equation 3-13:

$$s'_m = \frac{s_m}{5} \tag{3-13}$$

The relations to define the stress at the free edge are:

$$s_z = \frac{14M(z)}{45h_b^2} \tag{3-14}$$

$$M(z) = \int_z^h s_y(x)(x-z)dx \tag{3-15}$$

For our calculations, the h_b in the stress expression represents the boundary layer and is therefore the thickness of the top flange. The h value in Equation 3-15 is the distance from the midplane to the top of the cross section (10.16 cm ; 4.0 in). The value of *z* is the distance from the midplane to the interface being considered. The expressions are then evaluated at each interface, to determine the interfacial σ_z at the free edge. The coordinate system and variable definitions are shown in Figure 3- 10.

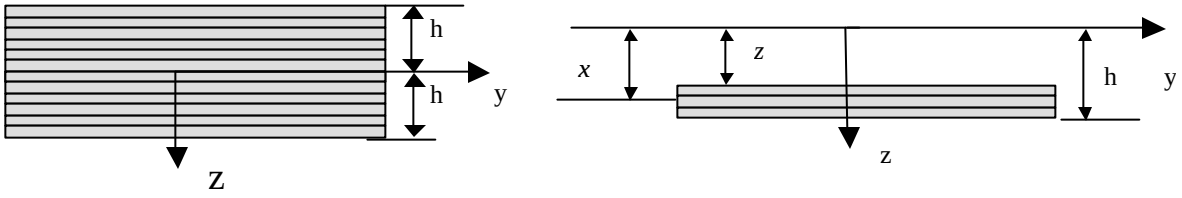

Figure 3- 10: Variable Definition for the Primitive Delamination Model

Since σ_y is linear over each layer, the integral can be computed by looking at the sum of the moments of the layers above or below the respective interface. From CLT, the stresses at the top and bottom of each layer are known, making the linear relationship for σ_y through a ply to be:

$$s_{y,i}(x) = \frac{s_{y,2,i} - s_{y,1,i}}{t_i} x + C_{o,i} \qquad C_{o,i} = s_{y,2} - \frac{s_{y,2,i} - s_{y,1,i}}{t_i} z_{2,i} \qquad (3\text{-}16)$$

In these equations $\sigma_{y,1}$ and $\sigma_{y,2}$ are the stresses at the top and bottom of a layer respectively. The thickness of the layer is t_i, z_2 is the location of the bottom of the layer with respect to the neutral axis of the section. The integral of the expression for an interface then becomes:

$$M_i = \frac{s_{y,2,i} - s_{y,1,i}}{t_i} \frac{x^3}{3} + \left(C_{o,i} - \frac{s_{y,2,i} - s_{y,1,i}}{t_i} z_{int} \right) \frac{x^2}{2} - C_{o,i} z_{int} x \Bigg|_{z_2}^{z_1} \qquad (3\text{-}17)$$

where z_{int} represents the interface being evaluated and z_1 and z_2 are the z locations at the top and bottom of the ply respectively. The moments are then summed for the plies above or below the interface being evaluated and this value of M(z) is used in Equation 3-17 to determine the stress at the free edge.

The resulting ply-level stress distribution in the top flange of σ_z under the ultimate moment is shown in Figure 3- 11 and Figure 3- 12 for both methods of approximating EI_{eff}. The ultimate load is the average moment capacity of all of the beams tested at all spans, M_{ult} = 135 kN-m (100 kip-ft). This value will be used for all of the calculations in the remainder of the chapter. The moment balance for the analysis is completely dependent on the σ_y values. Comparison of the approximated in-plane stresses to Laminated Beam Theory did not clearly indicate which stiffness approximation is best for $\sigma_{y,}$ therefore both are compared in the figures below. The use of 1 equivialent ply for the section is more conservative, as it yields the higher stress levels by as much as 16%.

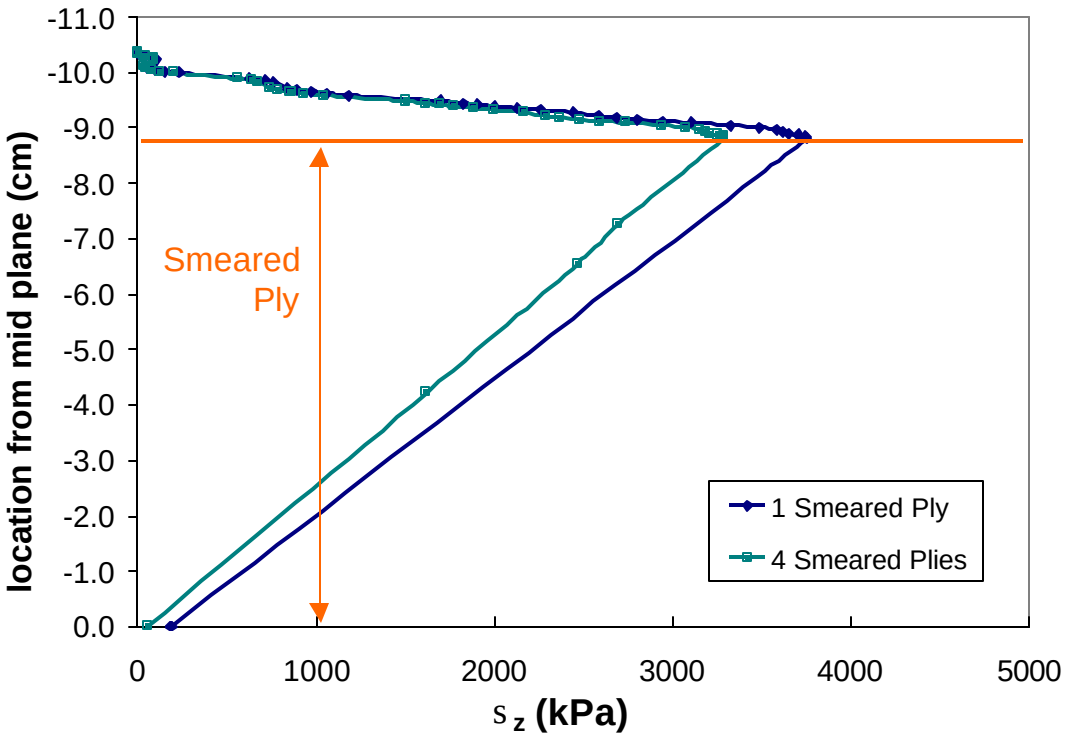

Figure 3- 11: Stress Distribution through top half of beam cross section at failure loading using the Primitive Delamination model

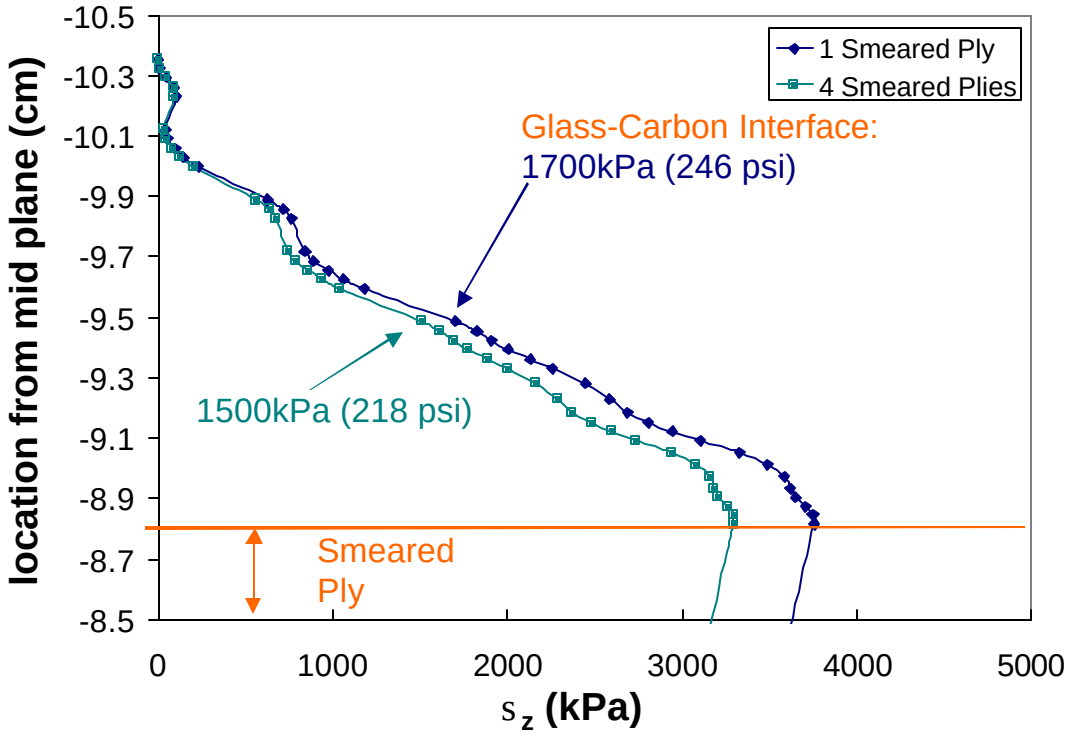

Figure 3- 12: Stress distribution "zoomed-in" on top flange using the Primitive Delamination Model

The Primitive Delamination Model continuously sums the effects of the plies above it, therefore it suggests that the maximum σ_z is actually reached at the bottom of the top flange. Based on this, the stress free conditions are certainly not met at the bottom face of the flange. Experimentally, the failure is consistently occurring at the first carbon matrix interface from the midplane, so the critical free edge stress will be considered the maximum σ_z at that interface, called out in Figure 3- 12

3.1.3.2 Minimization of Complementary Energy

The second approach, more appropriate for the non-symmetric top flange laminate, is the Minimization of Complementary Energy. This approach is outlined in Reference [49] and will be summarized below.

In order to simplify the mathematics, a new coordinate system is introduced. The zero value is shifted to the free edge and normalized:

$$\bar{y} = \frac{b - y}{h} \tag{3-18}$$

Additionally, a local coordinate, z_p , is introduced for each ply. At the bottom of the ply, $z_p = 0$, and at the top of the ply, $z_p = t^k$, where t^k is the thickness of ply k. See Figure 3-13.

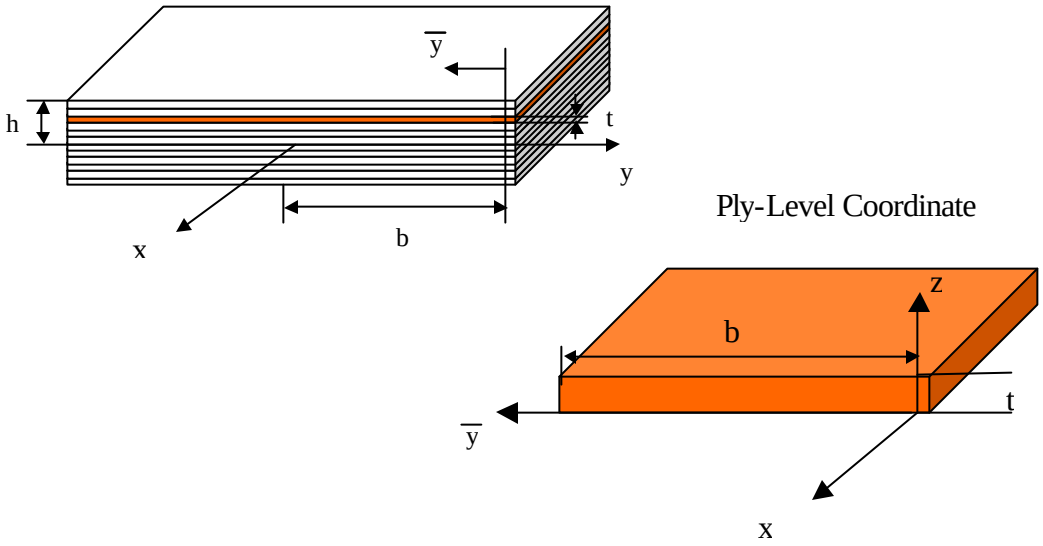

Figure 3- 13: Coordinate System for interfacial stress analysis using the Minimization of Complementary Energy approach

The stresses are assumed independent of the x direction and multiplicatively independent of y and z. For the most general loading conditions the in-plane stresses cannot be more than linear in z, and must regain the CLT values away from the free edge. The stresses for a given ply are assumed to take the form:

$$s_y^k = (1 + g_1(\bar{y}))(A_o^k + A_1^k z_p) \tag{3-19}$$

$$s_{xy}^k = (1 + g_2(\bar{y}))(B_o^k + B_1^k z_p) \tag{3-20}$$

The equilibrium equations, in accordance with the above assumptions, become:

$$\frac{1}{h}\frac{\partial s_{xy}}{\partial \bar{y}} = \frac{\partial s_{xz}}{\partial z_p} \qquad \Rightarrow \qquad s_{xz}^{k} = \frac{g_2'(\bar{y})}{h}\left(D_o^k + B_o^k z_p + B_1^k \frac{z_p^{\,2}}{2} \right) \tag{3-21}$$

$$\frac{1}{h}\frac{\partial s_{y}}{\partial \bar{y}} = \frac{\partial s_{yz}}{\partial z_p} \qquad \Rightarrow \qquad s_{yz}^{k} = \frac{g_1'(\bar{y})}{h}\left(C_o^k + A_o^k z_p + A_1^k \frac{z_p^{\,2}}{2} \right) \tag{3-22}$$

$$\frac{1}{h}\frac{\partial s_{yz}}{\partial \bar{y}} = \frac{\partial s_{z}}{\partial z_p} \qquad \Rightarrow \qquad s_{z}^{k} = \frac{g_1''(\bar{y})}{h^2}\left(C_1^k + C_o^k z_p + A_o^k \frac{z_p^{\,2}}{2} + A_1^k \frac{z_p^{\,3}}{6} \right) \tag{3-23}$$

The g_1 and g_2 functions are solved for the entire laminate, where as the other constants change for each ply, as indicated by the k superscript. At the free edge, stress free conditions must be met:

$$s_{y}^{k}(0) = 0 \qquad \Rightarrow \qquad g_1(0) = -1 \tag{3-24}$$

$$s_{xy}^{k}(0) = 0 \qquad \Rightarrow \qquad g_2(0) = -1 \tag{3-25}$$

$$s_{yz}^{k}(0) = 0 \qquad \Rightarrow \qquad g_1'(0) = 0 \tag{3-26}$$

In order to regain the CLT values, the following conditions must be met away from the free edge:

$$\lim_{\bar{y}\to\infty} g_1(\bar{y}) = 0 \qquad \text{and} \qquad s_{y,CLT}^{k} = A_o^k + A_1^k z_p \tag{3-27}$$

$$\lim_{\bar{y}\to\infty} g_2(\bar{y}) = 0 \qquad \text{and} \qquad s_{xy,CLT}^{k} = B_o^k + B_1^k z_p \tag{3-28}$$

To attain the CLT stresses, using the local ply coordinate system, the constants are defined from the CLT solution are are:

$$A_o^k = s_{y,CLT,bottom}^{k} \tag{3-29}$$

$$A_1^k = -\left(\overline{Q}_{12} k_x^o + \overline{Q}_{22} k_{yx}^o + \overline{Q}_{23} k_{xy}^o\right) \tag{3-30}$$

$$B_o^k = s_{xy,CLT,bottom}^{k} \tag{3-31}$$

$$B_1^k = -\left(\overline{Q}_{13} k_x^o + \overline{Q}_{23} k_{yx}^o + \overline{Q}_{33} k_{xy}^o\right) \tag{3-32}$$

The constants for the first ply can be found by knowing that the top of the laminate is stress free:

$$s_{yz}^{1}(z_p = t^1) = 0 \qquad \Rightarrow \qquad C_o^1 = -\left(A_o^1 (t^1) + A_1^1 \frac{(t^1)^2}{2}\right) \tag{3-33}$$

$$s_{z}^{1}(z_p = t^1) = 0 \qquad \Rightarrow \qquad C_1^1 = -\left(C_o^1 t^1 + A_o^1 \frac{(t^1)^2}{2} + A_1^1 \frac{(t^1)^3}{6}\right) \tag{3-34}$$

$$s_{xz}^{1}(z_p = t^1) = 0 \qquad \Rightarrow \qquad D_o^1 = -\left(B_o^1 t^1 + B_1^1 \frac{(t^1)^2}{2}\right) \tag{3-35}$$

Using the matching conditions at the ply interfaces, the constants can be defined as follows for the other plies:

$$s_{yz}^{k}(z_p = t^k) = s_{yz}^{k+1}(z_p = 0) \quad \Rightarrow \quad C_o^k = -\sum_{i=1}^{k}\left(A_o^i (t^i) + A_1^i \frac{(t^i)^2}{2}\right) \tag{3-36}$$

$$s_{z}^{k}(z_p = t^k) = s_{z}^{k+1}(z_p = 0) \quad \Rightarrow \quad C_1^k = -\sum_{i=1}^{k}\left(C_o^i t^i + A_o^i \frac{(t^i)^2}{2} + A_1^i \frac{(t^i)^3}{6}\right) \tag{3-37}$$

$$s_{xz}^{k}(z_p = t^k) = s_{xz}^{k+1}(z_p = 0) \quad \Rightarrow \quad D_o^k = -\sum_{i=1}^{k}\left(B_o^i t^i + B_1^i \frac{(t^i)^2}{2}\right) \tag{3-38}$$

The stress functions are now only functions of g_1 and g_2 and the appropriate derivatives. The functional forms are found using the minimization of complementary energy and variational calculus. The expression for the complementary energy is:

$$\Pi_c = \sum_{i=1}^{n} \left[\iiint_V s^T \bar{S} s \, dV \right] \tag{3-39}$$

where $s^T = \left[s_x, s_y, s_z, s_{yz}, s_{xz}, s_{xy} \right]$ and $\bar{S}$ is the 6 x 6 matrix as defined in Appendix-A.

For a given ply, in the top half of a symmetric laminate, the expression of complementary energy becomes:

$$\Pi_c^k = \iiint \left[\left(\bar{S}_{22} - \frac{\bar{S}_{12}^2}{\bar{S}_{11}} \right) \frac{s_{22}^2}{2} + \left(\bar{S}_{33} - \frac{\bar{S}_{13}^2}{\bar{S}_{11}} \right) \frac{s_{zz}^2}{2} + \frac{\bar{S}_{44}}{2} s_{2z}^2 + \frac{\bar{S}_{55}}{2} s_{1z}^2 + \left(\bar{S}_{66} - \frac{\bar{S}_{16}^2}{\bar{S}_{11}} \right) \frac{s_{12}^2}{2} \right.$$
$$\left. + \left(\bar{S}_{33} - \frac{\bar{S}_{13}\bar{S}_{12}}{\bar{S}_{11}} \right) s_{22} s_{zz} + \left(\bar{S}_{26} - \frac{\bar{S}_{16}\bar{S}_{12}}{\bar{S}_{11}} \right) s_{22} s_{12} + \left(\bar{S}_{36} - \frac{\bar{S}_{16}\bar{S}_{13}}{\bar{S}_{11}} \right) s_{zz} s_{12} + \bar{S}_{45} s_{22} s_{1z} \right] dx d\bar{y} dz \tag{3-40}$$

Calculus of variation procedures, give the governing equations for $g_1(\bar{y})$ and $g_2(\bar{y})$ to be of the form:

$$\frac{d^2}{d\bar{y}^2}\left(\frac{\partial \Pi_c}{\partial g_1''} \right) - \frac{d}{d\bar{y}}\left(\frac{\partial \Pi_c}{\partial g_1'} \right) + \frac{\partial \Pi_c}{\partial g_1} = 0 \tag{3-41}$$

$$\frac{d}{d\bar{y}}\left(\frac{\partial \Pi_c}{\partial g_2'} - \frac{\partial \Pi_c}{\partial g_2} \right) = 0 \tag{3-42}$$

The solution is outlined in Reference 49 and results in the solution for $g_1(\bar{y})$ and $g_2(\bar{y})$ to be:

$$g_1 = S_1 e^{m_1 \bar{y}} + S_2 e^{m_2 \bar{y}} + S_3 e^{m_3 \bar{y}} \tag{3-43}$$

$$g_2 = \bar{S}_1 e^{m_1 \bar{y}} + \bar{S}_2 e^{m_2 \bar{y}} + \bar{S}_3 e^{m_3 \bar{y}} \tag{3-44}$$

In these equations the m_1, m_2 and m_3 values are the complex roots to the characteristic equations with negative real parts. The constants can be solved for by recalling the boundary equations (3-24 through 3-26)

In summary the stresses have the form:

$$s_y^k = (1 + S_1 e^{m_1 \bar{y}} + S_2 e^{m_2 \bar{y}} + S_3 e^{m_3 \bar{y}})(A_o^k + A_1^k z_p)$$

$$s_{xy}^k = (1 + \bar{S}_1 e^{m_1 \bar{y}} + \bar{S}_2 e^{m_2 \bar{y}} + \bar{S}_3 e^{m_3 \bar{y}})(B_o^k + B_1^k z_p)$$

$$s_{xz}^k = \frac{1}{h}\left(\bar{S}_1 m_1 e^{m_1 \bar{y}} + \bar{S}_2 m_2 e^{m_2 \bar{y}} + \bar{S}_3 m_3 e^{m_3 \bar{y}}\right)\left(D_o^k + B_o^k z_p + B_1^k \frac{z_p^2}{2}\right)$$

$$s_{yz}^k = \frac{1}{h}\left(S_1 m_1 e^{m_1 \bar{y}} + S_2 m_2 e^{m_2 \bar{y}} + S_3 m_3 e^{m_3 \bar{y}}\right)\left(C_o^k + A_o^k z_p + A_1^k \frac{z_p^2}{2}\right)$$

$$s_z^k = \frac{1}{h^2}\left(S_1 m_1^2 e^{m_1 \bar{y}} + S_2 m_2^2 e^{m_2 \bar{y}} + S_3 m_3^2 e^{m_3 \bar{y}}\right)\left(C_1^k + C_o^k z_p + A_o^k \frac{z_p^2}{2} + A_1^k \frac{z_p^3}{6}\right)$$

An example of the stress distribution is shown along the y-direction of the carbon-glass interface in Figure 3- 14. The solution is symmetrical, over the full beam width, and only one half is shown. The shaded area represents the boundary layer region, equal to the thickness of the top flange. The plot represents the solution for the case when 4 smeared plies are used. The in-plane σ_y and τ_{xy} do return to the CLT values outside of the boundary layer, and the maximum σ_z and τ_{xz} occur at the free edge. The value of τ_{yz} is significant within the boundary layer region, and is nearly as large as the in plane stress value. It should be noted that the σ_x mismatch at this interface is large. The stress value in the carbon ply is 689 MPa (100 ksi) and in the glass ply is 86.2 MPa (12.5 ksi).

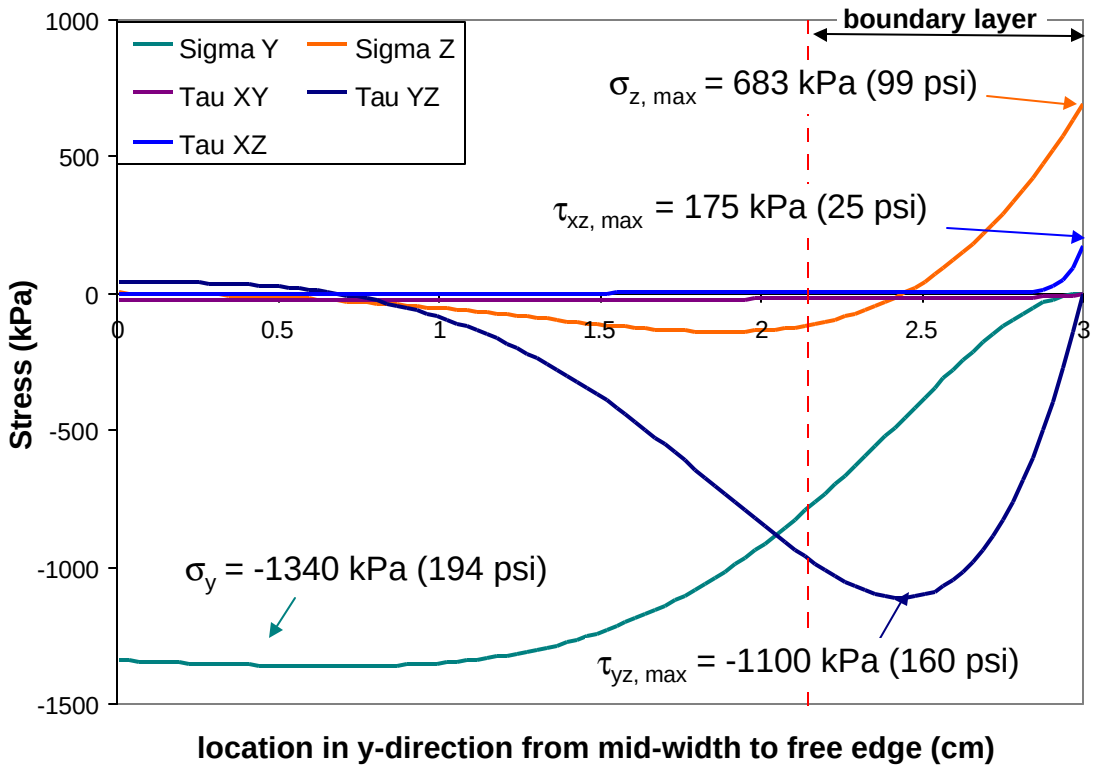

Figure 3- 14: Stress distribution at failure interface using the minimization of complementary energy using four smeared plies to represent the web and internal flanges.

The stress distribution through the top flange, using the one and four ply approximations, are shown in Figure 3- 15 and Figure 3- 16. The figures show the maximum values for σ_z within a given ply at a given *z* location. The out-of-plane stresses are continuous as required by the boundary conditions. The *z*-face stresses do not return to zero at the bottom of the laminate because of the smeared properties.

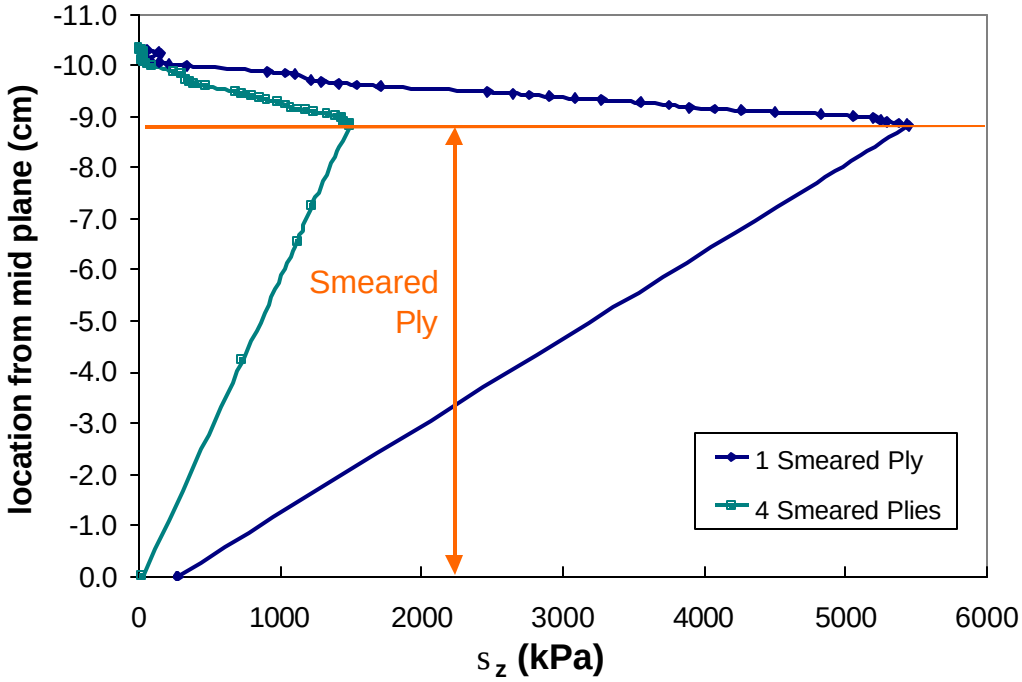

Figure 3- 15: : Stress Distribution through top half of beam cross section at failure loading using the Minimization of Complementary Energy approach

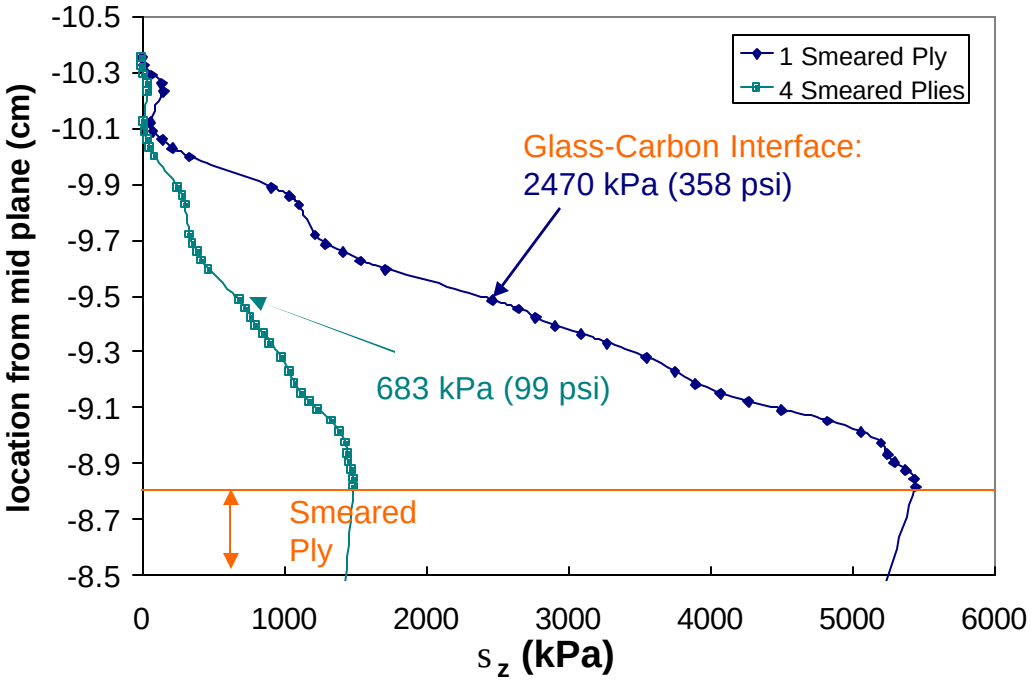

Figure 3- 16: : Stress Distribution "zoomed-in" through top flange at failure loading using the Minimization of Complementary Energy approach

3.1.3.3 Model Comparison

The overall shapes of the models are very consistent, demonstrated in Figure 3- 17. Both models have the highest stress for a glass-carbon interface at the location of the failure experimentally. Each model is a summation of the properties in the plies above a given infterface, and therefore the models both reach the maximum values at the bottom of the flange. There is a significant increase in the stresses across through the stiffer carbon plies in each model. The energy method uses all the in-plane stresses for the analysis and is therefore more sensitive to the stress approximation used. The models range from 683 kPa to 2470 kPa (99 psi –358 psi) at this critical carbon-glass interface, under the ultimate loading. The use of one smeared ply yields the more conservative result in each model. The stress values at the critical carbon-glass interface will be used in life prediction as the out-of-plane strength values for the beam, Z_t.

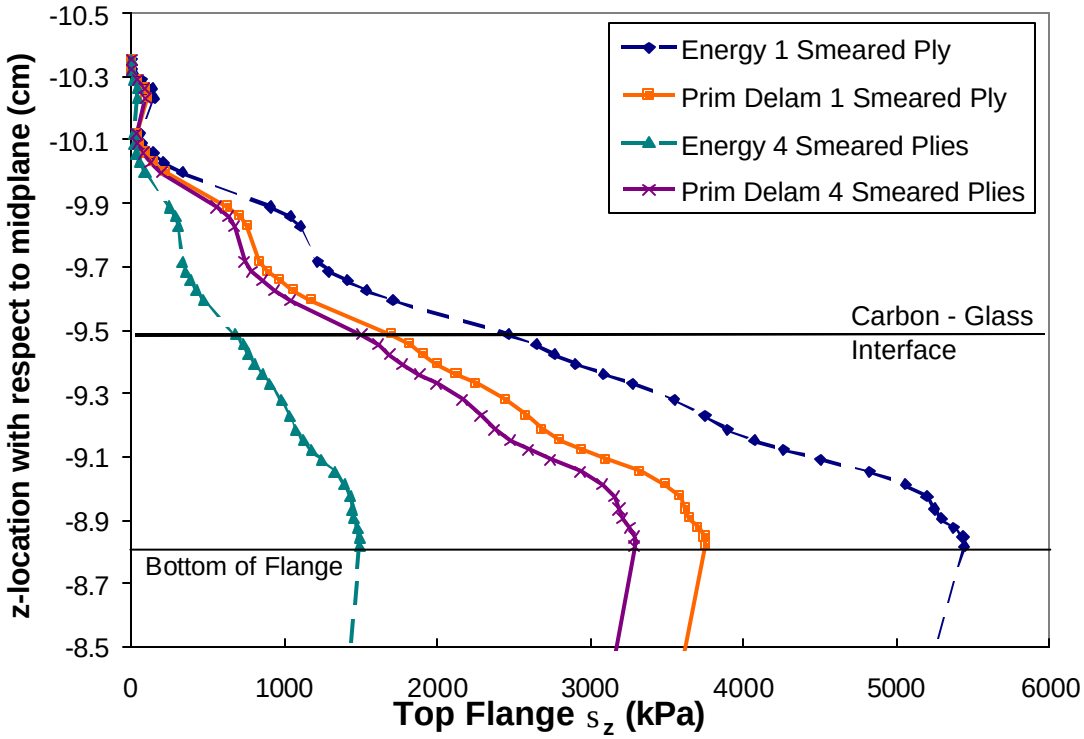

Figure 3- 17: Comparison of the two out-of-plane stress models, and the equivalent property approximations

3.2 Life Prediction

Knowledge of the stiffness properties and ply level stresses and strains allows for a life prediction model to be developed. The model employs the idea that initially stiffness reduction only occurs in the tensile flange. As the stiffness of the bottom flange is reduced, there is a redistribution of strain to the compressive flange and an inherent shift in the neutral axis. A remaining strength approach [61], in conjunction an iterative stress analysis is then used to determine the onset of delamination and the crack growth to failure. The assumptions employed in the residual strength model include:

- Reduction in tensile stiffness of the beam will be evaluated, based on tensile coupon data of similar material conducted by Phifer [18] which focuses on off-axis plies .
- The unidirectional carbon plies do not experience any stiffness reduction.
- Strength reduction is uniform for both the tensile and compression flanges and is related to the in-plane strength reduction of the tensile flange.
- The carbon acts stiffer in tension than in compression, therefore the neutral axis is initially offset toward the tensile flange but during loading shifts toward the compressive side.
- The tensile out-of-plane strength (Z_t) is calculated from the M_{ult} found from quasi-static failure testing.
- Once delamination initiates, stiffness reduction must be accounted for in the compression flange in addition to the tensile flange.
- Crack growth, once delamination is initiated, is symmetric from each side of the beam, across the width of the beam (in the y-direction)
- Failure occurs when the crack propagates across the width of the beam or if the in-plane remaining strength matches the loading.

The flow chart, Figure 3- 18, demonstrates the process up to delamination inititaion, and the steps are further detailed in the sections to follow. The process begins by inputting the geometry, layup and loading. Using this information the stresses and strains are evaluated. The free edge stresses are then compared to the strength of the top flange. If the stress exceeds the strength, delamination is assumed. If the stress does not exceed the strength, the stiffness in the tensile flange is reduced based on a maximum strain

criterion. The neutral axis shift corresponding to the stiffness reduction is then calculated. The new stiffness and neutral axis location are used in Laminated Beam Theory to determine the new EI_{eff} and curvature. The κ_x^o becomes the new loading condition for the stress evaluation. The process is continued until delamination initiation.

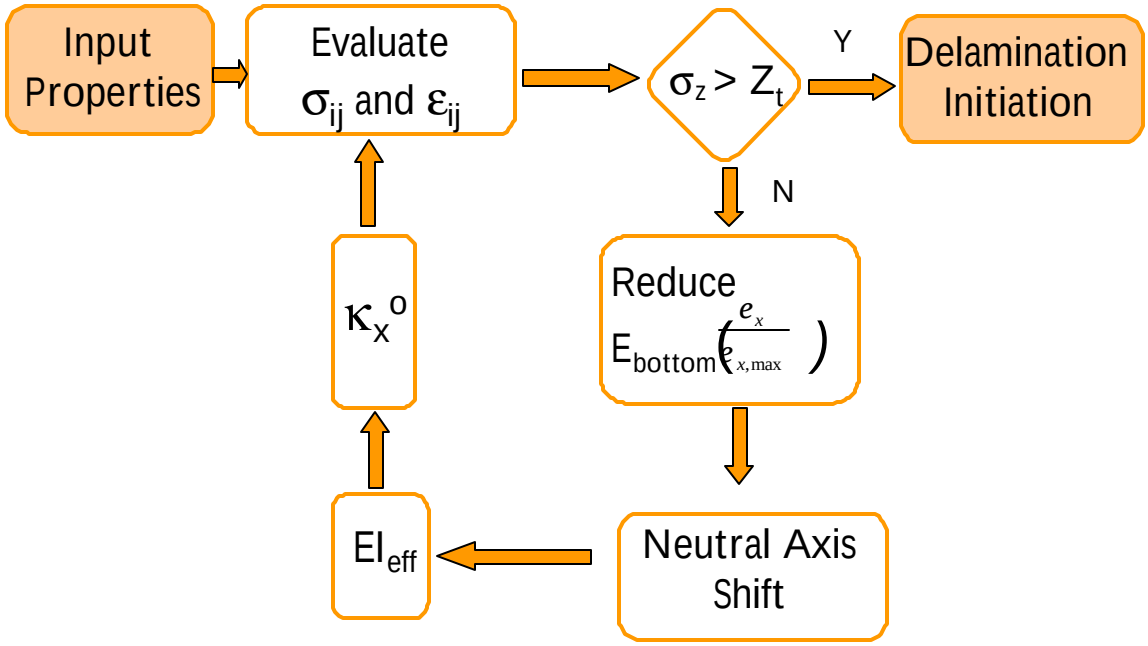

Figure 3- 18: Flow Chart of Stress Analysis and Stiffness reduction up to delamination

3.2.1 Stiffness Reduction

3.2.1.1 Stiffness reduction of the Tensile Flange

All of the initial stiffness reduction is assumed to occur in the tensile flange, based on what was seen experimentally. Prior tensile fatigue testing of pultruded, E-glass, vinyl ester laminates is used to characterize the stiffness reduction of the bottom flange. The dynamic stiffness reduction was monitored in the tests; and indicates a linear reduction in stiffness occurs with respect to cycles at a given load [18], following an intial drop off. The carbon plies are assumed to experience no stiffness reduction in the analysis. The flange is divided into sublaminates that mimic the cross-ply and quasi-isotropic coupons tested, and the stiffness reduced on a sub-laminate basis. A summary of the initial properties for the crossply CP1 lamaintes, $(0/90)_{5T}$, and the quasi-isotropic QI2 laminates $(0/90/+45/-45/90/0)_{2T}$ is given in Table 3- 2 .

Table 3- 2: Summary of coupon laminate properties tested in tensile fatigue by Phifer

	Ply Orientation	V_f % Fiber Volume	E_T Tensile Modulus GPa (Msi)	e_{90f} 90° % Failure Strain	e_f % Failure Strain	X_t Ult Strength MPa (ksi)
CP1	$(0/90)_{5T}$	56.2	27.3 (3.96)	.32	2.077	430 (62.4)
QI2	$(0/90/+45/-45/90/0)_{2T}$	56.3	24.1 (3.50)	.37	2.060	357 (51.9)

Based on the fatigue data, Phifer used a linear fit was to describe the dynamic modulus reduction. The cross-ply laminate stiffness reduction (Figure 3- 19) was dependent on the load level, resulting in two different fits, where Fa represents the ratio of the load to the ultimate load. For the quasi-isotropic laminates both overall laminate reduction was determined and the reduction of the off-axis plies was also calculated as shown in Figure 3- 19. Although the linear fit does not capture the initial degradation of the laminate, it is representative thereafter.

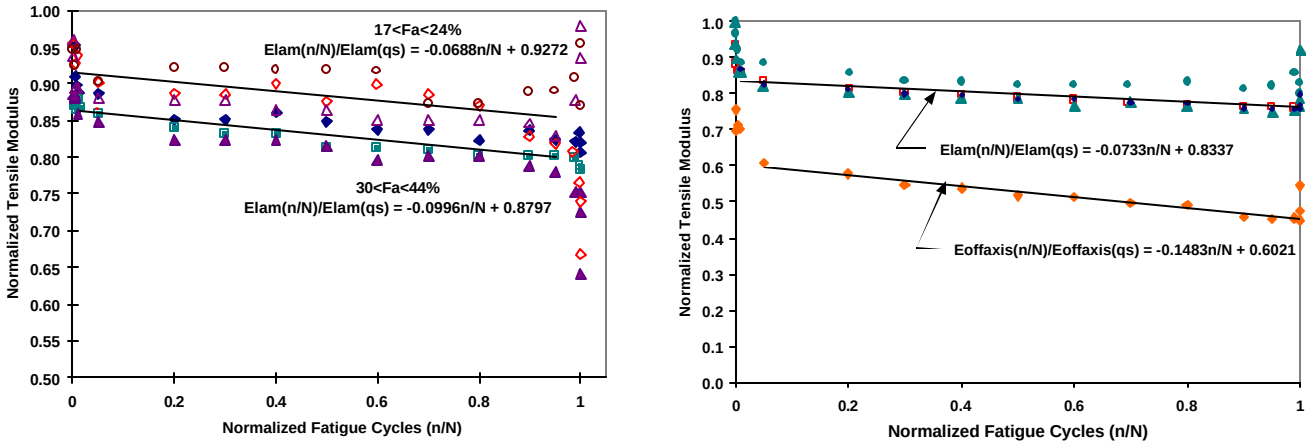

Figure 3- 19: Linear curve fits used by Phifer for tensile coupon fatigue data of Quasi-Isotropic (Left) and Cross-Ply (right) laminates

For modeling the beam, it seems that the initial coupon degradation is similar to what occurs in the beam itself, therefore the data was fit to a logarithmic curve to capture the initial area, and then flatten out. It is also important to note that the inplane strains in the beam are lower than what the coupon tests are loaded to. Therefore the data was averaged using the lower Fa ($\varepsilon_{applied}/\varepsilon_{max}$)values. The data and fit are shown for the quasi-isotropic laminates in Figure 3- 20 and the cross-ply laminates in Figure 3- 21. The resulting curve fits were:

$$\text{Quasi-Isotropic: } \frac{E_x}{E_o} = -0.0124 \ln\left(\frac{n}{N}\right) + .8281 \qquad (3\text{-}45)$$

$$\text{Cross Ply: } \frac{E_x}{E_o} = -0.0118 \ln\left(\frac{n}{N}\right) + .8933 \qquad (3\text{-}46)$$

The sublaminate reductions are comparatively plotted in Figure 3- 22. The reduction of the Quasi-Isotropic laminates is more severe initially, but both have similar attributes thereafter due to the nature of the logarithmic curve fit.

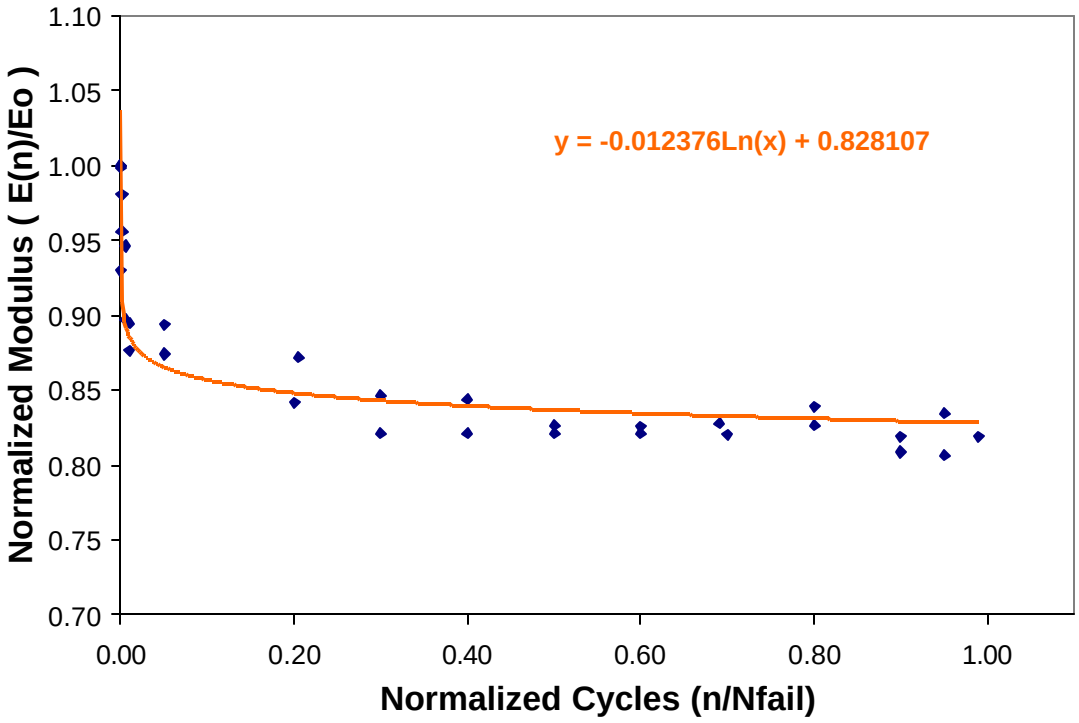

Figure 3- 20 : Curve fit of coupon dynamic stiffness reduction for quasi-isotropic laminates

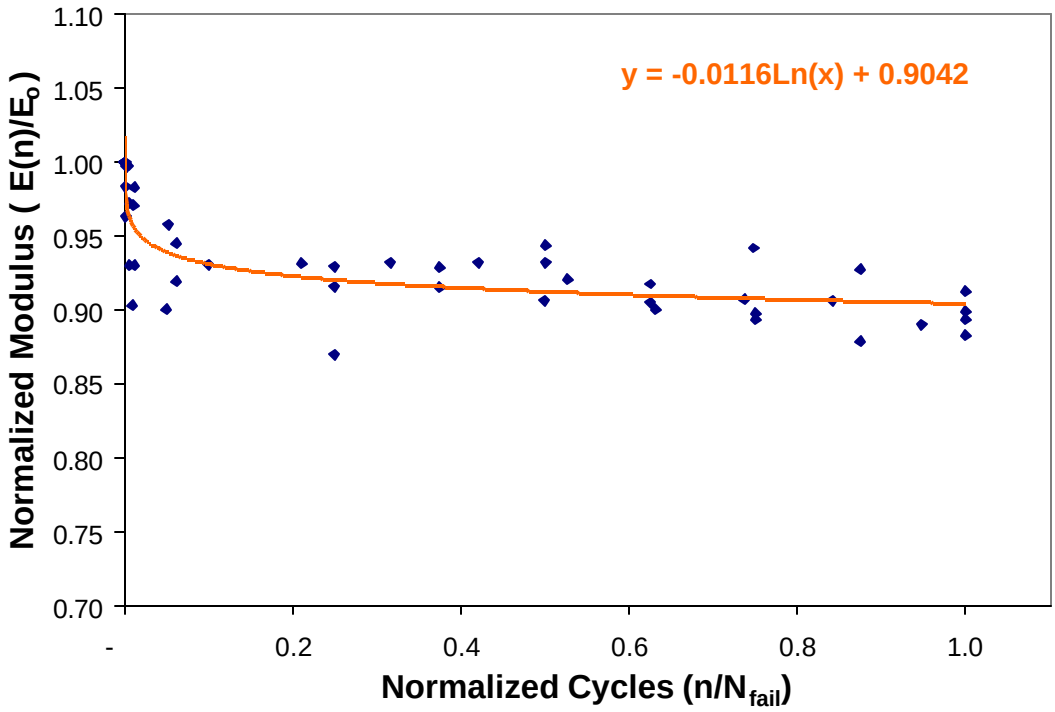

Figure 3- 21: Curve fit of coupon dynamic stiffness reduction for cross-ply laminates

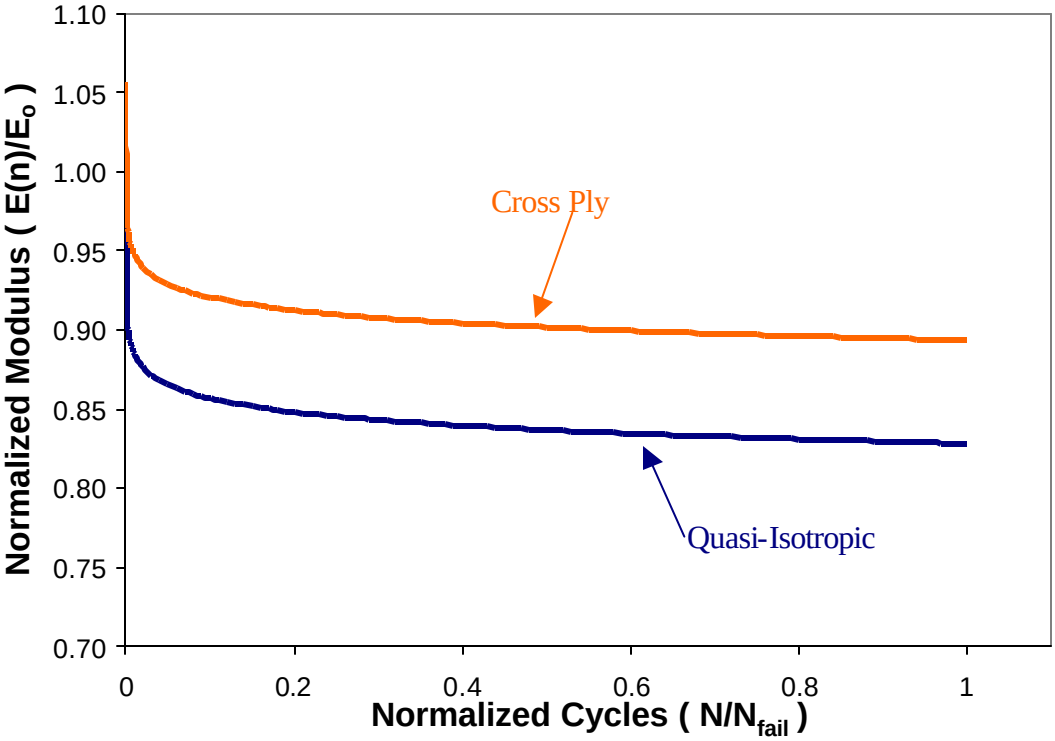

Figure 3- 22: Comparison of sub-laminate level stiffness reductions

3.2.1.2 Flange Stiffness Calculation

In the analysis, the effective modulus of a sublaminate is found from a rule of mixtures approach:

$$E_{eff} = \frac{\sum E_{x,i} t_{i\,i}}{\sum t_i} \tag{3-47}$$

where $E_{x,i}$ is the equivalent modulus in the axial direction for a ply of any orientation and t_i is the thickness of the respective ply. This effective stiffness was then used in the same manner to determine the stiffness of the entire flange. For the entire flange the $E_{x,i}$ and t_i are the sublaminate E_{eff} and thickness respectively.

The use of the inverse ABD values to attain the effective stiffness was also considered:

$$E_{eff} = \frac{1}{a_{11} t} \tag{3-48}$$

Jones notes that this expression is not accurate for laminates with plies of different thicknesses [62]. It also needed to be used at the sublaminate level and then to determine the overall stiffness of the flange, doubling the inaccuracy and adding complexity. This approach also results in a different E_x for the top and bottom flanges, which are symmetric to each other, prior to any reduction.

The EI_{eff} values using both approaches are compared to LBT in Table 3- 3.

Table 3- 3: Comparison of approximated EI_{eff} values to Laminated Beam Theory results

	Rule of Mixtures MPa-m^4 (psi-in^4)	**Inverse ABD** MPa-m^4 (psi-in^4)	**LBT** MPa-m^4 (psi-in^4)
Top Flange	1.10 (3.83×10^8)	1.02 (3.57×10^8)	1.14 (4.00×10^8)
Bottom Flange	1.10 (3.83×10^8)	.832 (2.91×10^8)	1.17 (4.09×10^8)

The rule of mixtures approach yields a modulus value closer to the Laminated Beam Theory prediction. It is also simpler to employ, and is used in the model.

3.2.1.3 Stiffness Reduction of the Compression Flange

Stiffness reduction occurs only in the tensile flange until delamination initiates. The reduction is then controlled by the number of delaminations and the crack length. This method will be further described in the section following.

3.2.1.4 Neutral Axis Shift

Initially, the neutral axis shift is toward the tensile flange, as carbon acts stiffer in tension than in compression. As the stiffness of the flanges change, there is a shift in the neutral axis. This shift inherently changes the strain distribution across the section and will influence the in-plane stiffness reduction. Initially, the neutral axis moves toward the compression flange, and once delamination occurs, it begins to shift toward the bottom flange. The location of the neutral axis is simply found by considering the effective E_x for the top and bottom flanges, in the standard mechanics of materials calculation:

$$NA = \frac{\Sigma E_{x,i} t_i \bar{y}_i}{\Sigma E_{x,i} t_i} \tag{3-49}$$

The influence of the neutral axis shift on the inertia properties is negligible and is not accounted for in the analysis. A .635 cm (0.25 in) shift, representing the carbon acting 76% less stiff in compression, results in a less than 1% change in inertia values.

3.2.2 Strength Properties

The out-of-plane strength in the z-direction (Z_t) is assumed to be the maximum σ_z at the critical glass carbon interface at failure. The average moment capacity of the beam is used in the previously defined stress analysis yielding Z_t. The strength values are summarized for the different methodologies in Table 3- 4

Table 3- 4: Summary of predicted strength values at the critical interface

	Strength Values Z_t kPa (psi)	
Model	1 Smeared Ply	4 Smeared Plies
Minimization of Energy	2470 (358)	683 (99)
Primitive Delamination Model	1700 (246)	1500 (218)

3.2.3 Prediction of Remaining Strength

For the analysis, the strength reduction of the beam is considered to be uniform and is evaluated with consideration to the stiffness reduction of the bottom flange until the onset of delamination. This selection was made since fatigue is assumed to initially occur in the tensile bottom flange due to in-plane effects. Based on the increased curvature and stresses from the reducing EI_{eff} value, the remaining strength of the beam is then predicted using the following expression [61] :

$$Fr = 1 - \{\int_0^n (1 - Fa)^{1/j} \frac{dn}{N_{fail}}\}^j \qquad (3\text{-}50)$$

In Equation 3-50, the *Fr* term represents the percentage of the strength remaining due to the loading over *n* cycles. *Fa* is a failure criteria selected for a given system, and will be further defined for the ply-level and sublaminate level reduction schemes. The parameter *j*, is a material parameter, which is taken to be 1.2, based on experimental curve fits from characterizing a similar material [63]. The value of N_{fail} represents the predicted number of cycles to failure at a given load level, and is therefore a function of *Fa*. N_{fail} is taken from coupon fatigue data [18].

3.2.3.1 Failure Criteria for Sub-Laminate Level Reduction

For each sublaminate, a value *Fa* is calculated based on the in-plane tensile loading in the sublaminate. *Fa* for this application is also a maximum strain criterion, and is defined as

the ratio of the average strain in the laminate to the experimental strain to failure of the respective test laminate summarized above in Table 3- 2 .

$$Fa(n) = \frac{e_{ave}(n)}{e_{\max,\ laminate}} \tag{3-51}$$

The N_{fail} values are then calculated for each respective sublaminate using Equation 3-52, which is directly from the coupon fatigue data by Phifer.

$$N_{fail,sublam} = \left\{ -\frac{1}{c} \ln\left(\frac{Fa(n) - a}{-b} \right) \right\}^{1/d} \tag{3-52}$$

The constants in Equation 3-52 and the strain values they are valid for are in Table 3- 5 :

Table 3- 5: Constants for defining the number of cycles to failure for the sublaminates

	a	b	c	d	Valid for *Fa(n)* >
QI2	1.0000	.82203	15.803	-.43840	.16
CP1	.69202	.55922	142.86	-.61808	.14

Due to the low loading in the tensile flange, relative to the coupon tests conducted, extrapolation of the data was necessary for many of the simulations. At the ultimate moment, the strains are between 26% and 29% of the failure strain values, which is lower than the loading many of the coupon tests were conducted at. The data was linearly extrapolated, on the log scale, and the final piecewise continuous curves are shown in Figure 3- 23 for both types of laminates. The fatigue life is plotted vs the maximum strain criterion, over the range that this analysis will focus on. After N_{fail} is determined for each sublaminate, the limiting, least number of cycles to failure, value is then used to evaluate the remaining strength for the entire beam.

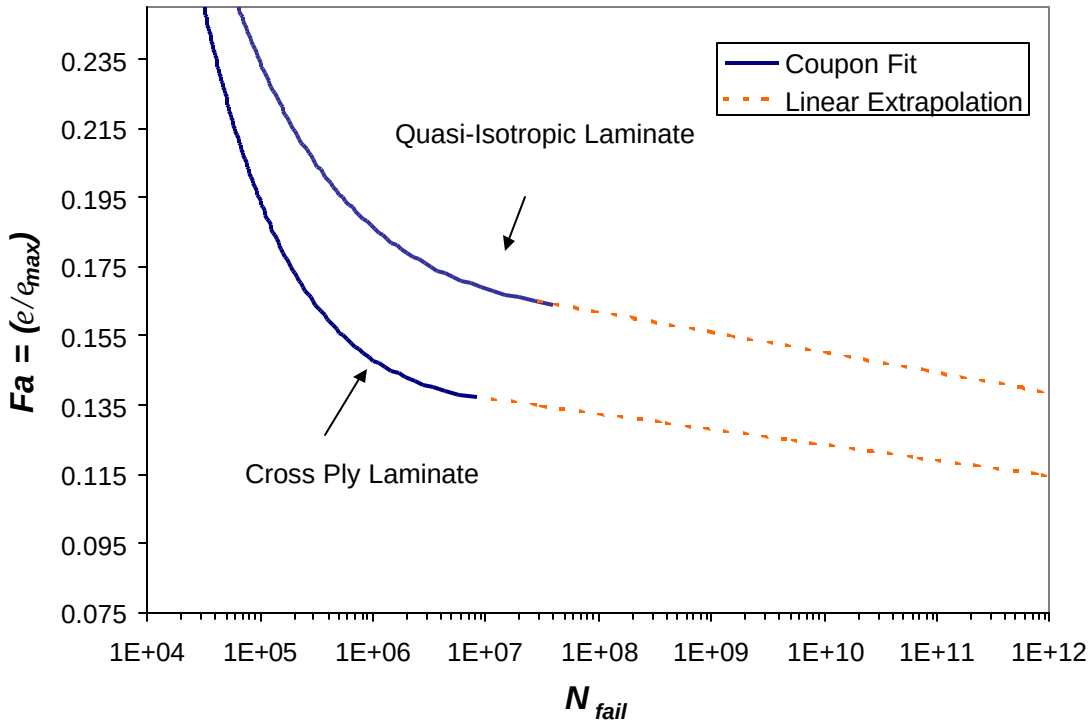

Figure 3- 23: Fit for prediction of number of cycles to failure based on maximum strain criteria

3.2.3.2 Strength Reduction

The analysis is iterative and the reduction can be summed over set increments (Δn) [64]. For each iteration, the Fa and N_{fail} value will change, as the strain values will be gradually increasing. In order to determine the strength reduction, the ΔFr_i must be calculated for the interval and then summed and raised to the j power as shown in Equation 3-54.

$$\Delta Fr_i = (1 - Fa(n))^{1/j} \frac{\Delta n}{N_{fail}(n)} \qquad (3\text{-}53)$$

And the remaining strength in the beam then becomes:

$$Fr = 1 - \left(\sum \Delta Fr_i \right)^j \qquad (3\text{-}54)$$

The Fr value calculated was then considered to be the overall reduction in strength of the beam. Since the beam is considered to degrade uniformly, this reduction will also adjust the Z_t value. Knowing the reduction in strength, the criteria for initiation of delamination can be evaluated.

3.2.3 Delamination and Crack Growth

The quadratic failure criterion was used to predict the onset of delamination in the compression flange. Following the onset of delamination, stiffness reduction of the compressive flange must also be considered with the tensile in-plane effects. These effects are also coupled with the crack growth and propagation to predict the ultimate failure of the beam. The reduction scheme is shown in Figure 3- 24. Once delamination is predicted, the length of the crack can be calculated and compared to the width of the beam. If the crack has fully propagated across the width ultimate failure is assumed, otherwise the stiffness of the top flange is reduced. This stiffness reduction is used in with the continued modulus reduction in the bottom (tensile) flange to determine the neutral axis shift. The new stiffness values and neutral axis location are then used to determine EI_{eff} and κ_x^o that allow for calcuation of the stress state. The drop in stiffness and increase in curvature will inherently raise the stresses and may cause additional failures. The initial crack, and any newly formed cracks, are then monitored and continue through this evaluation cycle until failure.

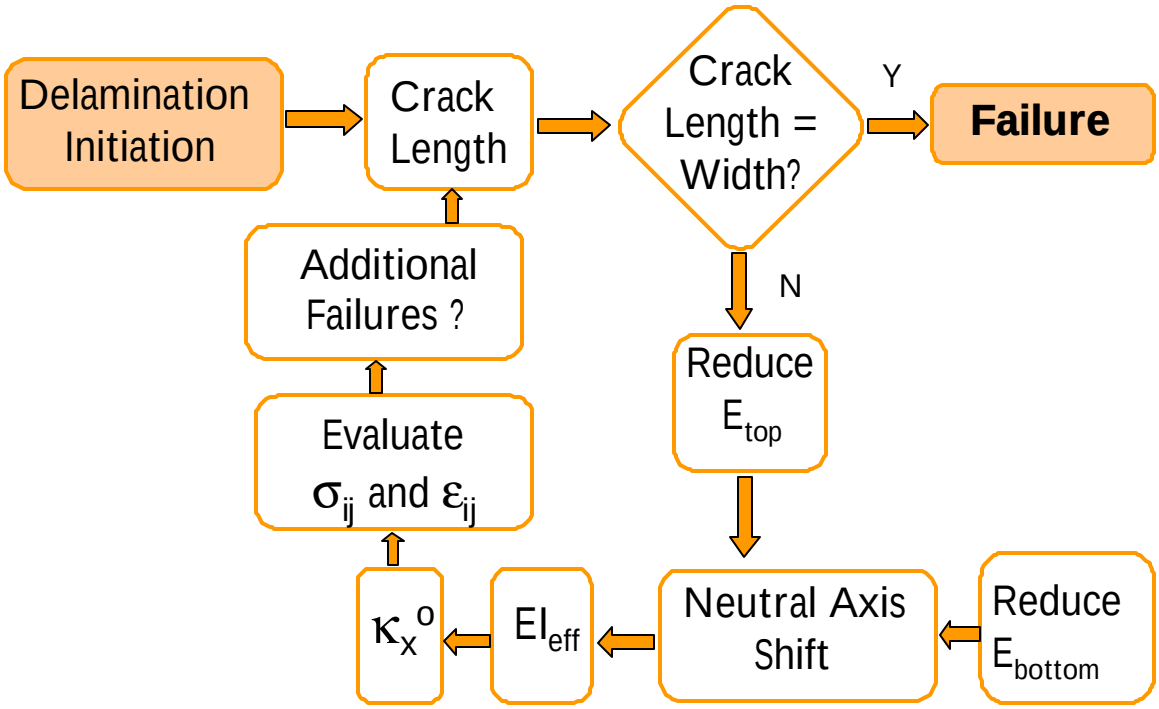

Figure 3- 24: Flow chart of stiffness reduction and stress redistribution following delamination

3.2.3.1 Quadratic Delamination Theory

The Quadratic Delamination Theory proposed by Brewer and Lagace [56] predicts delamination initiation, based on the out-of-plane stresses and strengths. Failure is assumed when Equation 3-55 is satisfied.

$$\left(\frac{t_{xz}}{Z_{xz}}\right)^2 + \left(\frac{s_z}{Z_t}\right)^2 \geq 1 \tag{3-55}$$

The value of τ_{xz} is negligible in this analysis when compared to the matrix strength, allowing the criteria to be simplified. Also, on the assumption that the Z_t strength degrades the same as the in-plane strength, the failure is assumed when:

$$\frac{s_z}{Z_t Fr} \geq 1 \tag{3-56}$$

This essentially becomes a maximum stress criterion in the out-of-plane direction.

3.2.3.2 Compressive Flange Stiffness Reduction and Crack Growth

Once delamination is initiated, indicated by the delamination criterion exceeding 1, further reduction of top flange stiffness needs to be included in the reduction scheme. The new modulus calculations implement a rule of mixtures approach developed by O'Brien [51].

$$E_x = (E^* - E_{lam})\frac{a}{b} + E_{lam} \tag{3-57}$$

In Equation 3-57, a is the crack length of the largest crack in the laminate, b is the half width of the laminate, E^* represents the effective modulus of the laminate if the layers are completely delaminated from each other (Equation 3-59), and E_{lam} is the initial effective modulus value of the laminate. The variables are demonstrated in Figure 3- 25.

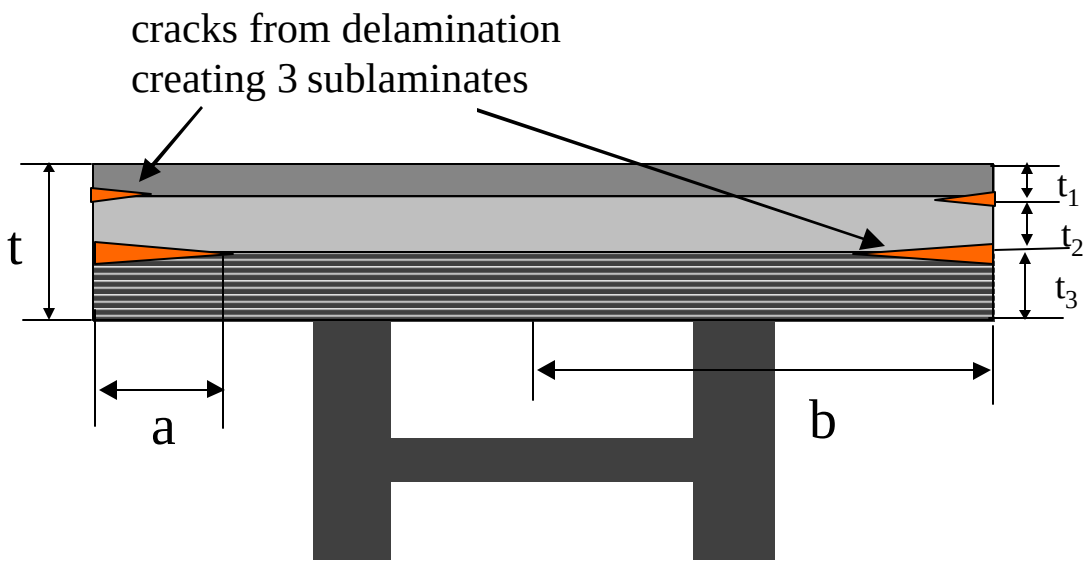

Figure 3- 25: Variable definition for crack growth prediction

Despite the issues discussed above, in accordance with O'Brien's approach, an effective modulus can be calculated using Equation 3-58 where a_{11} is from the inverse ABD matrix and t is the total thickness of the laminate being evaluated.

$$E_{eff} = \frac{1}{a_{11} t} \tag{3-58}$$

The rule of mixtures is used to determine E* :

$$E^* = \frac{\sum E_{x,i} t_i}{t} \tag{3-59}$$

where $E_{x,i}$ and t_i represent the effective modulus and thickness of the sublaminates formed by the cracks (See Figure 3- 25).

3.2.3.3 Crack Growth

Once delamination initiates, crack growth is considered symmetric from each free edge of the beam. O'Brien has shown a good estimation of crack growth is based on the relation [51-54]:

$$\frac{da}{dn} = \left(\frac{b}{E^* - E_{LAM}}\right)\left(\frac{dE}{dn}\right) \tag{3-60}$$

dE/dn is the change in modulus over the step size, all other terms are consistent with their definitions above. The crack growth rate (*da/dn*) is not constant, since it is dependent on the number of layers that have delaminated at a given time, thus as more layers delaminate, the rate of crack growth increases.

3.2.3.4 Determining Failure of the Beam

The model predicts failure due to in-plane effects and also due to delamination. Failure is assumed when either of the following criteria are met:

1. The crack completely propagates across the width of the beam
2. The remaining strength of the beam matches the loading (*Fa=Fr)*.

CHAPTER 4: ANALYTICAL RESULTS

The results of model developed in Chapter 3 will be discussed in this chapter. The model will be compared to experimental results in Chapter 5, the purpose of this chapter will be to understand how the parameters in the model effect the predicted fatigue life and failure mode. S-N curves were developed by running the model at numerous load levels, and are then compared to understand the important parameters in the model.

4.1 Life Prediction Model Output

Regardless of the strength values used or the method to predict σ_z the program always predicts out-of-plane failure prior to in-plane tensile failure of the bottom flange. The results shown are typical and are used to demonstrate the program output. The plots are from an input load of 58% of the ultimate moment, using the Minimization of Energy approach to solve for σ_z, and one ply to represent the webs and flange.

Using the MRLife methodology, failure will occur at the intersection of the remaining strength curve and the applied load curve. In Figure 4- 1 both the out-of-plane stress criteria and in-plane maximum strain criteria are shown with the remaining strength curve. For this case, delamination occurs at 401,000 cycles, the intersection of the curves. Ultimate failure is at 404,500 when the crack has propagated across the entire width of the beam. The crack growth is shown in Figure 4- 2. The points on the plot are over equal intervals, thus the rate of crack growth increases, as further stiffness is lost. At the load considered here, there is a 2% loss in modulus in the tensile flange over the first 50,000 cycles (Figure 4- 3). There is no loss in stiffness in the top flange until delamination, followed by a sudden drop in the modulus. These modulus changes are reflected in the neutral axis location, which shifts toward the stiffer flange as demonstrated in Figure 4- 4

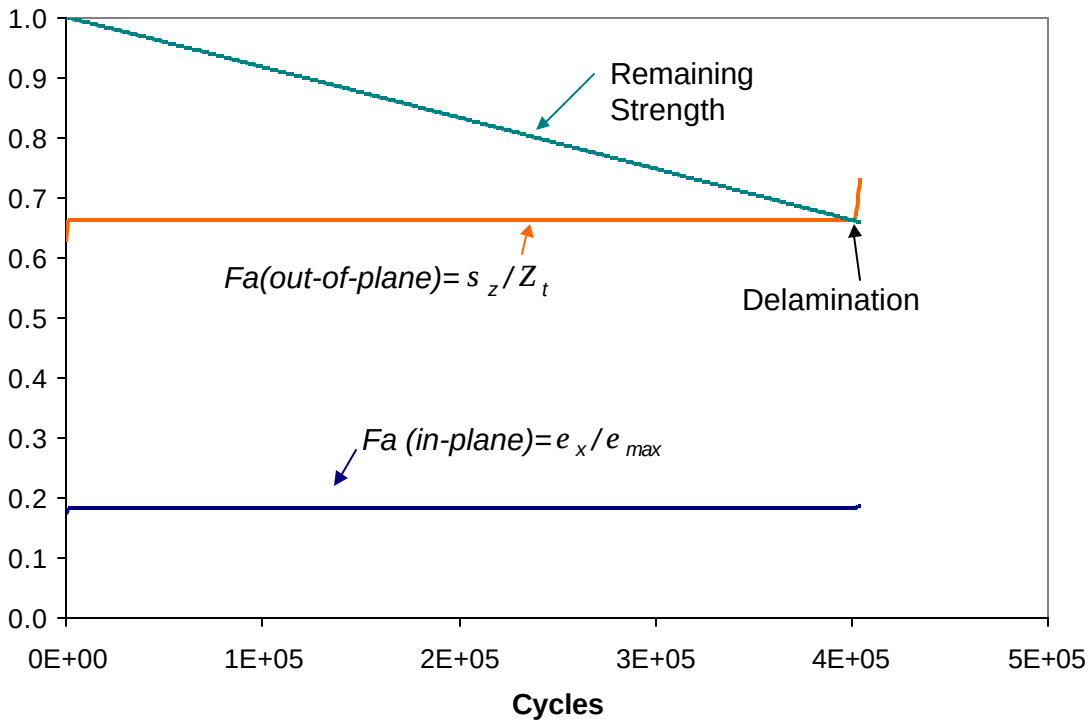

Figure 4- 1: MRLife plot of remaining strength and in-plane and out-of-plane normalized loading

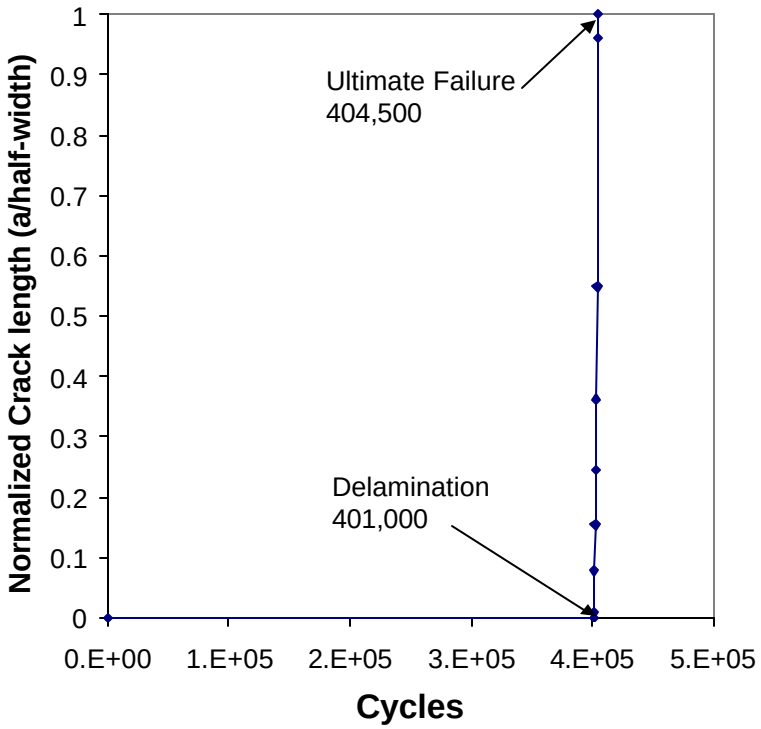

Figure 4- 2: Crack growth in the top flange following delamination initiation

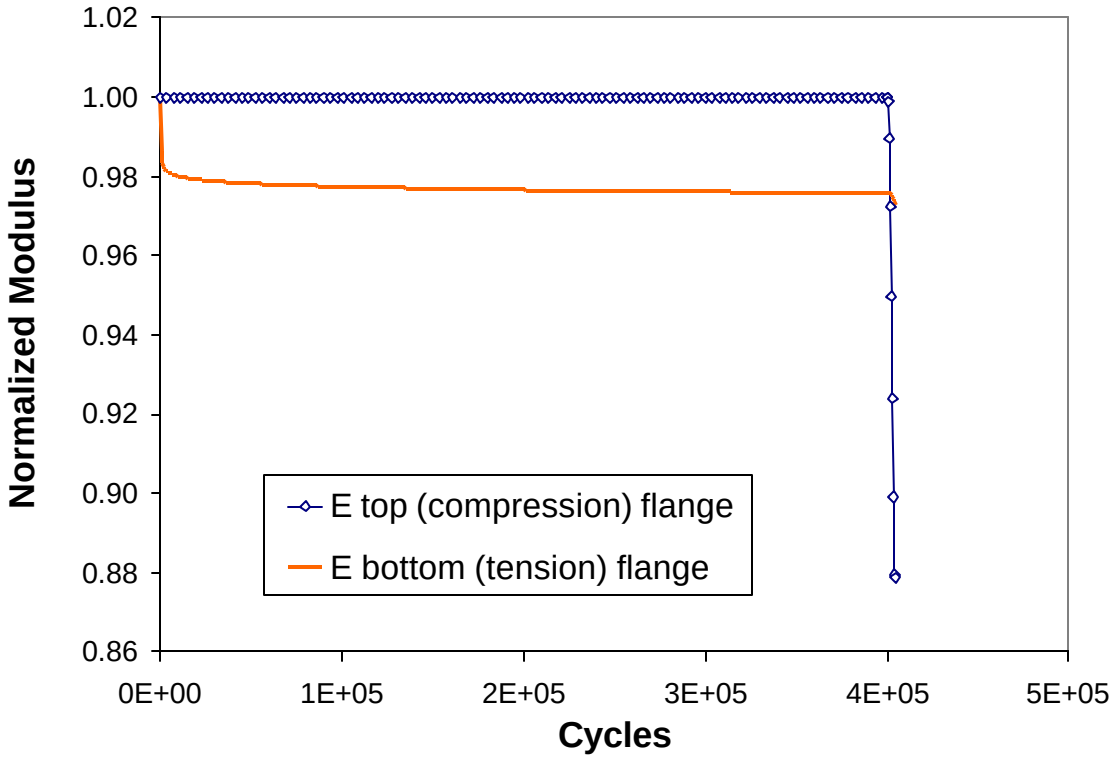

Figure 4- 3: Top and bottom flange stiffness reduction, normalized to the initial stiffness

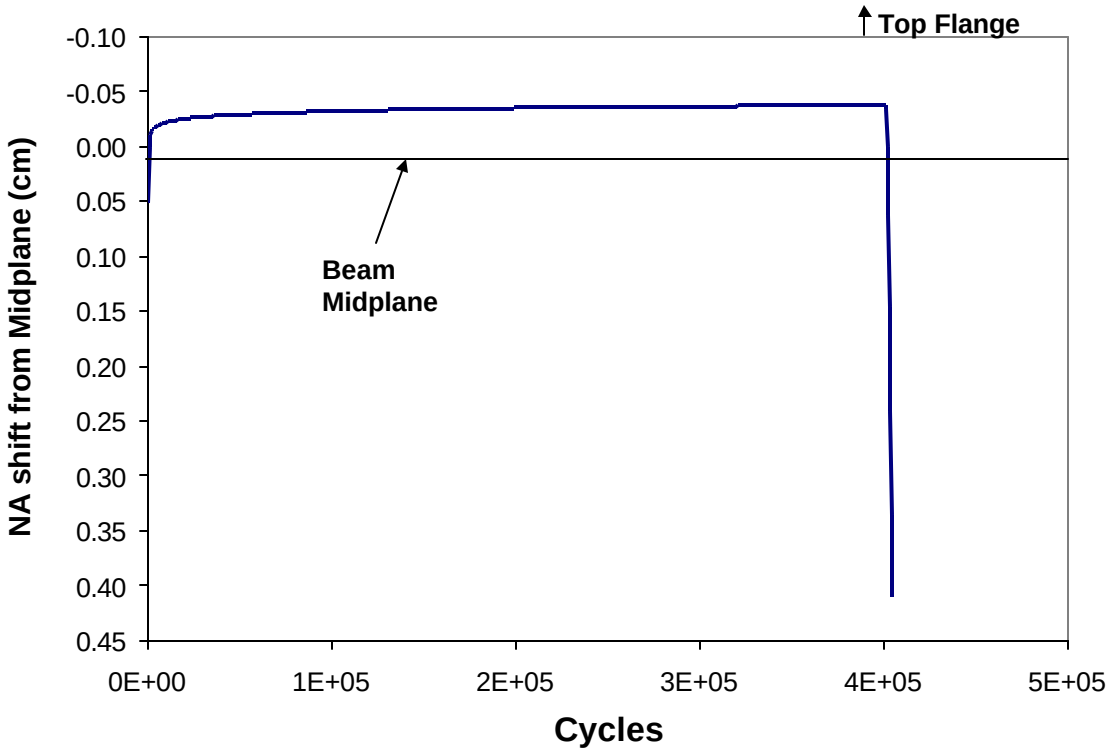

Figure 4- 4: Neutral Axis Shift from the midplane predicted by the life prediction model

4.2 Model Comparison Using Calculated Strength

The strength values (Z_t) were calculated for each model based on the average M_{ult} found in experimental testing of all the beams. The four different out-of-plane strengths are summarized in Chapter 3. When the calculated strength values are used in their respective models, as expected, the same S-N curve is attained for the beam. The coincident curves are plotted in Figure 4- 5. The matching results occur because this technique normalizes out the different strengths in the failure criterion which is a ratio of σ_z to Z_t. Attaining the same S-N curve using the calculated strength values confirms that the model is consistent in the life prediction calculations. Additionally, if a strength value is calculated for a model from the M_{ult} of the beams, the use of any model and its respective strength can be used without altering the life prediction.

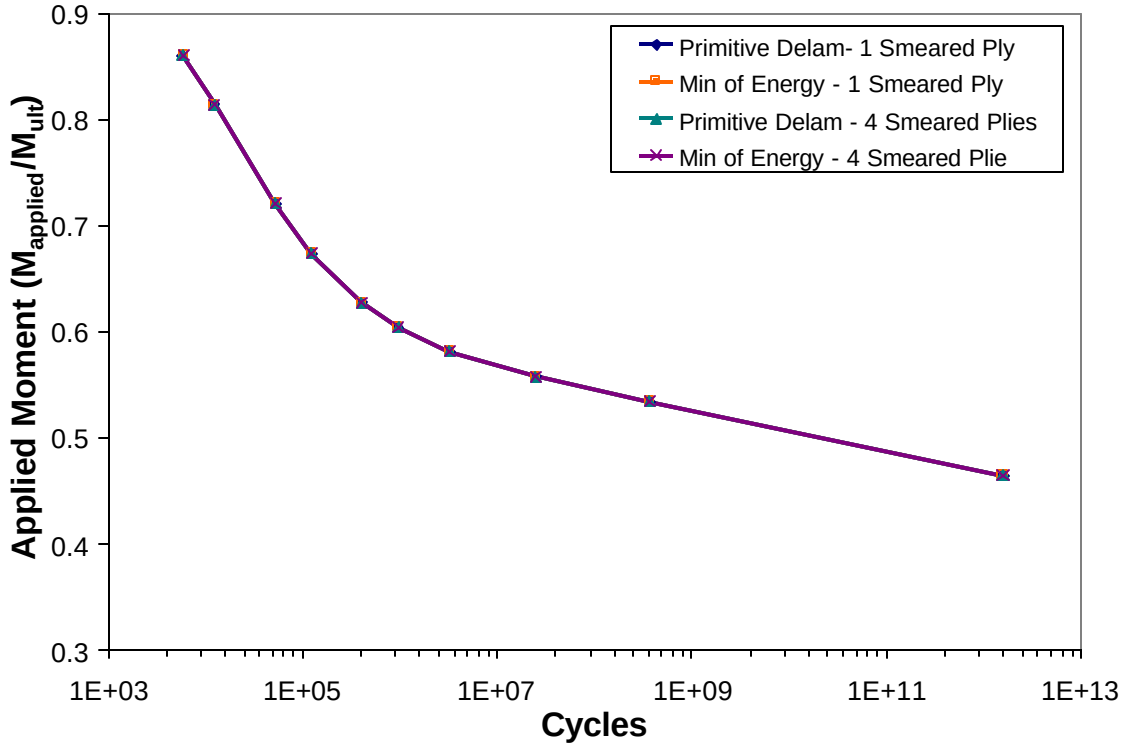

Figure 4- 5: Comparison of S-N curves for different methods of calculating s_z and approximating the effective stiffness

4.3 Model Sensitivity to Strength Value

The data by Garcia [23] on the strength of the top flange was then used with the four combinations as the Z_t value. Figure 4- 6 shows the S-N curves using this approach and compares them to the curve developed from the calculated Z_t. The energy method curves using the experimental data deviate from the prior calculations (dashed line in the plot) more than the curves found using the primitive delamination model. This is the result of the calculated strength values for the method being closer to the experimental strength. The percent change in strength values are compared to the percent change in life in Table 4- 1 for four different loads. The change in life is both a function of the change in strength value and the loading applied.

Table 4- 1: Influence of strength value on the fatigue life

% change Z_t	% change life 46% M_{ult}	% change life 58% M_{ult}	% change life 63% M_{ult}	% change life 81% M_{ult}
-23%	-27%	-34%	-57%	-98%
12%	10%	13%	21%	65%
27%	19%	25%	40%	125%
179%	58%	75%	122%	378%

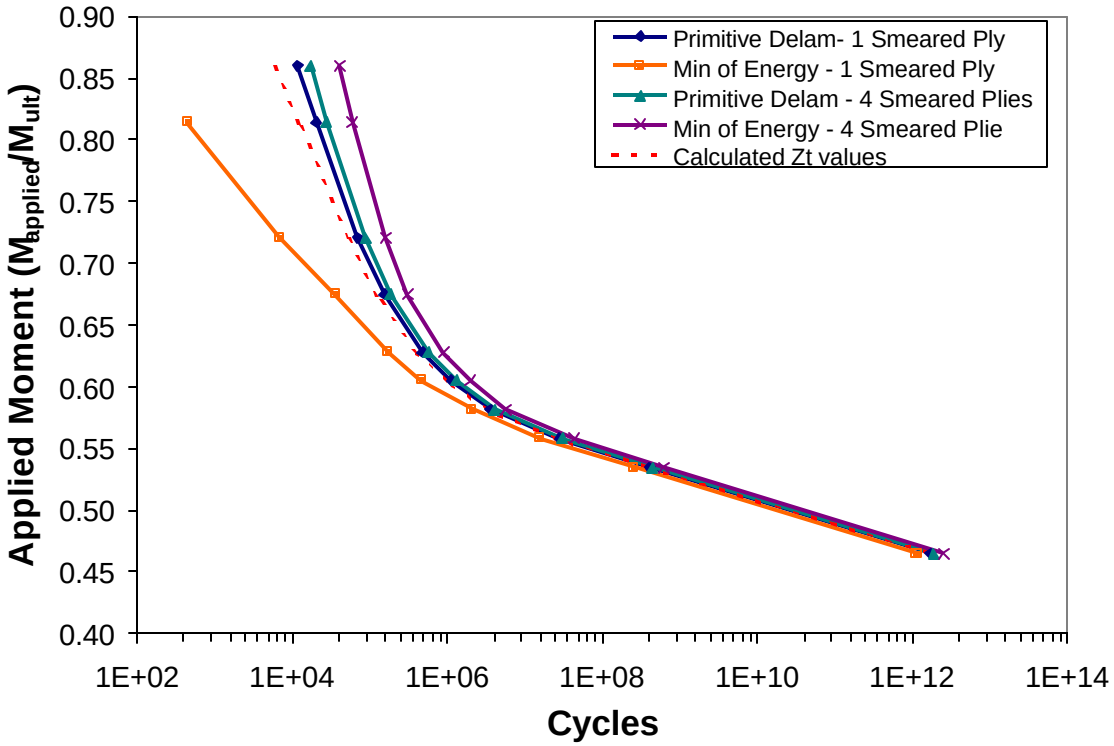

Figure 4- 6: S-N curves developed using the experimental out-of-plane strength value

4.4 Influence of Neutral Axis on Life Prediction

The influence of an initial neutral axis offset is investigated for the model based on using the Primitive Delamination Model and 1 smeared ply. Three cases are considered, where the neutral axis is initially shifted toward the bottom tensile flange, as often seen experimentally:

1. Increasing the carbon stiffness in the tensile flange by 10%
2. Decreasing the carbon stiffness in the compression flange by 10%
3. Increasing the carbon stiffness in the tensile flange by 5% and decreasing the carbon stiffness by 5%

The resulting S-N curves are shown in Figure 4- 7, where the dashed line is the nominal value. The prediction is dominated by the properties of the tensile flange. Any increase

in stiffness in the tension flange increases the predicted life, even with the compression flange degraded. Additionally, the shift in the S-N curve for an increase in the tension flange is greater than the shift in the opposite direction for a degradation of equal magnitude in the compression flange.

The shift in the neutral axis for all of the cases is plotted at 63% of the ultimate moment in Figure 4- 8. The higher the effective modulus of the tensile flange, the more gradual the shift in stress is to the top flange, increasing the life. Figure 4- 9 demonstrates the influence of the in-plane *Fa* value on the remaining strength curve. The slight differences in *Fa* result in a large change in the slope of the remaining strength curves also controlling the life prediction..

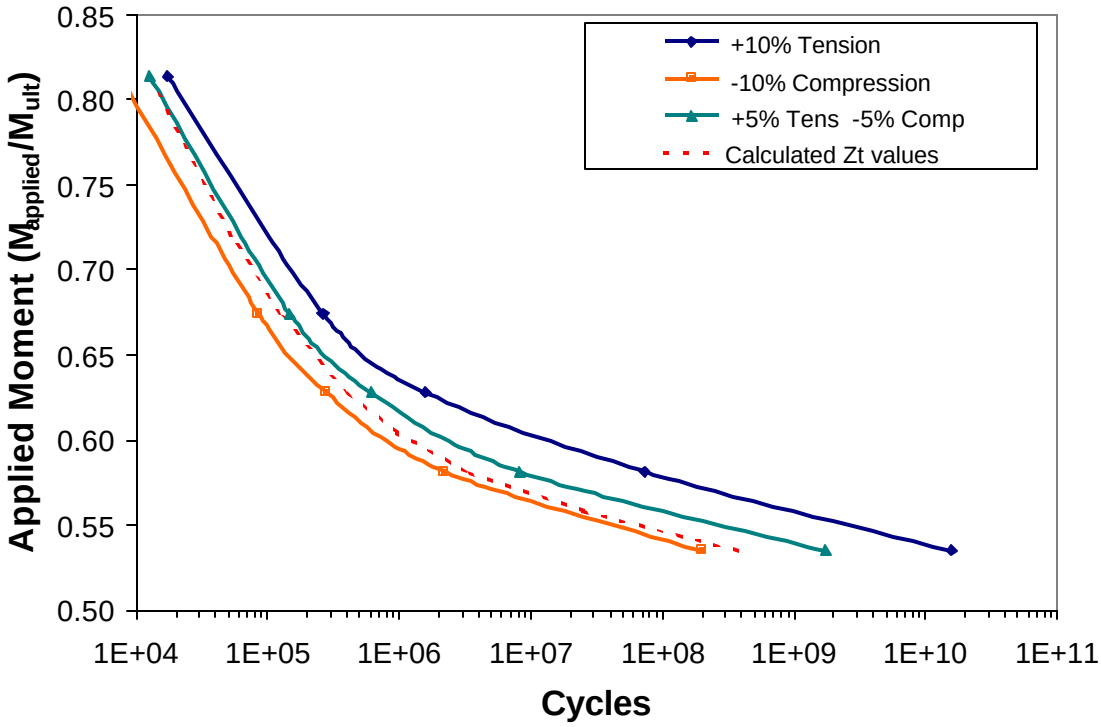

Figure 4- 7: Comparison of Life prediction for different carbon stiffness values

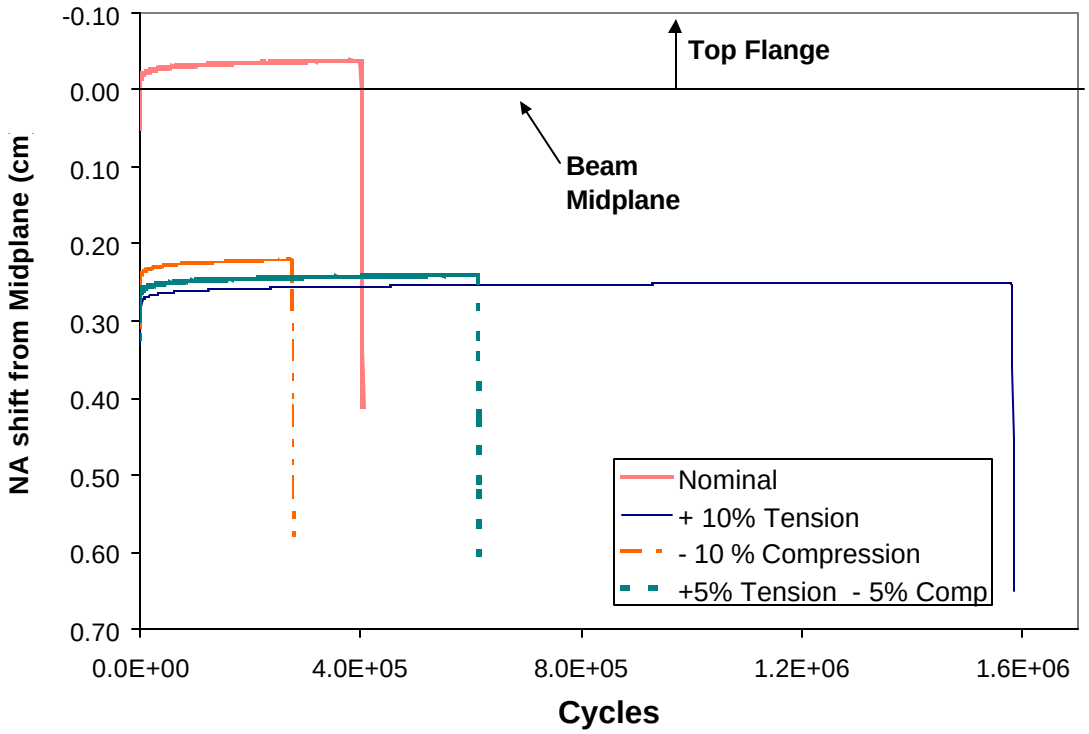

Figure 4- 8: Comparison of the neutral axis shift for different carbon stiffness values

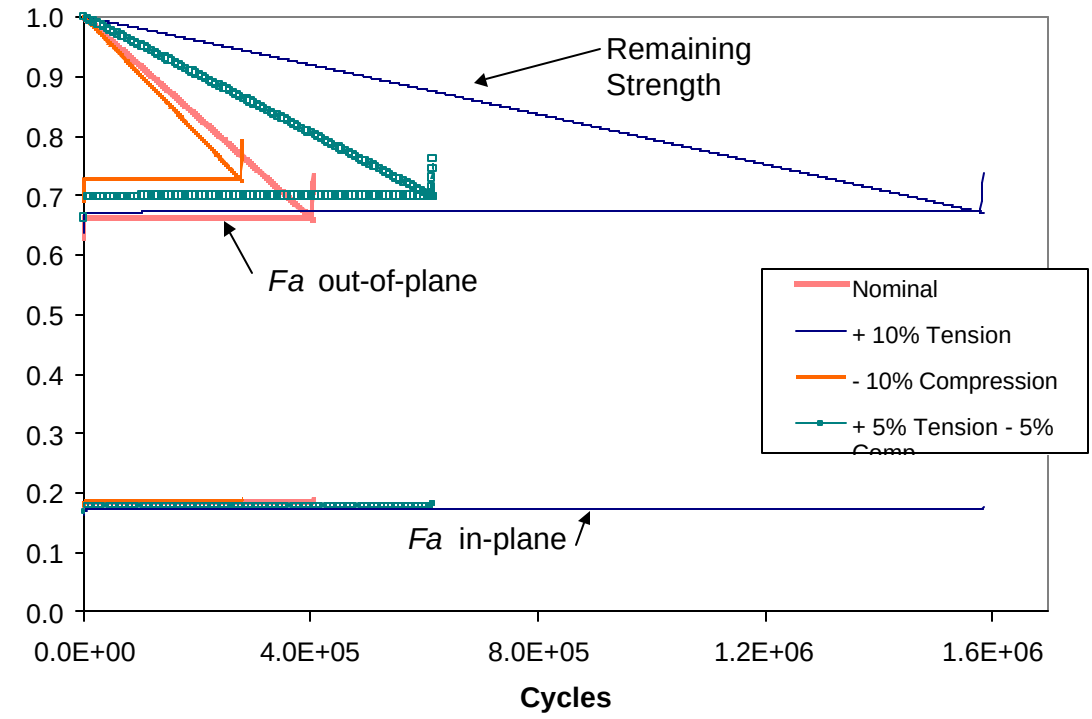

Figure 4- 9: Comparison of reamaining strength curves for different carbon stiffness values

4.5 Summary

The program output gives reasonable results and suggests that delamination is the controlling failure mechanism, and in-plane fiber failure will not occur prior to failure of the top flange. The calculated neutral axis shift and stiffness reductions follow the anticipated trends.

The sensitivity of the model to several parameters was investigated. The predicted life is not sensitive to the method used to calculate σ_z or the number of plies used to mimic the webs and internal flange. The strength value used in the model becomes of greater importance at higher loads; a slight change in the value can result in a large change in the life predictions at loading over 75% of the ultimate moment. Finally the model indicates that the life is controlled by the stiffness of the tensile flange. An increase in stiffness of the tensile flange (or a neutral axis shift toward the tensile flange) even with a decrease in the properties of the compression flange will shift the S-N curve right, increasing the life. The tensile flange stiffness controls the redistribution of stresses and also the slope of the remaining strength curve.

CHAPTER 5: COMPARISON OF ANALYTICAL AND EXPERIEMENTAL RESULTS

In order to validate the analytical ideas developed in Chapters 3 and 4 the calculated values must be compared to experimental results. The comparison of these values will be shown in the sections that follow

5.1 Comparison to Laminated Beam Theory

Laminated beam theory was used to predict the stiffness, deflections and strain values for the beam under four-point bend loading. Using this method to predict the beam response assumes and ideal case where plies are of uniform thickness and do not have any ply waviness. In reality, manufacturing of the section by pultrusion results in plies with varying thicknesses and flaws such as fiber undulation. Despite the simplification used in the analysis, the effective stiffness values compared well as shown in Table 5- 1.

Table 5- 1: Comparison of predicted and experimental stiffness values

	EI_{eff} (MPa-m^4)	EI_{eff} (Mpsi-in^4)	% error (data-prediction)/data * 100%
Prediction	**2.41**	**841**	
400 Series (14 ft)	2.29	798	-5.39 %
500 Series (20 ft)	2.45	855	1.58 %
Average	2.37	826	-1.78 %

The mid-span deflection, calculated using beam theory was then compared to experimental results. The calculations do not account for shear deformation, and are therefore conservative as seen in Figure 5- 1. The average error between the calculated values and the prediction is 9.52 %, which is the same as the shear contribution to deflection found in the fatigue test. The experimental points shown are from the quasi-

static tests to failure and initial readings on the beams that underwent fatigue. This includes data from both batches of beams.

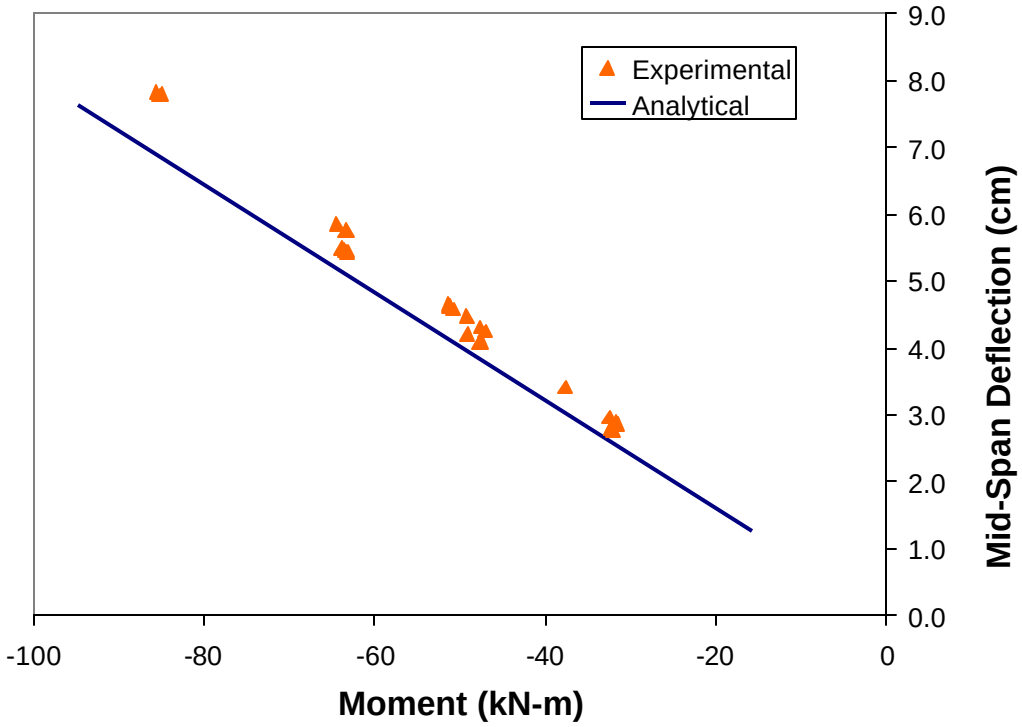

Figure 5- 1: Comparison of predicted and experimental mid-span deflection values

The axial strain values measured at the mid-span of the beam (ε_x) at both the top and bottom of the beam were compared to the predicted CLT strain values (Figure 5- 2 and Figure 5- 3). The experimental points shown are from the same samples as the deflection data was taken from. The correlation between these values is excellent.

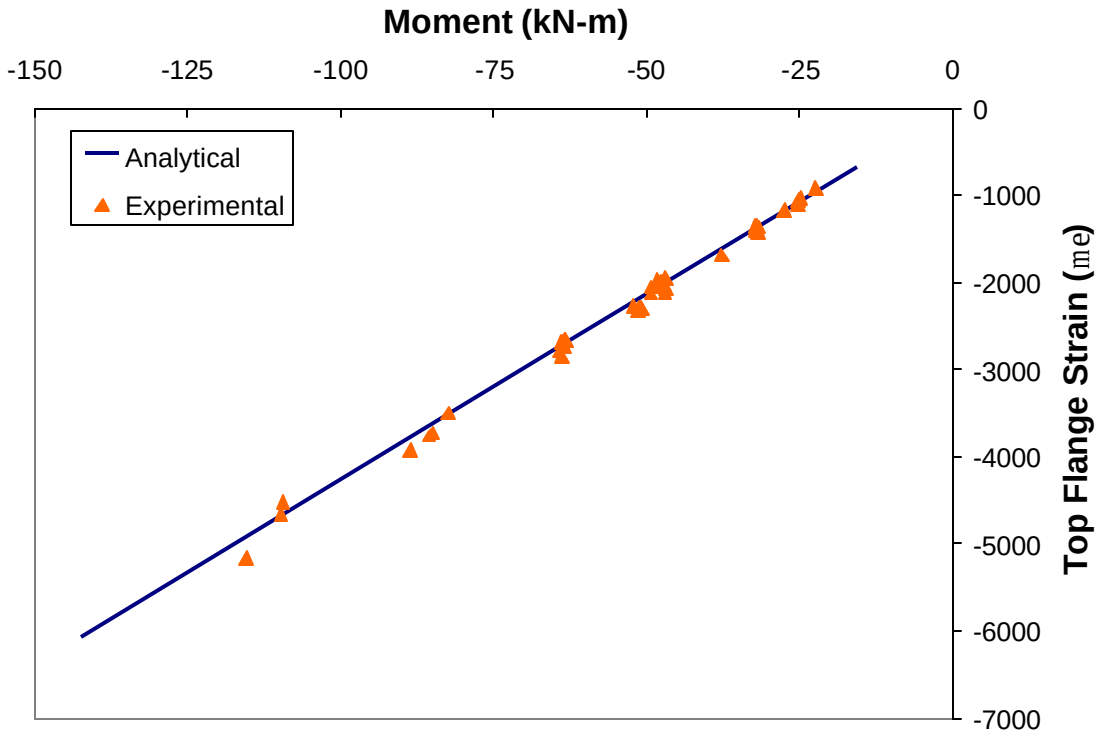

Figure 5-2: Comparison of predicted and experimental axial top flange strain values

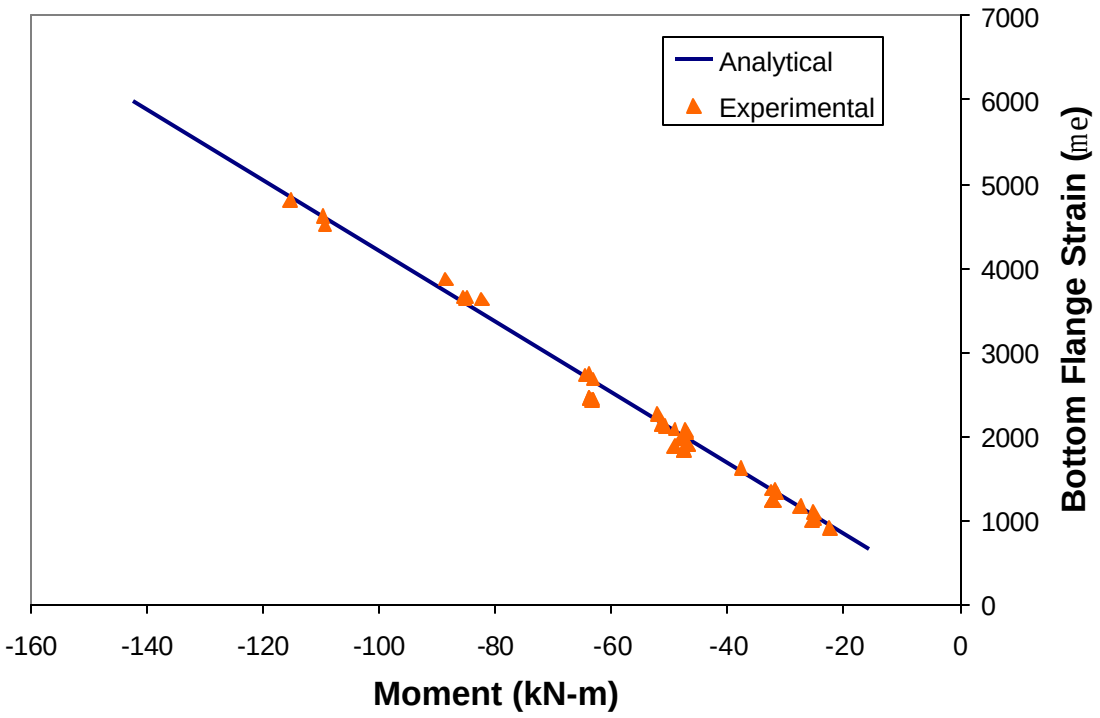

Figure 5-3: Comparison of predicted and experimental axial bottom strain values

5.2 Out-of-Plane Stresses

The prior testing by Garcia, discussed in Chapter 1, resulted in a Weibull out-of-plane strength of the specimens of 1900 kPa (276 psi). The failure was at the first carbon-glass interface from the midplane. The stresses at this interface at the failure moment for the two batches are summarized in Table 5- 2. The predictions are in reasonable agreement with the tested strength values, and encourage the use of these simple models. The use of one smeared ply for both models gives a better approximation to the strength value seen in the test.

Table 5- 2: Summary of predicted strength values at the carbon-glass interface for each series of beams

	Primitive Delamination Model		Minimization of Energy	
	1 Smeared Ply kPa (psi)	4 Smeared Plies kPa (psi)	1 Smeared Ply kPa (psi)	4 Smeared Plies kPa (psi)
400 Series	1760 (255)	1550 (225)	2540 (369)	703 (102)
500 Series	1250 (182)	1110 (161)	1820 (264)	503 (73)

The prediction for the all glass beams was also examined at the ultimate loading under four-point bend. The predicted value using the primitive delamination model with four smeared plies is 3658 kPa (530 psi), at the same interface. This is reasonable agreement with the known value of over 2100 kPa (300 psi).

5.3 Life Prediction comparison

An S-N curve was created based on the average failure moment from the 14 ft and 20 ft quasi-static tests. The predicted curve is calculated using the Primitive Delamination

Model for σ_z and the calculated value for Z_t at the ultimate moment of 120 kN-m (88.7 kip-ft). No neutral axis shift was considered, based on the average data for the beams.

The experimental points and the predicted S-N curve are plotted in Figure 5- 4 normalized to the average ultimate moment of all of the hybrid beams tested from both batches. The beam failure at 53% (Beam #425) is about 6 orders of magnitude from the prediction. The two beams (#514 & #421) which experienced runout at 8 and 10 million cycles were under the predicted failure. Beam #517 failed at 370,000 cycles at 71% of the ultimate moment agrees well with the prediction of 300,000 cycles at the same load. Without further data, the validity of the model overall cannot be determined.

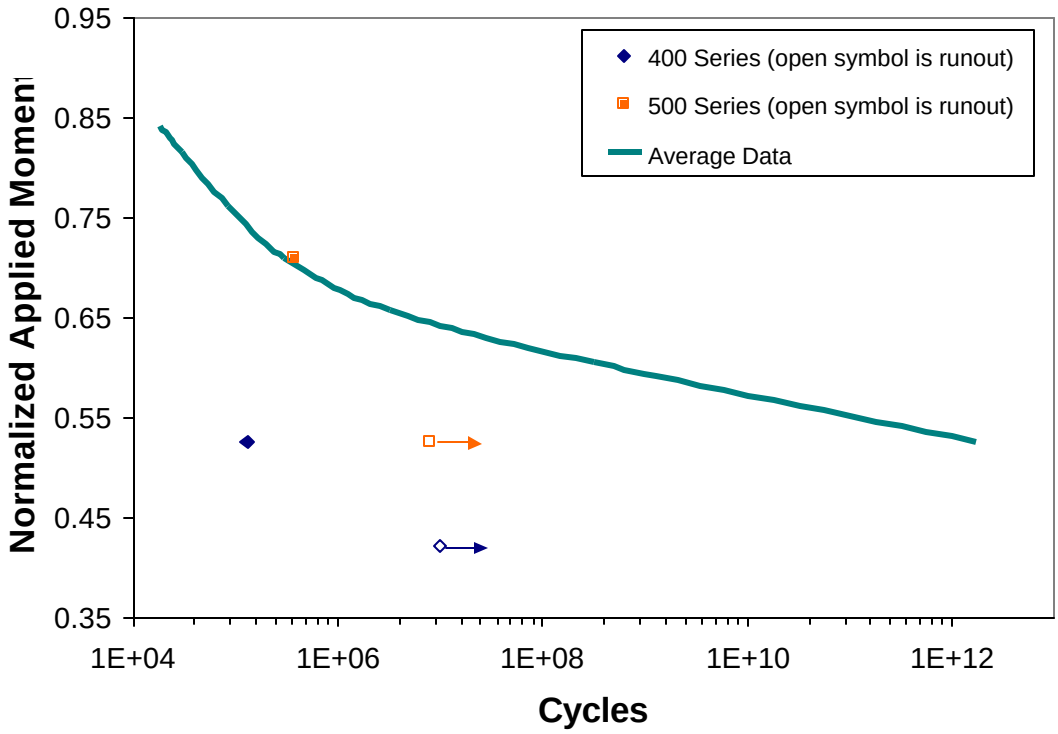

Figure 5- 4: Comparison of predicted S-N curve to experimental data

5.4 Comparison of Prediction to Beam #517

The overall life prediction of Beam #517 based on average strength values had excellent agreement. The correlation between the model at the experimental data is looked at in further detail below. The results shown account for the initial neutral axis shift of the beam. Experimental results indicate this shift was 0.14 cm (.055 in) toward the tensile flange. Since the 500 series is stiffer than the overall average, the shift was attained by increasing the stiffness of the carbon by 6.0% in the tensile flange, rather than decreasing the stiffness of the carbon flange. The strength value was calculated based on the ultimate moment of the batch, 101 kN (74.6 kip-ft). The resulting remaining strength plot is show in Figure 5- 5. Using these inputs the predicted life is 265,000 cycles. This life is shorter than the prediction using the average data. The increase in stiffness and decrease in the in-plane *Fa* values did not offset the decrease in strength and increase in the out-of-plane *Fa*, thus predicting a shorter life. These trends are identified in Figure 5- 6.

The modulus values, normalized to their respective initial stiffness are compared in Figure 5- 7. The initial reduction in the tensile flange matches well, although the model does not predict any reduction in the compression flange, which experimentally reduces about 1%. The final stiffness after delamination, is predicted based on different flanges, but is about 89% of the initial stiffness in both cases. The compression flange stiffness experimentally can not be determined once the flange fails, because the gage is in the buckled zone. In the model, the final stiffness is controlled by the compression flange. The shift in neutral axis is related to the changes in relative stiffness and compared in Figure 5- 8. The model under-predicts the shift, but captures the region of the most change. Finally, the deflection values are compared. The model does not account for shear deformation, and therefore underestimates the total measured deflection. When compared to the calculated "non-shear" deformation (as discussed in Chapter 2), the prediction matches the data, including the final increase in deflection after failure.

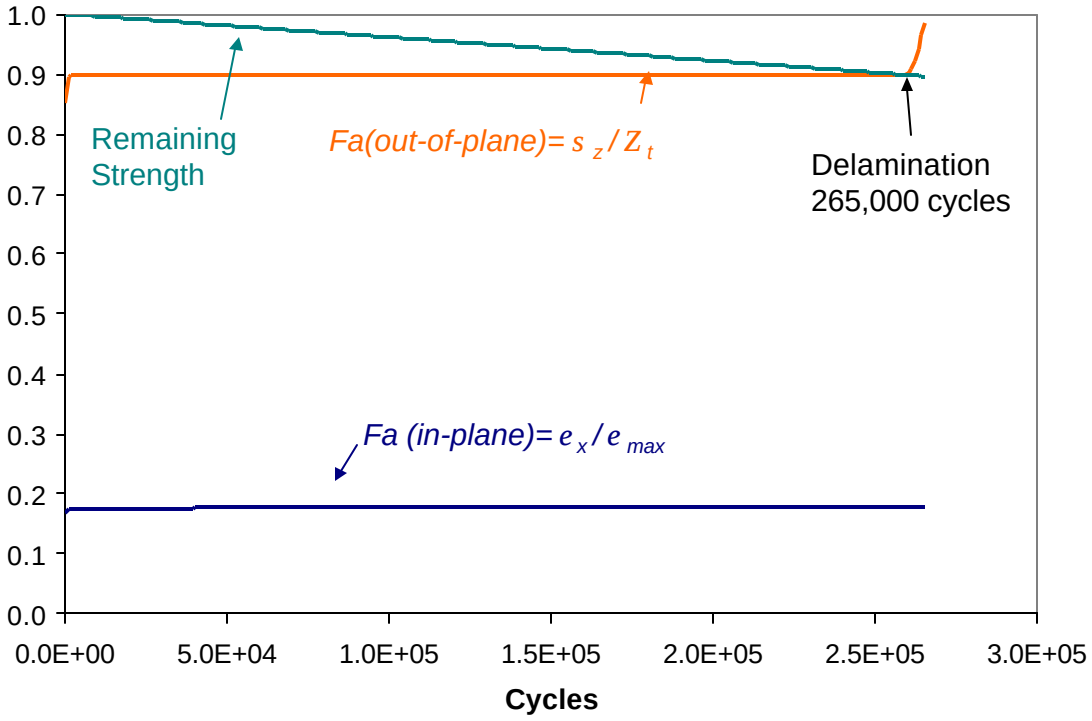

Figure 5- 5: Remaining strength plot for Beam #517 using batch properties

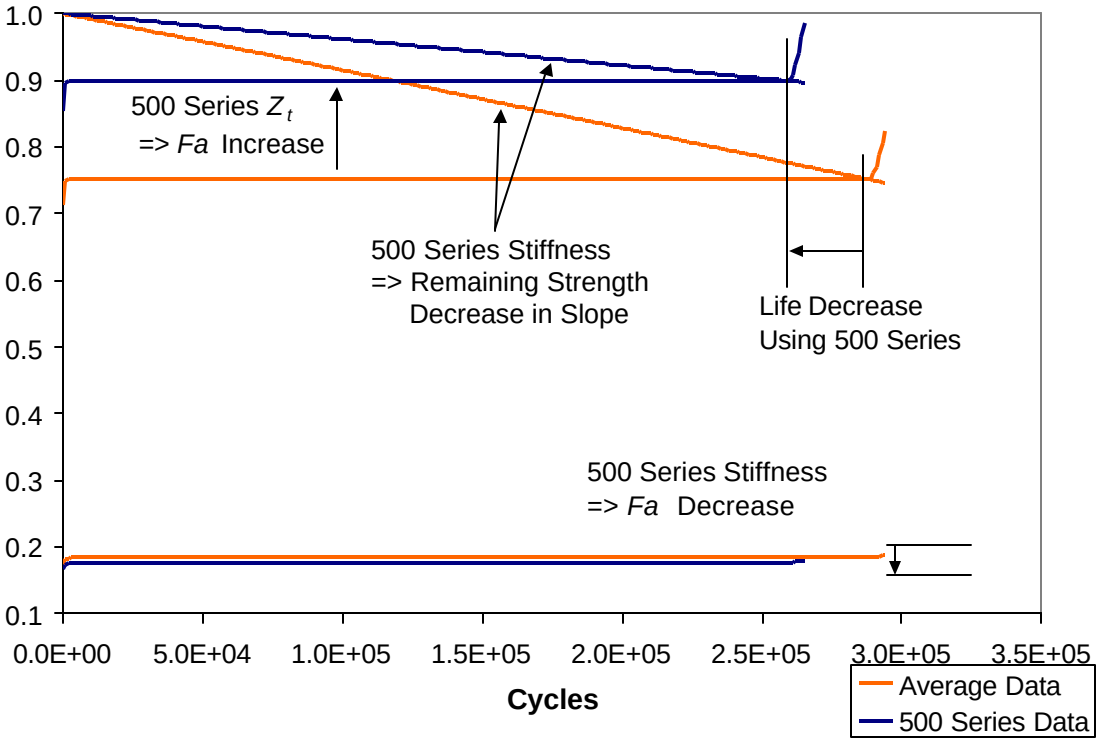

Figure 5- 6: Life Prediction comparison for Beam #517 using average and batch M_{ult} data

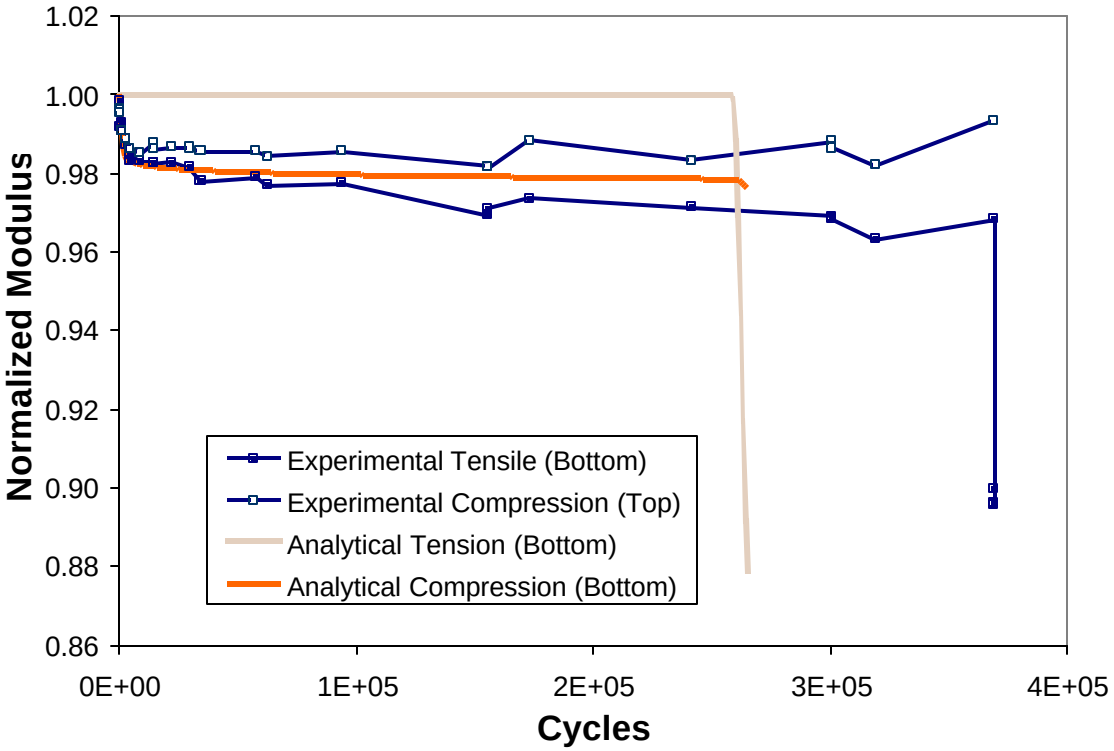

Figure 5- 7: Comparison of predicted stiffness reduction to experimental results for Beam #517

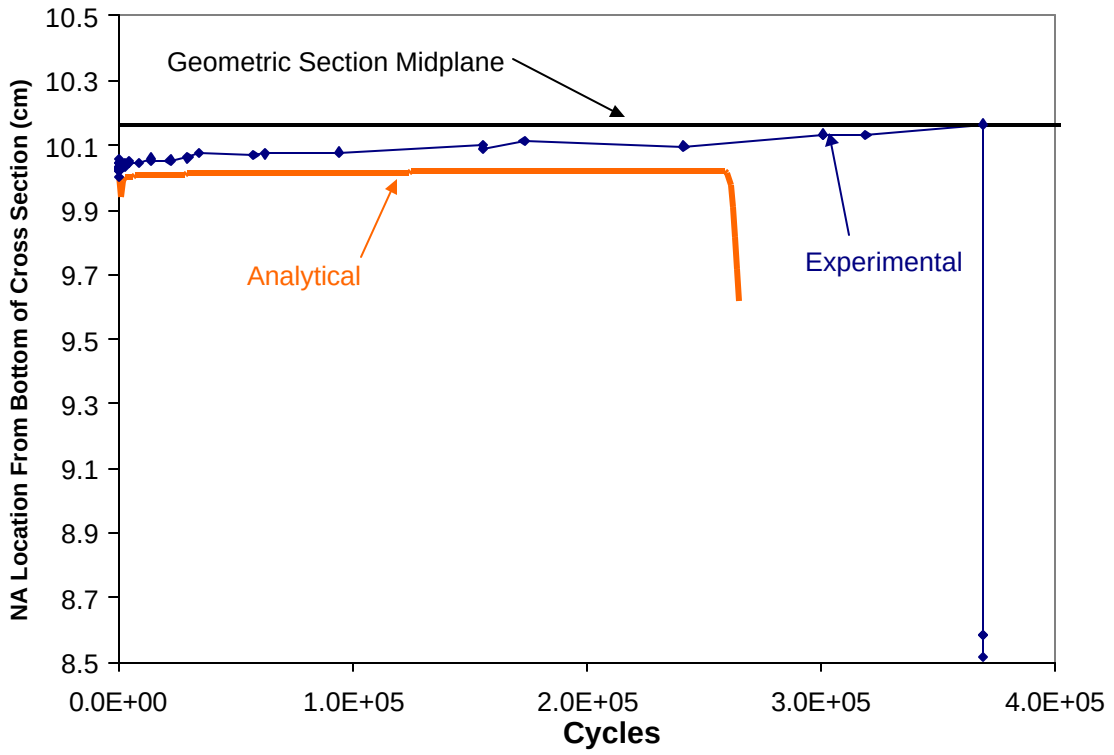

Figure 5- 8: Comparison of the predicted and experimental neutral axis shift for Beam #517

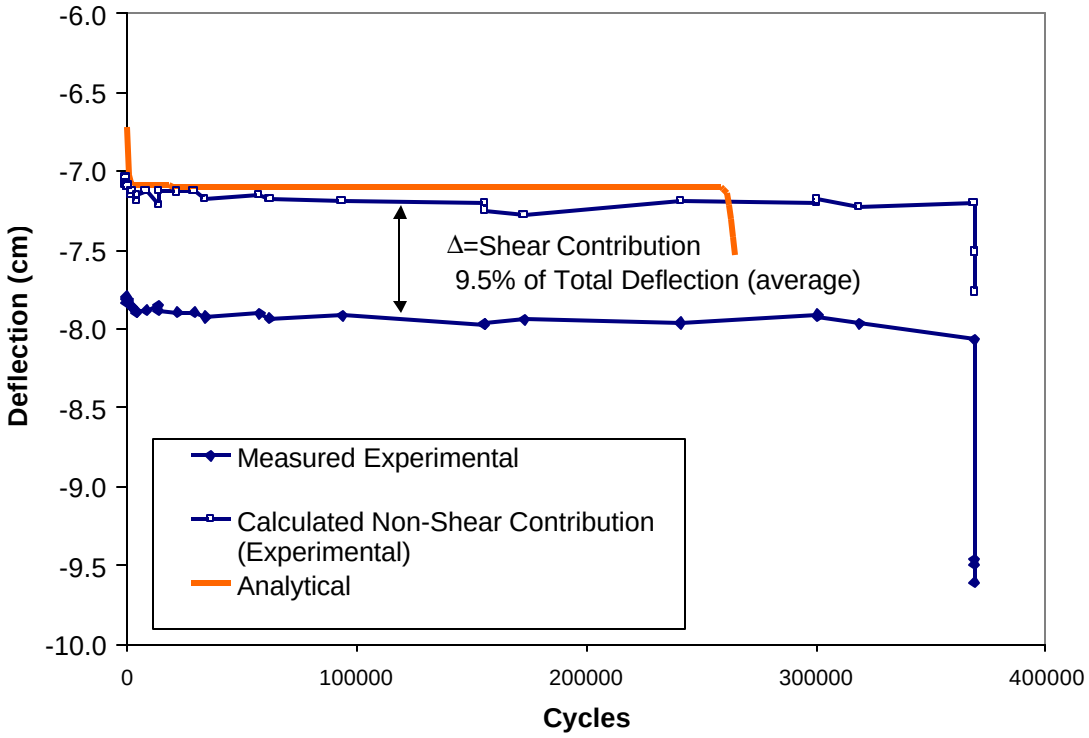

Figure 5- 9: Comparison of the predicted and experimental mid-span deflection for Beam #517

5.5 Comparison of Prediction to Beam #514

The data for Beam #514 is also compared to the model, although not failed in fatigue. The initial neutral axis shift of the beam is accounted for based on the experimental shift of 0.44 cm (.173 in) toward the tensile flange. As in the comparison above, the shift was attained by increasing the stiffness of the carbon in the tensile flange, for this case by 18.0%; and the strength value was calculated based on the ultimate moment of the 500 series. The model predicted a life of greater than 10^{11} cycles under these conditions.

The beam response is compared over 8 million cycles between the experimental results and the analytical model. The modulus values, normalized to their respective initial stiffness are compared in Figure 5- 10. The model predicts a negligible amount of stiffness reduction in either flange, which does not match well with the actual data. This may be the result of the lack of tensile coupon data at this loading, and the linear

extrapolation used to determine the stiffness reduction. Because of the lack of stiffness reduction, the shift in neutral axis is also very slight (Figure 5- 11). The deflection data, as before agrees with the non-shear portion of the deformation, exhibited in Figure 5- 12.

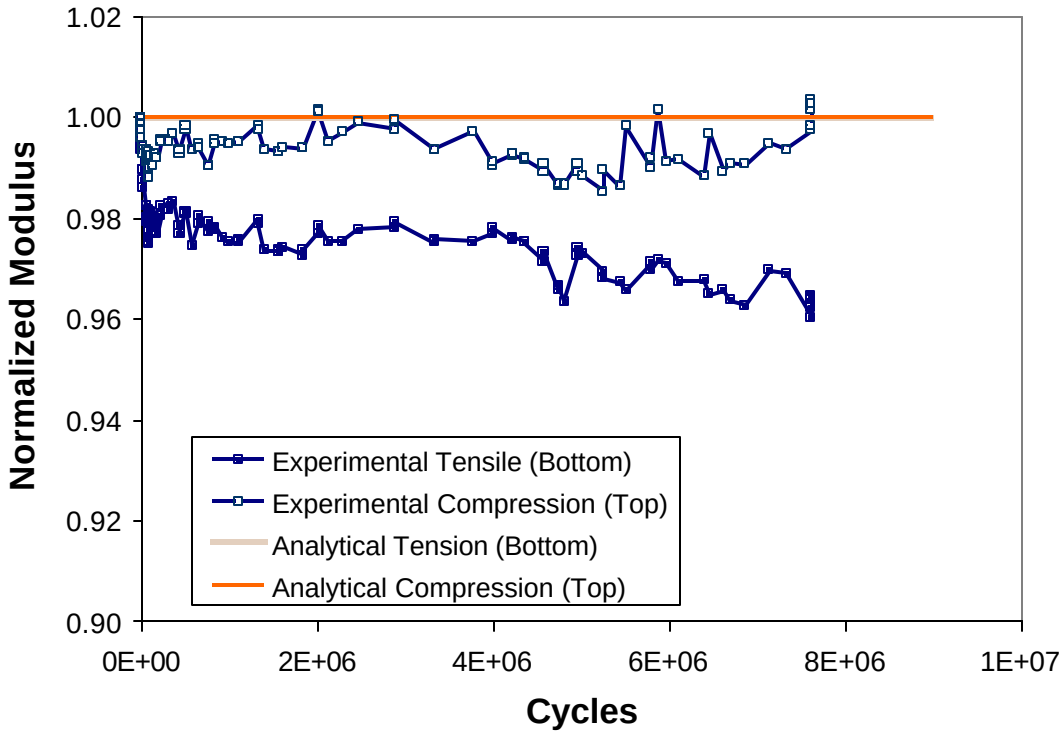

Figure 5- 10: Comparison of predicted and experimental modulus values for Beam #514

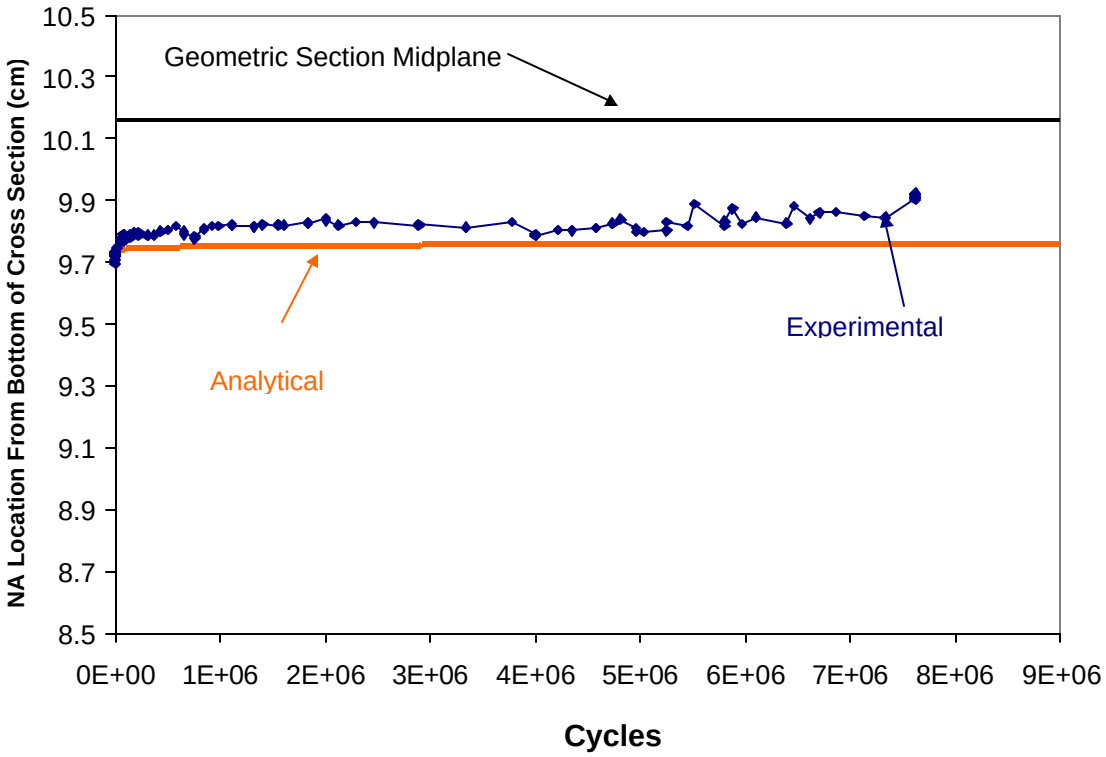

Figure 5- 11: Neutral Axis shift, experiemental and predicted response Beam #514

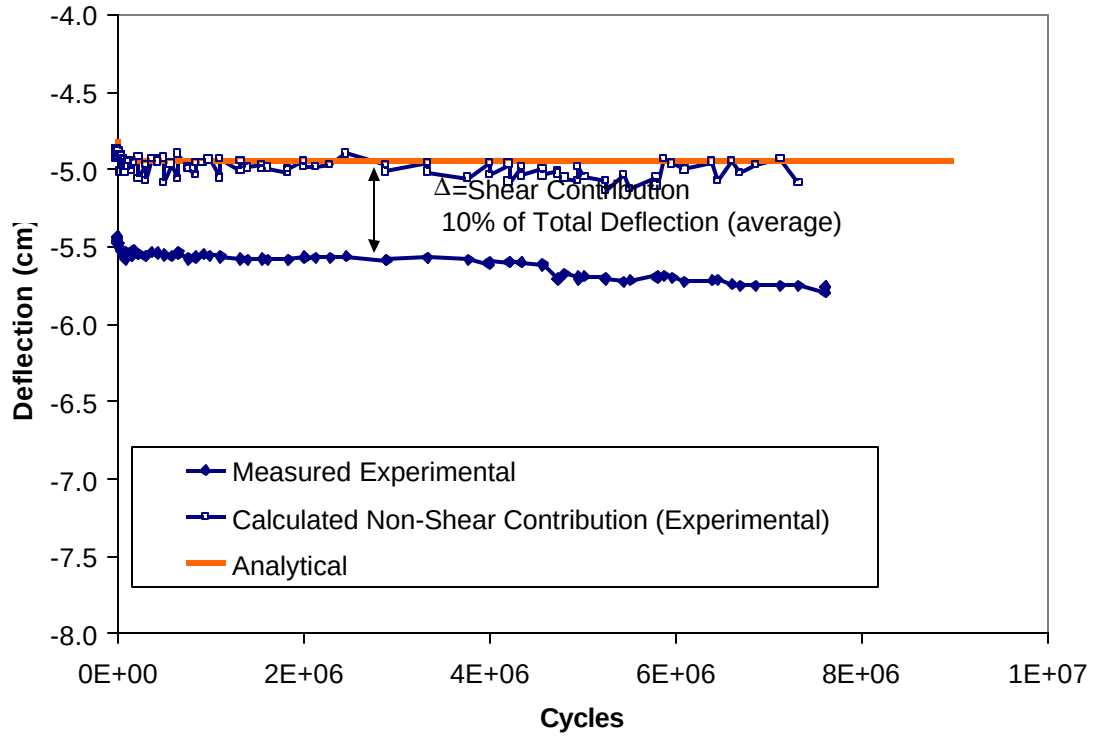

Figure 5- 12: Comparison of deflection values for the Beam #514

CHAPTER 6: CONCLUSIONS AND RECOMMENDATIONS

6.1 Conclusions

The work presented is an analytical and experimental study of the response of hybrid FRP composite beams under four-point bend fatigue loading. This loading requires both the tension and compression response of the material to be accounted for. The beams tested and analyzed were the 8" pultruded beams used in the Tom's Creek Bridge in Blacksburg, VA. Beyond predicting the life of the beams for that structure, understanding the durability and failure mode of such members is essential for the infrastructure community to accept FRP materials for larger scale applications. Prior quasi-static testing indicated the failure of the beams was due to delamination in the compression flange. In the beams under bending, at the failure load, the in-plane strains are insignificant when compared to failure strain levels. Commonly, fatigue life of laminated structures is the result of in-plane fiber or matrix damage, for which fatigue life is fairly well understood. Delamination is an out-of-plane failure mode, therefore many of the techniques developed could not be used in their entirety, requiring a new methodolgy to be investigated.

Experimentally, the beams were subjected to cyclic four-point bend load. Two batches of beams were tested, wherein the batch with a higher stiffness had a lower ultimate moment. The beams from the first batch were tested at 35% and 46% of their ultimate moment. The beam at 46% failed after 130,000 cycles and the test was stopped at 10 million cycles for the second beam. The first beam from the second batch was tested at 65% (same actuator load as the 46% beam from batch #1) and was stopped after 7.6 million cycles. The final beam failed at 370,000 cycles at 82% of the ultimate moment. The beams that failed, exhibited failure by delamination, as seen in quasi-static testing.

The test was periodically stopped to capture data and characterize the stiffness response of the beam. The modulus was monitored based on the strain in the top and bottom flanges and also from mid-span deflection. Testing indicated an initial drop in stiffness to a value that was then maintained for the remainder of the test. The stiffness reduction seems to be controlled by the tensile flange, while the compression flange maintains its properties until delamination occurs. There is a shear component to the response, accounting for on average 10% of the total deflection, and remains constant with cyclic loading. The test results indicate that the fatigue life is dependent on the stiffness of the beam rather than the strength, and is a strain controlled problem.

A model to predict the life of the beams under the same loading was developed in accordance with the experimental observations. The methodology accounts for the different response of the flanges under tension and compression, and predicts the out-of-plane failure mode of delamination. In order to predict delamination, a three-dimensional stress analysis must be done on the top flange. Laminated beam theory is used to determine the in-plane stresses in the flanges. Two approximations are then used to attain the out-of-plane stresses at the free edge, the Primitive Delamination Model, and the Minimization of Complementary Energy.

The model then uses the critical element residual strength theory to degrade the properties based on assumptions made in conjunction with experimental results. The overall stiffness reduction is controlled purely by the tensile flange, which results in a redistribution of strains and a shift in the neutral axis. As the stiffness is reduced, the overall strength of the beam is also degrading until the stresses reach a critical level at the free edge in the compression flange resulting in delamination initiation. The compression flange does not have any stiffness reduction until delamination, and then degrades further as the crack grows until ultimate failure.

The stiffness degradation scheme is based on experimental fatigue data. Prior fatigue testing by Phifer on pultruded laminates under tension showed a similar trend to what was exhibited in the tensile flange of the beams. There was an initial drop in stiffness

followed by a constant region. Therefore, the coupon laminate data was used to characterize sublaminate stiffness reduction in the tensile flange, and the carbon was assumed to retain all of its stiffness.

The static analysis from the model agreed well with experimental data. The predicted EI_{eff} was under 6% error from the measured value, and the top and bottom flange strains were with 2% of the measured values. Comparison of the S-N curve to the four experimental data points suggested the life prediction model is reasonable. A detailed comparison of Beam #517 to the model accounting for the initial neutral axis offset and 500 series strength, suggests the model captures the data trends. The model predicted a life of 265,000 cycles compared to the actual 370,000 cycles and accurately characterized the stiffness reduction of the tensile flange.

In conclusion, a life prediction model has been developed which predicts delamination of the top flange as the dominant failure mode. The use of coupon fatigue data to characterize the stiffness reduction results in correlation to the fatigue response of the entire structure. The simplified methods of calculating the out-of-plane stresses also seem reasonable for this application. The model could act as a design tool for predicting the stiffness and ultimate moment of similar structures.

6.2 Recommendations for Future Work

In order to truly understand the correlation of the model to what is actually occurring further full-scale fatigue testing is necessary. The beams from the fatigue tests which were stopped, should be failed to determine the residual strength. Using the analysis and conducting tests on other layups, such as the all glass beam is also advised.

The strength value used in the model, and the out-of-plane stress values are crucial to characterizing the fatigue life based on delamination. The simplified calculations for stresses need to be compared to more exact solutions, such as Finite Element Analysis or

elasticity. Additionally, further experimental data on the out-of-plane strengths should be obtained.

The tension coupon fatigue data characterized the response of the tensile flange well for the loading investigated. This correlation was in the region where the coupon tests were run. The agreement in the region where the data was extrapolated is not known. Attaining coupon data at these lower regions to avoid the extrapolation will allow for a better prediction at the loads that the beams would actually see in service.

Finally, the compression response under fatigue needs to be understood and included in the model. This can be done based on compression coupon fatigue data similar to what is currently known for the tensile flange. The beam fatigue test resulted in reduction in stiffness of the compression flange although less than the tension flange. This reduction is not currently included in the model. Understanding the compression response will also allow for the remaining strength to be determined based on more than just the in-plane tensile response of the beam.

REFERENCES

[1] Lopez-Anido, R.,. Howdyshell, P.A, Stephenson, L.D., and Gangarao, H.V.S., "Fatigue and Failure Evaluation of Modular FRP Composite Bridge Deck", *International Composites Expo Proceedings,* SPI, New York; 1998, Session 4-B.

[2] P.Qiao, J.F.Davalos, E.J. Barbero, and D. Troutman, "Step-by-Step Engineering Desing Equations for FRP Structural Beams", *Procs International Composites EXPO '99*, Cincinnati, OH, May 1999. pp.9-E/1-7.

[3] M. D. Hayes, J.J. Lesko, J. Haramis, T. E. Cousins, J. Gomez, P. Massarelli, "Laboratory & Field Characterization of the Tom's Creek Bridge Composite Superstructure," Accepted to the *ASCE, Journal of Composites for Construction*, to be published Nov. 1999.

[4] "Proposed Bridge on Tom's Creek Road Over Tom's Creek Bridge, Town of Blacksburg," Tom's Creek Bridge design plans, Commonwealth of Virginia Department of Transportation, May 8, 1997.

[5] Hayes, M.D., **"**Characterization and Modeling of a Fiber-Reinforced Polymeric Composite Structural Beam and Bridge Structure for Use in the Tom's Creek Bridge Rehabilitation Project"**,** M.S. Thesis, Virginia Polytechnic Institute and State University, December 1998.

[6] Neely, W.D., "Evaluation of the In-Servic Performance of the Tom's Creek Bridge", M.S. Thesis, Virginia Tech, May 2000

[7] J. Haramis, K.N.E. Verghese, J.J. Lesko, & R.E. Weyers, "Characterization of Freeze-Thaw Damage Mechanisms in Composites for Civil Infrastructure," SAMPE 2000, May 21-25, 2000, Long Beach, CA.

[8] J. Haramis, K.N.E. Verghese, & J.J. Lesko, "Freeze-Thaw Durability of Composites for Civil Infrastructure," ANTEC 2000, May 7-11, 1999, Orlando FL.

[9] Verghese, K.N.E., M. R. Morrell, M.R. Horne, J. J. Lesko, J. Haramis, "Freeze-Thaw Durability of Polymer Matrix Composites in Infrastructure", *Proceedings of the Fourth International Conference on Durability Analysis of Composite Systems*, Duracosys 99/Brussels/Belgium, July 11-14, 1999, pp 457-464.

[10] S.P. Phifer, K.N.E. Verghese, J. Haramis, & J.J. Lesko, "Temperature-Moisture-Mechanical Response of Vinyl Ester Resin and Pultruded Vinyl Ester/E-glass Laminated Composites," ANTEC 2000, May 7-11,1999, Orlando, FL.

[11] S.P. Phifer, K.N.E. Verghese, J. Haramis, & J.J. Lesko, "Temperature-Moisture-Mechanical Response of Vinyl Ester Resin and Pultruded Vinyl Ester/E-glass Laminated Composites," 3rd International Conference on Advanced Composite Materials in Bridges and Structures, August 15-18, 2000, Ottawa, Canada.

[12] F. McBagonluri**, K. Garcia✞, M. Hayes**, N. Verghese**, & J. J. Lesko, "Characterization of Fatigue and Combined Environment on Durability Performance of Glass/Vinyl Ester Composite for Infrastructure Applications" *International Journal of Fatigue*, Vol. 22, Issue 1, 2000, pp. 53-64.

[13] Strongwell Extren DWB™ Design Guide

[14] "Development of Innovative Manufacturing Technology to Produce a Large Phenolic Composite Shapes", NIST Advanced Technology Program, Strongwell, Corp., 1995.

[15] "Composite Structural Shapes for Infrastructure", National Institute of Standards and Testing (NIST) Advanced Technology Program (ATP), 1994.

[16] "Pulturded Beams Reflect Design-For-Manufacture", *High Performance Composites*, May/June 1997, pp 23-26.

[17] Wilson, Brian A., Pultrusion Handbook of Composites, Peters, S.T., Editor, 1998.

[18] Phifer, S.P., "Quasi-Static and Fatigue Evaluation of Pultruded Vinyl Ester/E-Glass Composites", M.S. Thesis, Virginia Tech, May 1999.

[19] Haeberle, D., Personal Communication

[20] Kim, R.Y. and Soni, S.R. "Experimental and Analytical Studies On the Onset of Delamination in Laminated Composites," *Journal of Composite Materials*, Vol 18, Jan 1984, pp 70-80

[21] Verghese, K.N.E, "Durability of Polymer Matrix Composites for Infrastructure: The Role of the Interphase", Ph.D. Dissertation, Virginia Polytechnic Institute and State University, August 1999.

[22] Bump, M.B., Robertson, M.A.F., Broyles, N.S., Flynn, M.C., Verghese, K.E., Lesko, J.J., and Riffle, J.S., "Designed Polymeric Interphases for Vinyl Ester Composites," Proc. Int. Comp. Expo '98, Session 20-D, 1998.

[23] Garcia, K., Personal Communication

[24] Bank, L.C., M. Nadipelli, T. R. Gentry, "Local Buckling and Failure of Pultruded Fiber-Reinforced Plastic Beams", *Journal of Engineering Materials and Technology*, Vol 116, April, 1994, pp233-237.

[25] Khatri, S.C., M. J. Koczak, "Thick-section AS4-Graphite/E-Glass/PPS Hybrid Composites: Part II. Flexural Respons", *Composites Science and Technology*, Vol 56, 1996, pp 473-482.

[26] Hyer, M.W. Stress Analysis of Fiber Reinforced Composites; McGraw-Hill; Boston, 1998, pp212-305.

[27] Herakovich, C. T., Mechanics of Fibrous Composites; John Wiley & Sons, Inc.; New York, 1998, pp247-301.

[28] Herakovich, C. T., "On the Relationship Between Engineering Properties and Delamination of Composite Materials", *Journal of Composite Materials*, Vol 15, 1981, pp 336-348.

[29] Pipes, R. B. and Pagano, N. J., "Interlaminar Stresses in Composite Laminates Under Uniform Axial Extension", *Journal of Composite Materials*, Vol. 4, 1970, pp.538-548.

[30] Bogy, D. B., "Edge-Bonded Dissimilar Orthogonal Elastic Wedges Under Normal and Shear Loading", *Journal of Applied Mechanics*, Vol 35, 1968, p460.

[31] Hess, M. S. "The End Problem for a Laminated Elastic Strip – II. Differential Expansion Stresses", *Journal of Composite Materials*, Vol 3, 1969, p. 630.

[32] Pagano, N.J. and Pipes, R.B., "The Influence of Stacking Sequence on Laminate Strength", *Journal of Composite Materials*, Vol 5, 1971, pp. 50-57.

[33] Foye, R. L. and Baker, D.J., "Design of Orthotropic Laminates", presented at the 11th Annual AIAA Structures, Structural Dynamics, and Materials Conference, Denver, Colorado, April 1970.

[34] Rybicki, E. F. , "Approximate Three Dimensional Solutions for Symmetric Laminates Under In-Plane Loading", *Journal of Composite Materials*, Vol 5, 1971, pp. 354-360.

[35] Wang, A. S. D. and Crossman, F. W., "Some New Results on Edge Effect in Symmetric Composite Laminates", *Journal of Composite Materials*, Vol 11, 1977, pp. 92-106.

[36] Pagano, N.J. and Pipes, R.B., "Some Observations on the Interlaminar Strength of Composite Materials", *International Journal of Mechanical Sciences*, Vol 12 ,1973, pp 679-688.

[37] Pagano, N.J., Interlaminar Response of Composite Materials; Vol 5**,**Composite Materials Series, R.B.Pipes (Series,ed.); Elsevier; New York, 1989, pp. 1-25.

[38] Whitney, J. M. and Browning, C. E., "Free-Edge Delamination of Tensile Coupons", *Journal of Composite Materials*, Vol 6, 1972, pp 300-303

.

[39] Kim, R. Y. and Aoki, R. M., "Transverse Cracking and Delamination in Composite Materials", *Fibre Science and Technology,* Vol 18, 1983, pp.203-216.

[40] Pipes, R.B. and Pagano, N.J., "Interlaminar Stresses in Composite Laminates – An Approximate Elasticity Solution", *Journal of Applied Mechanics,* Vol 41, 1974, pp.668-672.

[41] Pagano, N.J. and Soni, S. R., "Global-Local Laminate Variational Model", *International Journal of Solids and Structures*, Vol 19, 1983, pp 207-228.

[42] Wang, S. S. and Choi, I., "Boundary-Layer Effects in Composite Laminates: Part 1 – Free-Edge Stress Singularities", *Journal of Applied Mechanics,* Vol 49, 1982, pp 541-548.

[43] Wang, S. S. and Choi, I., "Boundary-Layer Effects in Composite Laminates: Part 2 – Free-Edge Stress Solutions and Basic Characteristics", *Journal of Applied Mechanics,* Vol 49, 1982, pp 549-560

.

[44] Herakovich, C.T., Post, D., Buczek, M.B., Czarnek, R., "Free Edge Strain Concentrations in Real Composite Laminates: Experimental-Theoretical Correlation", *Jounal of Applied Mechnics,* Vol 52, 1985 pp 787-792.

[45] Brewer, J.C., C. Kassapoglou, P.A. Lagace, "An Efficient Method for the Calculation of Interlaminar Stresses due to Thermal Stresses in Composite Materials", *TELAC Report – Department of Aeronautics and Astronautics, Massachusetts Institute of Technology,* August 1987.

[46] Kassapoglou, C., P. A. Lagace, " An Efficient Method for the Calculation of Interlaminar Stresses in Composite Materials", *Journal of Applied Mechnics,* Vol 53, 1986 pp 744-750.

[47] Kassapoglou, C., Lagace, P. A., " Closed Form Solusions of the Interlaminar Stress Field in Angle-Ply and Cross-Ply Laminates", *Journal of Composite Materials,* Vol. 21, 1987 pp 292-308.

[48] Lin, C. and C. Hsu, "Interlaminar Stresses in General Laminates with Straight Free Edges", *American Institute of Aeronautics and Astronautics,* Vol. 33, August 1995, pp 1471-1476.

[49] Kassapoglou, C., "Determination of Interlaminar Stresses in Composite Lamines under Combined Loads", *Journal of Reinforced Plastics and Composites*, Vol. 9, Jan 1990, pp 33-58.

[50] Yin, W-L., " Simple Solutions of the Free-Edge Stresses in Composite Laminates Under Thermal and Mechanical Loads", *Journal of Composite Materials,* Vol. 28, No. 6, 1994, pp 573-587.

[51] O'Brien, T.K., "Generic Aspects of Delamination in Fatigue of Composite Materials," *Journal of the American Helicopter Society,* Vol 32, Jan 1987, pp 13-18.

[52] O'Brien, T.K., "Stacking Sequence Effect on Local Delamination Onset in Fatigue", *International Conference on Advanced Composite Materials,* The Minerals, Metals & Materials Society, 1993, pp. 399-406.

[53] O'Brien T.K., and Hooper, S.J. "Local Delamination in Laminates With Angle Ply Matrix Cracks, Part I: Tension Tests and Stress Analysis", *Composite Materials: Fatigue and Fracture*, Vol 4, 1993, pp 491-506.

[54] O'Brien T.K., "Local Delamination in Laminates with Angle Ply Cracks, Part II: Delamination Fracture Analysis and Fatigue Characterization", *Composite Materials: Fatigue and Fracture,* Vol 4, 1993, pp 507-538.

[55] Rybicki, E. F., D. W. Schmueser, and J. Fox, "An Energy Release Rate Approach For Stable Crack Growth in the Free-Edge Delamination Problem", *Journal of Composite Materials*, Vol. 11, Oct. 1977, pp 470-487.

[56] Brewer, J.C. and Lagace, P.A. "Quadratic Stress Criterion for Initiation of Delamination," *Journal of Composite Materials,* Vol 22, Dec 1988, pp1141-1155.

[57] Naik, R.A, Gillespie, J.W. and Eduljee, R.F., "Development of a Modified Tsai-Wu Criterion for Interlaminar Failure in Composite Laminates", *Proceedings of the Eighth Japan-U.S. Conference on Composite Materials,* 1998, pp639-648.

[58] Swanson, S.R., Introduction to Design and Analysis With Advanced Composite Materials; Prentice Hall; New Jersey, 1997, pp191-224.

[59] Davalos, J. F., H. A. Salim, P. Qiao, R. Lopez-Anido, E. J. Barbero, "Analysis and design of pultruded FRP shapes under bending", *Composites: Part B,* Vol 27, 1996, p 295-305.

[60] Lagace, P., J. Brewer and C. Kassapoglou, "The Effect of Thickness on Interlaminar Stresses and Delamination in Straight-Edged Laminates", *Journal of Composites Technology & Research,* Vol 8, No 3, Fall 1987, pp 81-87.

[61] Reifsnider K.L., Stinchcomb W.W.; "A Critical Element Model of the Residual Strength and Life of Fatigue-Loaded Composite Coupons;" Fatigue and Fracture, ASTM STP 907, 1986, pp.298-303.

[62] Jones, R. M., Mechanics of Composite Materials; Taylor and Frances1975, pp170-171.

[63] McBagonluri, F., K. Garcia, M. Hayes, K.N.E. Verghese, J.J.Lesko, "Characterization of Fatigue and Combined Environment on Durability Performance of Glass/Vinyl Ester Composite for Infrastructure Applications", *International Journal of Fatigue*, Vol 22, Jan 2000, pp 53-64.

[64] Case, S.W. and Reifsnider, K, Strength and Durability of Composite Materials Class Notes, Virginia Tech, 1999.

APPENDIX-A

The following are the terms of the symmetric 6 x 6 anisotropic compliance matrix used in the outlined analysis.

Note: m = cos θ; n = sin θ , and the *S* terms without an overbar are the compliances of a zero degree ply.

$$\overline{S}_{11} = S_{11}m^4 + (2S_{12} + S_{66})n^2m^2 + S_{22}n^4$$

$$\overline{S}_{12} = (S_{11} + S_{22} - S_{66})n^2m^2 + S_{12}(n^4 + m^4)$$

$$\overline{S}_{13} = S_{13}m^2 + S_{23}n^2$$

$$\overline{S}_{22} = S_{11}n^4 + (2S_{12} + S_{66})n^2m^2 + S_{22}m^4$$

$$\overline{S}_{23} = S_{13}n^2 + S_{23}m^2$$

$$\overline{S}_{33} = S_{33}$$

$$\overline{S}_{16} = 2S_{11}m^3n - 2S_{22}n^3m + (2S_{12} + S_{66})(n^3m - m^3n)$$

$$\overline{S}_{26} = 2S_{11}n^3m - 2S_{22}m^3n + (2S_{12} + S_{66})(m^3n - n^3m)$$

$$\overline{S}_{36} = 2(S_{13} - S_{23})m\ n$$

$$\overline{S}_{44} = S_{55}n^2 + S_{44}m^2$$

$$\overline{S}_{45} = (S_{55} - S_{44})m\ n$$

$$\overline{S}_{55} = S_{55}m^2 + S_{44}n^2$$

$$\overline{S}_{66} = 4(S_{11} + S_{22} - 2S_{12})n^2m^2 + S_{66}(m^4 + n^4 - 2m^2n^2)$$

VITA

Jolyn Senne was born in Ann Arbor, MI in 1976 to Steven and Judith Senne. She grew up in Wayne and Livonia, Michigan, and graduated from Livonia Churchill High School in 1994. From there, she headed north to the Upper Peninsula of Michigan to attend Michigan Technological University and pursue Mechanical Engineering. While attending MTU, she was involved in a local sorority Theta Chi Epsilon and was active on the Formula SAE team. She received several summer internships with Ford Motor Company before completing a B.S. in Mechanical Engineering in May of 1998. After completion of a B.S. she attended Virginia Tech in the Engineering Science and Mechanics Department. Following graduation in July of 2000, with a Master's of Science, she will begin work in Product Development with Ford Motor Company in Dearborn, Michigan.